EFFECT OF CO-FIRING TORREFIED WOODY BIOMASS WITH COAL IN A 30 kWt DOWNFIRED BURNER

A Dissertation

by

SIVA SANKAR THANAPAL

Submitted to the Office of Graduate and Professional Studies of
Texas A&M University
in partial fulfillment of the requirements for the degree of

DOCTOR OF PHILOSOPHY

Chair of Committee,	Kalyan Annamalai
Co-Chair of Committee,	Devesh Ranjan
Committee Members,	Andrea Strzelec
	Jim Ansley
Head of Department,	Andreas Polycarpou

May 2014

Major Subject: Mechanical Engineering

ABSTRACT

Mesquite and juniper can be beneficially utilized for gasification and combustion applications. Torrefaction has been considered to be one of the thermal pretreatment options to improve the chemical (e.g. heat content) and physical (e.g. grindability) properties of raw biomass. A simple three component parallel reaction model (TCM) was formulated to study the effect of heating rate, temperature, residence time and type of biomass on torrefaction process. Typically inert environment (e.g. N_2, He, Ar) is maintained to prevent oxidation of biomass during torrefaction. A novel method for utilization of carbon dioxide as the pretreatment medium for woody biomass has been investigated in the current study. Both raw and the torrefied biomass (TB) were pyrolyzed using TGA under N_2. The TB fuels were also fired with coal in a 30 kWt downfired burner to study the NOx emission. In addition, tests were also done using raw biomass (RB) (mesquite and juniper) blended with coal and compared with results obtained from cofiring TB with coal. A zero dimensional model has been developed to predict the combustion performance of cofired fuels.

The results are as follows. TGA studies yielded global kinetics based on maximum volatile release (MVR) method. TCM predicts higher loss of hemicellulose upon torrefaction when compared to the other components, cellulose and lignin resulting in improved heat values of TB. Comparable mass loss at lower temperatures, improved grindability, and improved fuel properties were observed upon using CO_2 as the torrefaction medium. Co-firing 10% by mass of raw mesquite with coal reduced the

NOx emission from 420 ppm to 280 ppm for an Equivalence ratio (ER) of 0.9. Further cofiring TB with coal reduced the NOx emission by 10% when compared to base case NOx emission from combustion of pure PRB coal. NOx emission decreased with increase in equivalence ratio. In addition, a term used in the biological literature, respiratory quotient (RQ), is applied to fossil and biomass fuels to rank the potential of fuels to produce carbon dioxide during oxidation process. Lesser the value of 'RQ' of a fuel, lower the global warming potential.

DEDICATION

This work is dedicated to my parents, Mr. Thanapal and Mrs. Manimoli, my brother, Dr Sivakumar Thanapal and my sister in law, Dr Gnanapriya Sivakumar. Their encouragement and support kept me motivated through the course of my research especially when situations got tough.

ACKNOWLEDGEMENTS

I thank my committee chair, Professor Kalyan Annamalai for admitting me into his research group and for his invaluable time, support, guidance, and for providing me with necessary resources for the experimental studies during my stay in Coal and Biomass Energy Lab, Texas A&M University. I also thank my co-chair, Dr Devesh Ranjan for his faith, suggestions and financial support which made this project possible. I thank my committee members, Professor Robert James Ansley for providing the biomass materials for this research work and Dr Andrea Strzelec for the useful discussions throughout the project. I thank all the professors and staff in the Department of Mechanical Engineering, Texas A&M University. I would like to acknowledge the help and guidance from my professors at College of Engineering Guindy, Anna University and my teachers at Jawahar Higher Secondary School, Neyveli, Tamil Nadu, India.

All my colleagues at Coal and Biomass Energy Lab, Department of Mechanical Engineering were of great help to me with setting up the reactor, suggesting modifications, troubleshooting the instruments and helping with running the experiments. Thanks to every one: Dr Ben Lawrence, Dr Wei Chen, Dr Mirik Mustafa, Dustin Eseltine, Aubrey Spear, Harikrishna Uggini, Arne Joachim Poestges, Marc Maindrault, Luis Martinez, Tiyawut Tiyawangsakul and Sam Pesek. A big thank you to Jason Caswell from the Department of Physics electronic shop for his help with circuits and experimental setup.

Thanks to my friends: Srikanth Pothiraj, Sankaranarayanan Ravi, Dr Sujeevraja Sanjeevi, Thanigaivel Kulandaivel, Rakesh Selvaraj, Arvind Chandran, Shreyas Balachandran, Seenu Gopalraju, Vivekanand Gurumoorthy, Elangovan Kembanur Natarajan, Rajesh Kumar Arunachalam, Ramanathan Swaminathan, Shriram Kalusalingam, Arun Palaniappan, Vaidyanathan Sambasivan, Karthik Raviprakash, Somasundaram Essakkiappan, Naresh Narayanan, Lakshminarasimhan Krishnan, Arun Selvakumar Dhandapani, Karthik Narayanan Ganesan, Prakash Elumalai and Sathish Kumar Raveendran were of tremendous support to me during the difficult times. I thank all my friends for their company. As per the saying by Tamil poet Thiruvalluvar,

தினைத்துணை நன்றி செயினும் பனைத்துணையாக்

கொள்வர் பயன்தெரி வார்.

Translated by George Uglow Pope, “Each benefit to those of actions fruit who rightly deem, though small as millet-seed, as palm-tree vast will seem”. Though the help extended by each and everyone around may be small, part of their small deeds contributed to the final outcome. I appreciate each and everyone’s help. Thanks to all my fellow aggies in Aggieland who were warm, friendly and made my stay at Texas A&M University, College Station more pleasant and memorable.

I would also like to acknowledge the financial support from 2013 Texas A&M University-CONACYT: Collaborative Research Grant Program, Texas Agrilife research, Sungrant Oklahoma, and the Department of Mechanical Engineering, Texas A&M University.

NOMENCLATURE

Ar	Argon
ar	as-received
A:F	Air to fuel ratio
Al_2O_3	Aluminum oxide
B/A	Basic to acidic oxides
B	Pre-exponential factor
BET	Brunauer-Emmett-Teller
BF	Burnt fraction
BMR	Basal metabolic rate
BTU	British thermal unit
C	Carbon
CABEL	Coal and Biomass Energy Lab
CaO	Calcium oxide
CFD	Computational Fluid Dynamics
Cl	Chlorine
CO	Carbon Monoxide
CO_2	Carbon dioxide
CO_{2e}	Carbon dioxide equivalent
CH_4	Methane
C_8H_{18}	Gasoline

$C_{12}H_{23}$	Diesel
C_2H_5OH	Ethanol
c_p	Specific heat at constant pressure
DAF	Dry ash free
d_p	Diameter of the particle
DSC	Differential Scanning Calorimetry
DTA	Differential Thermal Analysis
DTG	Differential thermogram
E	Activation energy
EIA	Energy Information Administration
EPA	Environment protection agency
ER	Equivalence ratio
f_k	Conversion of each component k
F	Overall conversion
FC	Fixed carbon
Fe_2O_3	Iron oxide
GJ	giga Joule
GWP	Global Warming Potential
H	Hydrogen
Hg	Mercury
ha	hectares
H/C	Ratio of hydrogen to carbon

HCN	Hydrogen cyanide
HEX	Heat exchanger
HHV	Higher heating value
HHV_{O2}	Higher heating value per kg oxygen consumed
H_2O	Water
H_2S	Hydrogen sulphide
IEA	International Energy Agency
K_2O	Potassium oxide
I.D	Inner diameter
kJ/kg	kilo Joule per kilo gram
kW	kilo Watt
kW_t	kilo Watt thermal
LASSDB	Low Ash Separated Solids Dairy Biomass
lb	Pound
LMTD	Log mean temperature difference
LPM	Liters per minute
L_{RZ}	Length of recirculation zone
M_i	Molecular weight of species i
m_0	Initial mass
m_k	Mass of component k
$m_{k,char}$	Mass of char in component k
m_{TB}	Mass of torrefied biomass

m_{RB}	Mass of raw biomass
MJ	mega Joule
MgO	Magnesium oxide
mmBTU	Million BTU
MVR	Maximum volatile release
MW	mega Watt
MW_e	mega Watt electrical
MW_t	mega Watt thermal
N	Nitrogen
NAAQS	National Ambient Air Quality Standards
Na_2O	Sodium oxide
N_2	Nitrogen
NH_3	Ammonia
NO	Nitric oxide
N_2O	Nitrous oxide
NOx	Nitrogen oxides
O	Oxygen
O.D	Outer diameter
O/C	Ratio of oxygen to carbon
OH	Hydroxyl
OHTC	Overall heat transfer coefficient
PAH	Polycyclic aromatic hydrocarbons

P_2O_5	Phosphorous (V) oxide
ppm	Parts per million
PRB	Powder river basin coal
$\bar{R}$	Universal gas constant (kJ/kmol-K)
RF	Radiative Forcing
RJ	Raw juniper
RM	Raw mesquite
RQ	Respiratory Quotient
S	Sulfur
SATP	Standard atmospheric temperature and pressure
SEM	Scanning Electron Microscope
SCFM	Standard Cubic Feet per Minute
SCR	Selective Catalytic Reduction
SLPM	Standard liters per minute
SiO_2	Silica
SMD	Sauter mean diameter
SNCR	Selective Non-Catalytic Reduction
SO_3	Sulfur trioxide
SOx	Sulfur oxides
t	Time
T	Temperature
T_g	Temperature of gas

T_p	Temperature of particle
T_{torr}	Temperature of torrefaction
T_{RCZ}	Temperature of recirculated gases
TCM	Three component model
TGA	Thermogravimetric analyzer
TiO_2	Titanium dioxide
TJ	Torrefied juniper
TM	Torrefied mesquite
TXLC	Texas Lignite Coal
U	Overall heat transfer coefficient
VM	Volatile matter
W	Watt
$\dot{w}_i$	Reaction rate of species i
WYC	Wyoming Coal
X_i	Mole fraction of species i
$X_{O2,flue}$	Mole fraction of oxygen in the flue gas
$X_{O2,amb}$	Mole fraction of oxygen in the ambient air
Y_i	Mass fraction of species i

Greek symbols

α	Liberated fraction
β	Heating rate

ρ	Density
ν_i	Stoichiometric amount of species i
ϕ	Equivalence ratio

TABLE OF CONTENTS

Page

LIST OF FIGURES

Page

Page

Page

Page

Page

Page

LIST OF TABLES

Page

Page

Page

1. INTRODUCTION

The world energy consumption is projected to increase with development and economic growth in developing countries. Fossil fuels play a major role in meeting the energy demand. In addition, different non- conventional energy sources such as wind, solar, nuclear, tidal and biomass are also being utilized to produce power. Of the different sources of energy currently used to produce electricity, coal still remains as one of the dominant source for power production. The use of natural gas for the production of power is projected to increase in the upcoming years due to development in shale gas, tight gas and coal bed methane [1]. It has been estimated that around 861 billion tons of coal reserves exist on earth as of 2013 and with the current rate of extraction and power generation these reserves can be used for another 109 years [2]. Around 44 % of total power produced in USA was from coal according to the 2011 data published by the Energy Information Administration [3]. Fig. 1 shows the amount of electricity generated from different fuels. The contribution of coal towards the total energy consumption in the world was 28% [4].

The major drawback with the utilization of coal is the amount of carbon dioxide (CO_2) being released into the environment which is considered to be a greenhouse gas which causes global warming. According to 2011 data published by Environment Protection Agency (EPA) [5], it was estimated that around 67% of the total greenhouse gas produced in the USA have been from power plants. Fig. 2 presents the contribution of different sources towards the greenhouse gas production in USA. The numbers

presented in Fig. 2 are expressed in carbon dioxide equivalent (CO_{2e}). The potential of different gases which causes global warming (methane, Nitrogen oxides, chlorofluorocarbons etc) varies with respect to each of the gases. CO_{2e} is used to represent the global warming potential (GWP) of the different gases based on the tendency of these gases to absorb heat. CO_{2e} for the different gases are calculated using the radiative forcing (RF) concept. It has been estimated that CO_{2e} of CO_2, CH_4 and N_2O are 1, 25 and 298 respectively on a time horizon of 100 years [6].

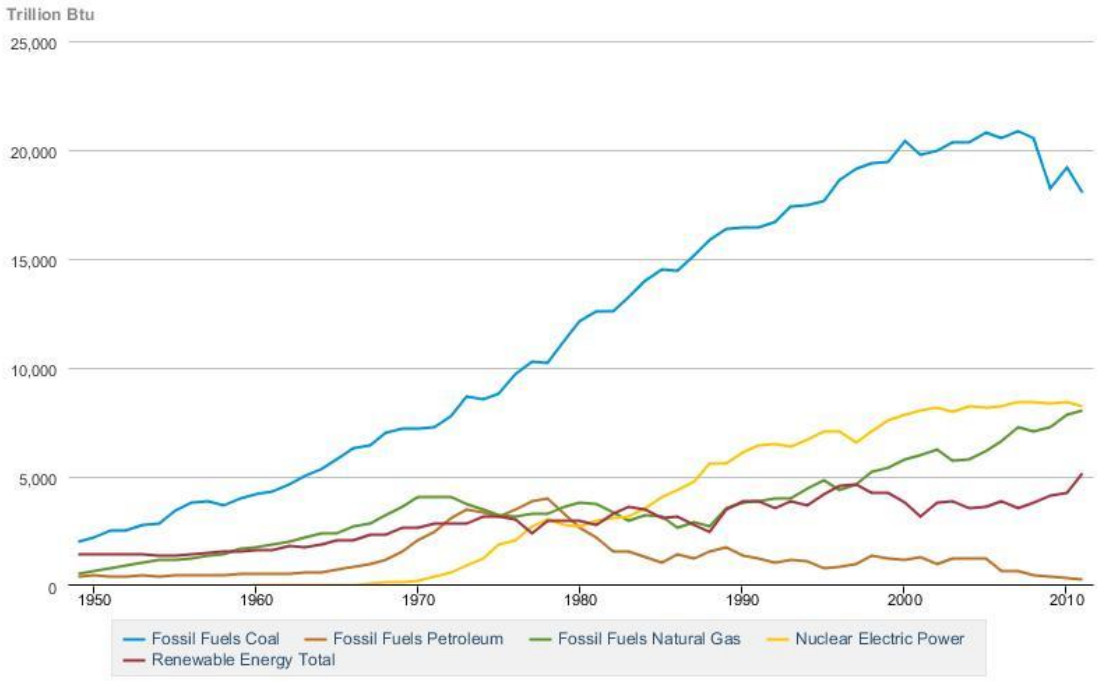

Fig. 1. Consumption of different fuels towards generation of electricity [4].

Along with CO_2, harmful pollutants such as nitrogen oxides (NOx), sulfur oxides (SOx) and mercury are also released during the combustion of coal in power generating

facilities. EPA, USA has set a strict cap for emissions from power plants and other sources which emit harmful pollutants into the atmosphere through the implementation of National ambient air quality standards (NAAQS). The cap on emissions has been slowly tightened to regulate harmful emissions. Table 1 shows the NAAQS set for six harmful pollutants [7].

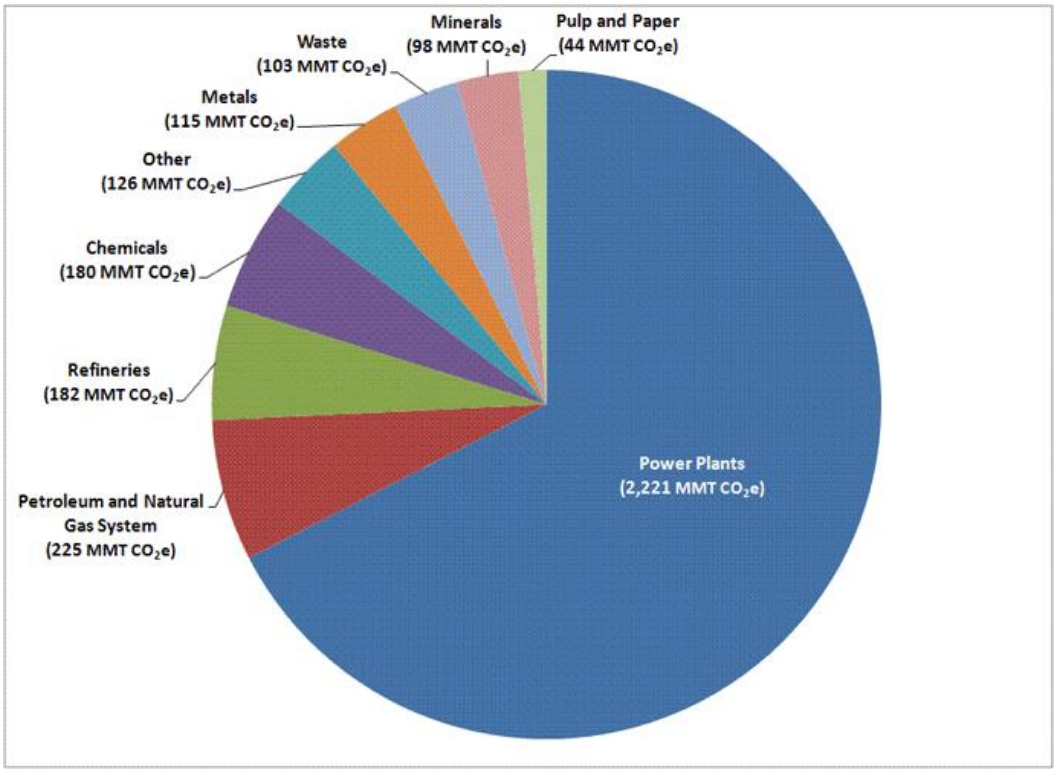

Fig. 2. Carbon dioxide emitted from different sources according to 2011 data published by EPA [5].

Table 1. National Ambient Air Quality Standards for six principal pollutants, adapted from [7].

Pollutant [final rule]		Primary/ Secondary	Averaging Time	Level	Form
Carbon Monoxide		primary	8-hour	9 ppm	Not to be exceeded more than once per year
[76 FR 54294, Aug 31, 2011]			1-hour	35 ppm	
Lead		primary and			
[73 FR 66964, Nov 12, 2008]		secondary	Rolling 3 month average	0.15 µg/m3 (1	Not to be exceeded
Nitrogen Dioxide					
[75 FR 6474, Feb 9, 2010]		primary	1-hour	100 ppb	98th percentile, averaged over 3 years
[61 FR 52852, Oct 8, 1996]		primary and			
		secondary	Annual	53 ppb (2)	Annual Mean
Ozone		primary and			
[73 FR 16436, Mar 27, 2008]		secondary	8-hour	0.075 ppm (3)	Annual fourth-highest daily maximum 8-hr concentration, averaged over 3 years
Particle Pollution	$PM_{2.5}$	primary	Annual	12 µg/m^3	annual mean, averaged over 3 years
		secondary	Annual	15 µg/m^3	annual mean, averaged over 3 years
		primary and secondary	24-hour	35 µg/m^3	98th percentile, averaged over 3 years
	PM_{10}	primary and secondary	24-hour	150 µg/m^3	Not to be exceeded more than once per year on average over 3 years
Sulfur Dioxide					
[75 FR 35520, Jun 22, 2010]		primary	1-hour	75 ppb (4)	99th percentile of 1-hour daily maximum concentrations, averaged over 3 years
[38 FR 25678, Sept 14, 1973]		secondary	3-hour	0.5 ppm	Not to be exceeded more than once per year

A number of techniques have been employed to reduce the emission of NOx, SOx, and Hg which includes pre-combustion techniques (Low NOx burners, using overfire air, Flue gas recirculation, operational modifications, reburning and cofiring) and post combustion techniques (selective catalytic reduction (SCR) and selective non catalytic reduction (SNCR)). More details on these techniques are available elsewhere [8]. In order to offset the total amount of CO_2 being released from coal power plants and to reduce the dependence on coal in producing power, biomass was thought of as a potential renewable fuel which is also considered to be carbon neutral.

The overall goal of the current study is to improve the suitability of carbon neutral biomass fuels for cofiring with coal in thermal power plants.

2. LITERATURE REVIEW*

The review section deals with the properties of fossil and biomass fuels, availability of mesquite and juniper for combustion applications, work carried out on the biomass pyrolysis, biomass torrefaction and cofiring biomass with coal.

2.1.Biomass and coal

Biofuels are one of the renewable energy sources which contribute about 10% of the total energy in the world [9]. Desired characteristics of biomass crops which can be used for power generation were listed by McKendry [10]. They include high yield, low energy input for production, low cost, low contaminants, and low nutrient requirements. Though wood was the dominant source of energy in the United States till 1850, its usage slowly decreased with the utilization of coal [11]. With current regulations on the emissions, the focus has again shifted towards the use of wood and other biomass fuels along with coal. The carbon dioxide emitted during the combustion of biomass fuels are supposed to be absorbed by the growing plants in the carbon cycle and hence biomass is considered to be carbon neutral. The term biomass includes wood, forest wood residues, agricultural wastes, energy crops, animal wastes and municipal solid wastes. Each of those biomass materials has different properties. Properties of some of the selected biomass which have been tested as fuel in cofiring studies are presented in Table 2.

*Reproduced in part with permission from Thanapal SS, Chen W, Annamalai K, Carlin N, Ansley RJ, Ranjan D. Carbon Dioxide torrefaction of woody biomass. Energy Fuels 2014; 28:1147–57. Copyright 2014 American Chemical Society.

Properties of more renewable and fossil fuels are available in TAMU fuel data bank, 2013. From Table 2, it can be observed that all the biomass materials have a higher percentage of volatile matter (species with CHNOS) and oxygen content. Table 3 gives the ultimate and proximate analysis of three types of coal. Coal has higher percentage of fixed carbon and lower oxygen content which results in higher heating value for the coal samples. Percentage of nitrogen in coal and biomass should also be noted here. Coal has comparatively higher percentages of nitrogen than agricultural biomass. However animal biomass also has much higher percentages of nitrogen.

Table 2. Properties of some of the selected biomass materials given on a dry basis.

Fuel (dry basis)	**Ash**	**VM**	**FC**	**C**	**H**	**N**	**S**	**O**	**Reference**
Hazelnut Shell	1.5	76.3	21.2	52.8	5.6	1.4	0.04	42.6	[12]
Sugarcane Bagasse	11.3	73.8	15	44.8	5.35	0.38	0.01	39.6	[13]
Switchgrass	8.9	76.7	14.4	46.7	5.9	0.8	0.19	37.4	[14]
Beech wood	0.5	82.5	17	49.5	6.2	0.4	0	41.2	[15]
Spruce wood	1.7	80.2	18.1	51.9	6.1	0.3	0	40.9	[15]
Cotton gin trash	17.6	67.3	15.1	39.6	5.26	2.09	0	36.38	[13]
Low ash Dairy biomass (LADB)	19.9	62.7	17.4	47.1	4.96	2.58	0.58	24.89	[16]
Litter Biomass	24.3	71	4.6	37.4	4.2	3.8	0.68	29.4	[17]
Meat bone meal	17.1	80.1	2.8	43.1	6.1	9.2	1.2	22.5	[17]

Amount of oxygen in the fuel samples decreases from biomass samples to higher rank coals which have higher carbon content. The ratio of oxygen to carbon (O/C) and hydrogen to carbon (H/C) in the fuels can be used to plot the coalification diagram. Fig. 3 shows the coalification diagram which represents the degree of loss in volatile matter

from biomass to coal. As coal is formed from biomass, the thermal and pressure effects within the ground over millions of years causes some of the volatile compounds to leave the biomass resulting in the formation of coal. Coals are ranked based on the amount of carbon present with anthracite having the highest carbon percentage when compared to peat and lignite which are low rank coals.

Table 3. Ultimate and proximate analysis of some of the coal samples given on a dry basis.

Fuel (dry basis)	**Ash**	**VM**	**FC**	**C**	**H**	**N**	**S**	**O**	**Reference**
Texas Lignite (TXL)	18.6	40.2	41.2	60.3	3.44	1.1	0.99	15.6	[18]
Wyoming Coal (PRB)	8.4	42.5	49.2	69.3	4.07	0.98	0.4	16.8	[18]
White oak (Utah Bituminous)	8.77	42.8	48.5	71	4.89	1.01	0.63	13.7	[14]

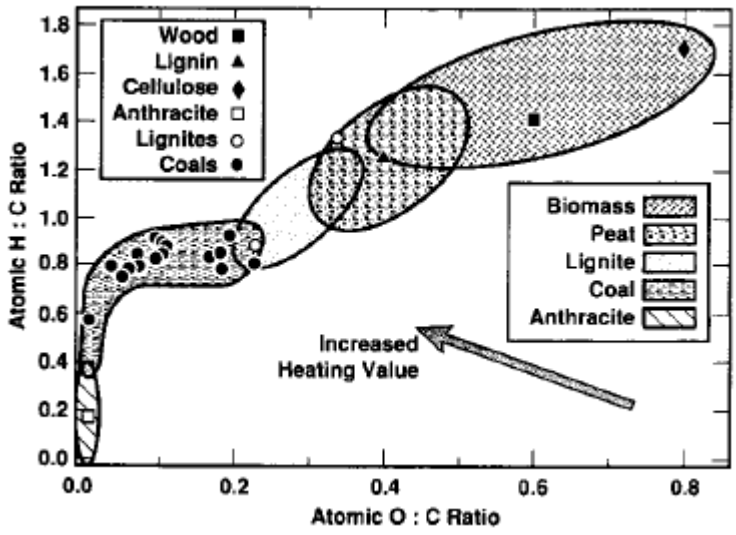

Fig. 3. Coalification diagram (Van Krevelen diagram) which shows the effect of oxygen composition for different class of fuel. Coal has the lowest O/C and H/C, adapted from [19].

In addition to the difference in the organic matter between the biomass and coals, wide differences are also observed with the composition of the inorganic material. Inorganic materials are important with respect to the slagging and fouling issues experienced within the boilers during the combustion process. The four mechanisms by which the fouling occurs are i) inertial impaction of the particles, ii) thermophoresis, iii) condensation of the inorganic vapors on the heat exchanger surfaces and iv) chemical reaction [19]. Inorganic properties of some of the biomass materials and coal are presented in Table 4 where LASSDB, TXLC and WYC stand for low ash separated solid dairy biomass, Texas lignite coal and Wyoming coal respectively.

Table 4. Inorganic properties of typical biomass fuels and coal.

Compositions	**Wheat straw**	**Walnut shell**	**Red Oak Wood**	**LASSDB**	**TXLC**	**WYC**
Silicon, SiO_2	48	23.1	49	31.36	48.72	31.73
Aluminum, Al_2O_3	3.5	2.4	9.5	2.89	16.04	17.27
Titanium, TiO_2	-	0.1	-	0.2	0.85	1.35
Iron, Fe_2O_3	0.5	1.5	8.5	1.62	7.44	4.61
Calcium, CaO	3.7	16.6	17.5	26.4	11.7	22.2
Magnesium, MgO	1.8	13.4	1.1	7.47	1.93	5.62
Sodium, Na_2O	14.5	1	0.5	2.28	0.29	1.43
Potassium, K_2O	20	32.8	9.5	6.9	0.61	0.67
Phosphorus, P_2O_5	3.5	6.2	1.8	6.01	0.1	0.8
Sulfur, SO_3	1.9	2.2	2.6	4.72	10.8	10.4
Chlorine, Cl	3.6	0.1	0.8	0.92	< 0.01	< 0.01
Carbon dioxide, CO_2	-	-	-	9.49	0.08	0.37
Basic/Acidic oxides, B/A	0.79	2.55	0.63	1.3	0.33	0.69
Reference	[15]	[15]	[15]	[8]	[8]	[8]

Basic constituents in the inorganic material include CaO, MgO, K_2O, Fe_2O_3 and Na_2O. SiO_2, Al_2O_3 and TiO_2 are the acid constituents in the ash. It can be observed from Table 4 that the base to acid ratio along with the percentage of Na_2O is very high for the case of biomass materials. This indicates a higher fouling potential [20, 21] of biomass based fuels when compared to that of coal. Different studies conducted to determine the effect of ash slagging and fouling will be presented later.

2.2.Mesquite and juniper

Honey mesquite (Kingdom – Plantae, Division – Magnoliophyta, Class – Magnoliopsida, Order - Rutales, Family – Fabaceae, Genus – Prosopis, Species - P glandulosa, Binomial name - Prosopis glandulosa L) [22] is a polymorphic woody legume that occurs on grasslands and rangelands in southwestern USA and occupies over 21 million ha in Texas alone [23]. The rate of increase in honey mesquite cover increased significantly with increase percentage of 2.2% units per year [24]. Redberry Juniper (Kingdom – Plantae, Division – Pinophyta, Class- Pinopsida, Order – Pinales, Family – Cupressaceae, Genus – Juniperus, Species – J pinchotti, Binomial name – Juniperus pinchotti) [25] is a basal sprouting conifer that has several stems arising from the base [26]. Its infestation has also increased by about 60% during the period 1948 to 1982 in a 65 county region in northwest Texas. It has been estimated that by 2000, redberry juniper would have invaded around 4.9 million ha or nearly a third of the 65 county region.

Both mesquite and juniper which have invaded the grasslands have a good heating value. A good heat content coupled with increased availability makes it a renewable energy crop which can be used as fuel for direct combustion or gasification. Harvesting the mesquite and utilizing it as a bioenergy feedstock has the following advantages. There are no planting, cultivation, irrigation and fertilization costs for this naturally occurring species. Also, the dry mass of 10 year old regrown mesquite (mesquite grown after harvest) was found to be 29.4 kg/tree with a typical tree density of 750 trees/ha which in turn gives an annual production of 2.2 tonnes/ha/yr. Mesquite and Juniper occur in warm, dry climate and they can be harvested year round thereby reducing fuel storage costs [23].

2.3.Biomass pyrolysis and kinetics

Different thermo-chemical methods which are used to extract the energy from biomass include pyrolysis, torrefaction, gasification and combustion [16]. Pyrolysis is the process of heating the biomass to temperatures of around 500˚C in an inert atmosphere to produce combustible gases, liquids and char which can be used for combustion applications. The three major components of plant based biomass include hemicellulose, cellulose and lignin. Utilization of biomass for thermal applications needs a proper understanding of the behavior of these components at different temperature conditions. Thermogravimetric studies have been done to extract the kinetic constants activation energy and pre-exponential factor. A number of studies have focused on determining the effect of heating rate on pyrolysis of biomass [27, 28]. Different

methods have been used to determine the kinetic constants to predict the release of volatile matter from biomass. Some of the common methods which are used to determine the reaction kinetics includes Broido- shafizadeh model for the pyrolysis of cellulose [29], Ozawa [30], single reaction conventional Arrhenius [31], independent parallel reactions [32-35], successive reactions [36] and distributed activation energy method [37, 38]. The kinetic parameters have been determined for individual components of biomass materials: hemicellulose [39], cellulose [40], lignin [41, 42] and extractives using the above mentioned methods. A comprehensive review by Di Blasi [43] gives detailed information on studies done on the pyrolysis of biomass including different models for pyrolysis process.

2.4.Biomass torrefaction

The major drawback of biomass to be used in direct combustion applications is its lower heating value, higher moisture content, poor grindability and lower bulk density [44]. Torrefaction is one of the thermochemical pretreatment techniques which has been used to improve the biomass properties with respect to heating value and grindability. Torrefaction is carried out in a temperature range of 200˚C to 300˚C in an inert environment to prevent biomass oxidation. Different gases which are used to maintain an inert environment includes nitrogen [44-46], argon [47] and recently wet torrefaction using hot compressed water was studied to improve the energy density of biomass [48]. Effect of using a small amount of oxygen on torrefaction was studied by Rousset et al. [49] and Wang et al. [50]. Effect of using CO_2 as the pretreatment

medium was studied by Eseltine et al. [51]. Using CO_2 resulted in comparatively higher mass loss at the temperature range commonly used for torrefaction.

Biomass composition influences the effect torrefaction has on the final product. Depending on whether the biomass is of fibrous type and woody type the percentage of lignin, cellulose and hemicellulose which make up the biomass will vary. Woody biomass may be either a hardwood or softwood. The percentage of hemicelluloses in the softwood is lower when compared to that of hardwood [52]. During torrefaction and pyrolysis studies, it was observed that hemicelluose is the component which degrades at a lower temperature range (220-315˚C) followed by cellulose (315-400˚C) and lignin (160-900˚C) [53]. Hence the mass loss percentage will vary for the torrefied samples based on the percentage of hemicelluose in the raw sample for different temperatures used.

Mesquite is a hardwood species while juniper is a softwood as evidenced from their division. Plants which are under Magnoliophyta are angiosperms (hardwood) and Pinophyta (softwood) are gymnosperms [52]. Analysis of hardwood shows increased presence of hemicelluloses when compared to softwood. Under the temperature range considered for torrefaction studies, it was observed that the hemicelluloses degrade first followed by cellulose. Hence a sample with higher amount of hemicellulose would be expected to show increased mass loss with increase in temperature during torrefaction due to breakdown of hemicellulose.

Hydrophilic nature of biomass is related to the presence of OH groups in biomass. Hemicellulose was found to have the highest potential to adsorb water followed

by cellulose and lignin. The reason behind the hydrophobic nature of torrefied biomass can be attributed to reduced amount of hemicelluloses and OH groups in the torrefied biomass during torrefaction [52]. Investigation on the moisture absorption tendency of the torrefied biomass by Acharjee et al. [54] and Medic et al. [55] revealed lower moisture adsorption tendency of the torrefied biomass when compared to the raw biomass.

Effect of temperature on the pyrolysis behavior of cellulose, hemicellulose and lignin were studied before by a number of researchers. Kinetics of pyrolysis of biomass and other fuels are useful for modeling the combustion reactions occurring within a burner. Also such kinetics can also be used to determine the amount of mass loss which occurs during thermal pretreatment processes such as torrefaction. Limited studies have focused on utilizing the kinetics extracted from the pyrolysis of biomass constituents on the modeling of torrefaction. Prins et al. [56] used a two-step reaction mechanism to model the torrefaction of willow in the temperature range of 200 to 300˚C. Repellin et al. [57] used three models to predict the mass loss during the torrefaction process. A simple model based on global weight loss kinetics, Di-blazi Lanzetta two step reaction model and Rousset model to study the torrefaction process.

Carbon dioxide is one of the green-house gases which is being released into the environment during combustion of fossil and renewable sources. Availability of hot gases from boiler exhaust with higher percentage of CO_2 makes it an attractive option to be used as the biomass pretreatment medium. Studies on utilizing CO_2 for the pyrolysis of lignocellulosic biomass between 25-900˚C showed enhanced cracking of released

volatile species resulting in increased concentration of H_2, CH_4 and CO upon using CO_2 compared to N_2 at a heating rates of 10˚C per minute and 500˚C per minute [58]. CO_2 also showed a tendency to mitigate the production of polycyclic aromatic hydrocarbons (PAH) during the pyrolysis of styrene butadiene rubber from 25-1000˚C. Presence of CO_2 as the medium of pyrolysis resulted in increased cracking of benzene derivatives and reduced gas phase addition to form PAH [59]. Limited studies were done on the torrefaction capability of CO_2. Studies done on TGA showed an increased mass loss with increase in pretreatment temperature on using CO_2 when compared to using N_2 as the torrefaction medium [51]. However the factors which might cause such an increased mass loss were not fully understood. Considering the temperature limits for Boudouard reaction, the effect of it under the pretreatment conditions (200˚C-300˚C) should be studied further [60].

2.5.Cofiring biomass with fossil fuels

Cofiring renewable fuels such as biomass along with coal has been studied earlier to reduce the total CO_2 and other harmful emissions from coal combustion. Different biomass materials including wood waste, agricultural residue, residues left after biomass processing, and municipal solid wastes have been tested for co-combustion with coal in small scale facilities as well as in bigger demonstration plants [14, 18, 61-68].

Sami et al. [67] presented a comprehensive overview on the status of cofiring biomass including agricultural and animal wastes with coal. Experience of cofiring

biomass with coal in utilities has been summarized by Tillman [14]. A number of pilot scale and bench scale studies have been done all around the world to understand the feasibility and consequence of cofiring different biomass materials with coal. The use of biomass in cofiring facilities, will also support the development of economy with respect to producing wood products in addition to reducing the emission of harmful pollutants [14]. It has been estimated that around 150 cofiring plants are currently in operation throughout the world with two thirds of it located in Europe [69]. Table 5 summarizes some of the work carried out on bench scale facilities and utilities cofiring biomass with coal.

From all the bench scale and large scale experiments, it was observed that the cofiring of biomass with coal reduces the emission of harmful pollutants such as NOx and SOx due to lower percentage of nitrogen and sulfur in the biomass fuels. In addition to reducing the harmful emissions, biomass also served to reduce the amount of CO_2 emitted into the environment due to its carbon neutrality. Combustion efficiency also improved on using biomass because of the rapid release of volatile matter from the biomass which results in improved combustion.

Table 5. Summary of some of the work carried on cofiring biomass with coal

System description	Fuel type	System capacity	Results	Reference
Grate fired burner	Coal and Wood chip blend; 10-20% wood		cofiring feasible only for 10-20%	[67, 70]
Wall fired dual fuel burner	Coal and sawdust blend	500 kW	Reduction in NOx emission, optimum cofiring percentage = 30%	[67, 71]
Multicirculating fluidized bed	Coal with straw and woodchips	20 MW	Alkali metals in the flue gas did not exhibit a steady output	[67, 72]
Downfired pulverized coal furnace	Coal with hardwood and softwood; 15% biomass in blend	38 kW	Cofiring unstaged decreased the NOx by 17% at 50% cofiring; Significant NOx reduction in staged combustion was not achieved until cofiring ratio was greater than 50%	[67, 73]
T fired boiler	Coal with wood waste; 15% biomass on heat basis	105 MW	Separate injection of biomass	[14]
Cyclone fired boiler	Petroleum coke and coal with urban wood waste; 10% biomass in blend	160 MW_e	Synergistic reduction of NOx	[61]
Wall fired boiler	Coal with wood waste; 10% biomass on heat basis	32 MW_e	Slight decrease in boiler efficiency and NOx.	[14]

Table 5. Continued

System description	Fuel type	System capacity	Results	Reference
Atmospheric Bubbling Fluidized Bed combustion	Lignite with Hazelnut shell and Cotton Residue; 10 - 40% biomass	0.3 MW_t	Hazelnut shell reduces NO, N_2O while cotton residue increases NO and N_2O emission	[65]
Atmospheric Bubbling Fluidized Bed combustion	Lignite with olive residue; 0 - 50% biomass in blend	0.3 MWt	Reduced N_2O and SO_2 emissions with increased combustion efficiency	[66]
Travelling grate boiler	Coal with bagasse, wood chips, sugarcane trash and coconut shell; 20%-60% biomass in blend	18.68 MW	Reduced NOx, SO_2 and suspended particulates.	[68]
Downfired pulverized coal furnace	Coal with Cotton Stalk, Sugarcane bagasse, shea meal and wood; 15% - 50% thermal based biomass blends	20 kW	Reduced NOx with increase in VM/FC in the blend, staging the air, introduction of enriched oxygen air and with NH3 injection through SNCR.	[74]
Circulating fluidized bed boiler	Coal with cotton stalk pellet; 10%-25% biomass in blend	50 MWt	Increased NOx emission with increase in biomass blend due to higher amount of primary air, catalytic effect of ash and higher bed temperature.	[75]
Downfired pulverized coal furnace	Pure russian coal	20 kW	Reduced NOx with reduction in primary burner zone SR and increase in oxygen enrichment with staging. Increased carbon burnouts were observed with enriched air.	[76]

The major drawback of biomass to be used in direct combustion applications is its lower heating value, higher moisture content, poor grindability, hydrophilic nature, lower bulk and energy density [44]. In addition to these factors, the ash constituents of the biomass are also different. Higher percentage of potassium, chlorine and sodium in the biomass ash increases the fouling tendency which will in turn decrease the effective heat transfer in the heat exchangers within the boiler. SCR deactivation was also observed due to the alkali in the biomass ash in a full scale cofired boiler [77]. Torrefaction of biomass is considered to be one of the better options to improve the quality of biomass for cofiring applications.

2.6.Co-firing torrefied biomass with coal

Limited literature are available on cofiring and direct combustion of torrefied biomass on boiler burner facilities and its effects on slagging and fouling on heat exchange tubes. 1n 2003, cofiring of torrefied wood was tested in Netherlands. The torrefied wood was mixed with coal upto 9% on energy basis [78]. Li et al. [79] simulated the effect of cofiring torrefied biomass with coal in a 220 MWe front wall pulverized coal boiler using CFD code. The model showed reduced NOx and CO_2 emissions when torrefied biomass was cofired with coal. Also, it was estimated that only 10% of the boiler load decreased when 100% of the coal was replaced with 100 % of torrefied biomass.

Effect of combustion of torrefied biomass in a downfired burner was studied experimentally and numerically on the flame characteristics by Li et al. [80]. The degree

of torrefaction, particle size, transport air velocity and oxygen concentration were the parameters varied to determine its effect of the flame volume and flame location. NO emissions were predicted numerically. It was found that the larger flame volume and lower NOx emissions will be obtained for lower percentage of oxygen in the incoming air. Also a longer flame will be obtained for lower air velocity with a higher flame lift off distance for the torrefied biomass with larger particle sizes.

2.7.Respiratory quotient (RQ)

Biology literature defines RQ as a ratio of moles of CO_2 produced (or CO_2 eliminated) to stoichiometric oxygen (O_2) moles consumed typically during oxidation reaction e.g. oxidation of nutrients in the body. The RQ factor for fat, protein and carbohydrates the three basic nutrients (Table 6) of the body, are 0.7, 0.8 and 1 respectively [81-84]. Thus with RQ you can determine which nutrient is being oxidized e.g. during exercise, if RQ = 0.7 and 1, you are oxidizing the fat and glucose respectively; when RQ is more than 1.0 it indicates anaerobic reactions (e.g. anaerobic digestion which simply "gasses" the nutrients to produce CO_2 and methane (CH_4) but do not consume O_2). Further RQ can also indicate energy released per liter of CO_2 produced. Note that H/C ratio is similar for glucose, fat and protein.

For human beings, while Sleeping, the basal metabolic rate (BMR) varies from 1.4 to 3.5 W/kg with a mean of 2.4 W/kg and RQ varies from 0.81 (glucose + fat) to 0.98 (glucose). Typically the RQ ratio normally falls between that for fat and glucose and RQ = 0.85 at rest [85].

Table 6. Properties of macronutrients, adapted from [86].

Nutrients	Formulae	M (kg/kmol)	St.O2 (kg/kg)	RQ	HHV (kJ/kg)	HHVO2 (kJ/kg O_2)
Glucose	$C_6H_{12}O_6$	180	1.066	1	15630	14665
Fat	$C_{16}H_{32}O_2$	256	2.869	0.7	39125	13635
Protein	$C_{4.57}H_{9.03}N_{1.27}O_{2.25}S_{0.046}$	119	1.54	0.8	22790	14705
Multiply HHV in kJ/kg by 0.43 to obtain BTU/lb						

It also indicates that the heat values of various nutrients expressed on kJ per kg of O_2 consumed (HHV_{O2}) is approximately constant at about 14000 kJ/kg of O_2. Hence by knowing the O_2 consumption, the amount of energy released in kJ can be estimated. Since about 100 W is required for 100 kg person, then for same O_2 consumed (7.1 mg of O_2 per s), higher RQ implies more release of CO_2 and more CO_2 needs to be removed from blood. It has been found that older people have difficulty in releasing the CO_2 from blood to alveoli in lungs. It also affects transfer of CO_2 from mitochondria (little combustion chamber within a cell). Thus lesser RQ diet is recommended for seniors.

From the review of the material in the literature it was found that no comprehensive experimental study has been done on the effect of cofiring torrefied biomass with coal on emission reductions. The current study focuses on studying the effect of different torrefaction mediums on thermal pretreatment of woody biomass and cofiring torrefied woody biomass with coal on emission reduction and heat transfer characteristics. Also the concept of respiratory quotient will be applied to determine the

global warming potential of these energy sources. In order to accomplish this objective the tasks proposed are outlined in the next section.

3. OBJECTIVES AND TASKS

The overall objective of the current research is to study the effect of cofiring torrefied woody biomass (TB) with sub-bituminous coal in a 30 kW_t downfired furnace and study the potential of the torrefied biomass in reducing emissions. Major focus will be on cofiring mesquite and juniper with coal and obtaining heat transfer and emission (CO, CO_2, NOx) characteristics. In order to achieve the objective the following tasks are proposed.

1. Obtain the raw biomass in processed form from the rangelands of Texas.
2. Obtain ground coal for the combustion studies from utilities.
3. Determine the chemical properties (ultimate and proximate analysis) of raw biomass and coal.
4. Conduct Torrefaction studies including model and experimentation.

   (i). Modify the current gasification facility to perform the torrefaction studies.

   (ii). Study the effect of torrefaction medium nitrogen (N_2) and carbon dioxide (CO_2) and the effect of torrefaction temperatures ranging from 200˚C to 300˚C on the mass loss characteristics of woody biomass.

   (iii). Study the effect of the torrefaction medium on the Brunauer–Emmett–Teller (BET) surface area and grindability of biomass using small scale ball mill.

   (iv). Determine the properties of the torrefied biomass.
5. Obtain kinetic parameters for the raw and torrefied biomass.

(i). Evaluate the mass loss characteristics of the raw and torrefied biomass in a TGA.

(ii) Determine the overall kinetic parameters for the biomass and coal samples using maximum volatile release (MVR) method.

6. Develop a three component model (TCM) to predict the mass loss behavior and heating value increase of biomass during torrefaction process.

7. Cofire biomass with coal in modified 30 kW burner facility.

(i). Modify the 30 kWt downfired burner to cofire solid fuels and study the heat transfer characteristics by mounting three heat exchanger tubes perpendicular to the flow of combustion exhaust gases.

(ii). Blend 10% of the ground raw and torrefied biomass samples with coal for the cofiring studies.

(iii). Study the effect of different biomass and equivalence ratio on the emissions and heat transfer characteristics from 30 kWt downfired burner.

(iv). Determine the emissions during cofiring raw biomass and torrefied biomass with coal using the zero dimensional model.

8. Modify the zero dimensional combustion model for the reburning process to study the combustion behavior in the cofiring process.

9. Respiratory quotient method in combustion applications.

(i). Apply the RQ concept for combustion applications and determine the RQ factor for different fuels.

(ii). Determine the RQ processing for mesquite and juniper biomass.

(iii). Expand the RQ concept to determine the total flue gas volume, burnt fraction and fuel RQ factor from the exhaust gas analysis.

4. METHODS AND EXPERIMENTAL PROCEDURE*

4.1.Three component model (TCM) for torrefaction

For a biomass material composed of hemicellulose, cellulose and lignin represented in a carbon normalized form CH_mO_n, mole balance can be represented as

$$CH_mO_n \rightarrow n_{hemi} * CH_{hh}O_{oh} + n_{cell} * CH_{hcell}O_{ocell} + n_{lig} * CH_{hl}O_{ol} \quad (1)$$

Where m and n stand for the number of hydrogen and oxygen atoms in the carbon normalized fuel. The N and S are considered as trace species. It can be included if more accuracy is desired. From the atom balance and composition of hemicellulose, cellulose and lignin, the percentage of each component in the biomass can be determined. The heating value of the biomass can be represented in terms of the composition of the individual components.

$$HHV_{biomass} = Y_{hemi} * HHV_{hemi} + Y_{cell} * HHV_{cell} + Y_{Lig} * HHV_{Lig} \quad (2)$$

where Y represents the mass fraction of different biomass components on DAF basis. The conversion of each of the biomass component (f_k) and the overall conversion (F) can be given as

*Reproduced in part with permission from Thanapal SS, Chen W, Annamalai K, Carlin N, Ansley RJ, Ranjan D. Carbon Dioxide torrefaction of woody biomass. Energy Fuels 2014; 28:1147–57. Copyright 2014 American Chemical Society.

$$f_k = \frac{m_k - m_{k,Char}}{m_{k,o} - m_{k,Char}} = \frac{Y_k - Y_{k,Char}}{Y_{k,o} - Y_{k,Char}} = \frac{\text{mass of k that could still be devolatilized}}{\text{Max mass of k that could be devolatilized}} \quad (3)$$

k = hemicellulose, cellulose and lignin.

$$F = \frac{m}{m_0} = \frac{\sum m_k}{m_0} = \left\{ f_k \left(Y_{k,o} - Y_{k,Char} \right) + Y_{k,Char} \right\} = \frac{\text{total mass left over}}{\text{Initial total mass}} \quad (4)$$

Where $Y_k = m_k/m_o$: m_0 is the initial mass of the component, m_k is the mass of the component after time t and m is the sum of all three components. $Y_{k,char}$ represents the mass fraction of k remaining in char at end of pyrolysis. The energy content ratio of the biomass after being heat treated for some time period can be determined from the remaining mass of the treated sample and heating value of individual components (see Eq. (2)).

Assuming first order pyrolysis, decomposition of each of the biomass component can be determined using the following expression

$$-\frac{dm_k}{dt} = B_k m_k \exp\left(\frac{-E_k}{\bar{R}T} \right), \text{k=Hemicellulose,Cellulose,Lignin} \quad (5)$$

Where m_k is the mass remaining in each of the components in sample (kg) which can be devolatilized. $m_k = (m_{k,0}-m_{k,char})-m_{k,lib}$. Amount of char ($m_{k,char}$) in each of the components was obtained from the pyrolysis data available elsewhere [53].

$$\frac{dm_{k,lib}}{dt} = B_k \left(m_{k,0} - \mathrm{m_{k,char}} - \mathrm{m_{k,lib}} \right) \exp\left(\frac{-E_k}{\bar{R}T} \right) \tag{6}$$

The above expression can be further simplified to

$$\frac{d\alpha_k}{dt} = B_k \left(1 - \alpha_k\right) \exp\left(\frac{-E_k}{\bar{R}T} \right) \tag{7a}$$

$$\frac{d\alpha_k}{dT} = \left(\frac{B_k}{\beta} \right) \left(1 - \alpha_k\right) \exp\left(\frac{-E_k}{\bar{R}T} \right) \tag{7b}$$

Where α represents the liberated fraction,

$$\alpha_k = \frac{m_{k,lib}}{m_{k,o} - m_{k,Char}} = \frac{\text{amount liberated}}{\text{maximum that could be liberated}} = \frac{m_{k,o} - m_k}{m_{k,o} - m_{k,Char}} = \frac{Y_{k,o} - Y_k}{Y_{k,o} - Y_{k,Char}} \tag{8}$$

When the sample is heated at a constant heating rate β, Eq. (7) reduces to

$$f_k = \left(1 - \alpha_k\right) = \exp\left[-\left(\frac{B_k}{\beta} \frac{E_k}{\bar{R}} \right) \cdot \left\{ \frac{\mathrm{E_2}\left(X_k\right)}{X_k} - \frac{\mathrm{E_2}\left(X_{k,0}\right)}{X_{k,0}} \right\} \right] \tag{9}$$

Where β=dT/dt [31]. Once the torrefaction temperature T_{torr} is reached the sample is maintained at T_{torr}, a constant value for a given residence time. From Eq. (7),

the mass loss during the isothermal torrefaction period for each of the component can be determined.

$$f_k = f_{k,TTorr} \exp\left\{-B_k \exp\left(\frac{-E_k}{\bar{R}T_{torr}}\right)(t - t_{start,fixed\,T})\right\} \quad (10)$$

Where B_k is the pre-exponential rate constant, E_k the activation energy for the kth component and R is the universal gas constant. Eq. (1) to Eq. (10) can be used to track hemicellulose, cellulose and lignin contents, heat values and total mass loss rate as a function of time or temperature (See Section 5).

4.2.Torrefaction

Fig. 4 shows the schematic of the batch type facility used for the current study. Well insulated batch type reactor which can pretreat around 500g sample per batch was used for the current study. A batch of sample (4) was first loaded into the reactor. Reactor was then closed with an assembly of auger (5) and bidirectional motor (6) in place to mix the samples and maintain the desired pretreatment temperature within the reactor. N_2/CO_2 was used to purge the reactor depending on the medium used for torrefaction. A constant flow of 30 SCFH (0.85 m^3/hr) of N_2/CO_2 was set using variable area mass flow controller (1) to maintain an inert/non reacting environment during the pretreatment period. A 1.8 kW band type electrical heater (3) was then turned on to heat the samples at a rate of 20˚C per minute. Two k-type thermocouples (2) connected to the

electrical heater were used to monitor the temperature and control the supply of power to the heaters. The samples were heated from room temperature to the desired temperature and kept constant at that temperature for 30 minutes. Residence time of 30 minutes was chosen based on the results from Arias et al. [45] and Sadaka and Negi [87] wherein it was observed higher residence times (more than 30 minutes) have minor effect on mass loss behavior. An auger coupled to the bidirectional motor was used to maintain a uniform temperature throughout the batch during the pretreatment period. A slightly negative pressure was maintained within the reactor by means of a vacuum fan (10) to remove the gases produced during torrefaction as well as the medium used for torrefaction. A shell and tube heat exchanger type condenser (7) was used to condense out any condensables from the gases produced during torrefaction. Since some of the condensables were condensed along the pathway, an accurate quantification of the condensables was not made. However a change in color of the condensables from light yellow to dark viscous liquid was observed with increase in pretreatment temperature. A small amount of the gases were filtered using inline filters (8) and their composition was analyzed using a Thermo Scientific Prolab mass spectrometer (9). The torrefaction medium had the highest concentration of the different species measured. The mass spectrometer was calibrated with gas mixtures of known composition to get accurate measurements [60].

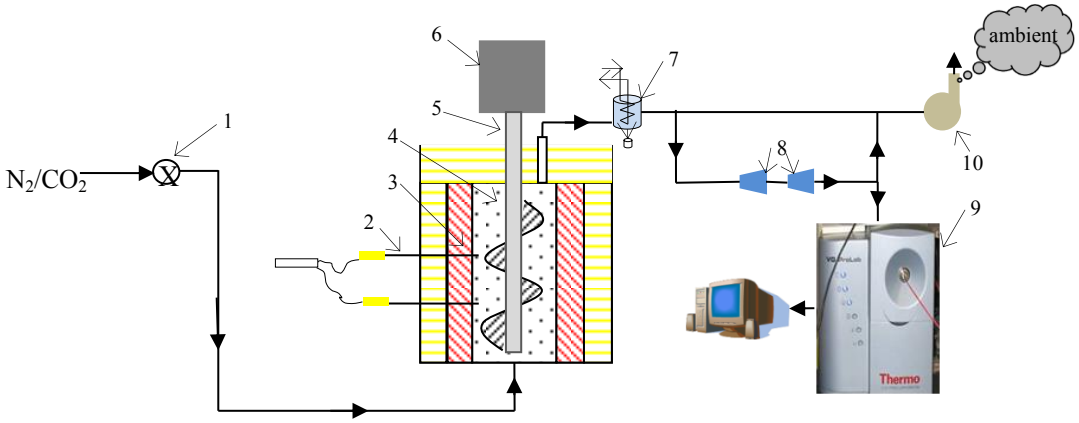

Fig. 4. Schematic of the batch torrefaction facility. 1) Flow controller, 2)Thermocouples, 3) Band heater, 4) Biomass, 5) Auger, 6) Bidirectional motor, 7)Condenser, 8) Line filters, 9)Mass spectrometer, 10) Exhaust fan, adapted from [60].

4.3.Grindability studies

In order to study for the grindability of torrefied samples, all the samples were ground for a constant time period of 20 minutes in a Sweco DM1vibro energy grinding mill (Fig. 5). This procedure was followed to have a constant power input for the mill to grind all the samples. The particle size distribution was obtained using Ro-tap testing sieve shaker with US standard sieves of numbers 8, 10, 20, 30, 100, 200 and 270 (these sieve numbers represent the following sizes: 2.4 mm, 2.2 mm, 1.42 mm, 715 microns, 370 microns, 112.5 microns and 64 microns respectively). The variation in particle size distribution with increase in torrefaction temperature was studied for both mesquite and juniper samples.

Fig. 5. Sweco DM1 vibro energy grinding mill used for the grindability studies.

4.4.TGA-DTG studies

Thermogravimetric analysis (TGA) of the raw samples and torrefied samples was carried out using TA instruments SDT-Q600. 10 mg of sample was loaded into the sample pan (Fig. 6) and 100 ml/min of nitrogen was used to maintain an inert environment during the TGA study. The samples were heated at a constant rate of 20˚C per minute from room temperature till 900˚C to study the sample behavior during pyrolysis. Simultaneous measurements of weight loss in the sample pan and temperature difference between sample and reference pan were made to get the TGA and differential thermal analysis (DTA) trace. 100 ml/min of air was used for the oxidation studies of the

raw samples and the torrefied samples in the TGA unit. Results obtained with air and N_2 was used to identify the ignition temperature.

The weight loss measurements made at different temperatures can then be used to determine the differential thermograms (DTG; dW/dT expressed in (% weight/˚C)) of the samples. The DTG traces obtained from the biomass pyrolysis curves can also be used to estimate the amount of the three components in the biomass. The three components in the biomass exhibit different pyrolysis behavior. Hemicellulose is the component which degrades first at lower temperatures of around 220-315˚C as mentioned earlier in the literature review section. Hence a biomass which has higher percentage of hemicellulose will exhibit a hump at lower temperatures of around 200-300˚C during pyrolysis process which indicates the degradation of hemicellulose. Similar observations were made by studies on biomass samples by Chen et al. [88], Biagini et al. [27], and Chen et al. [89].

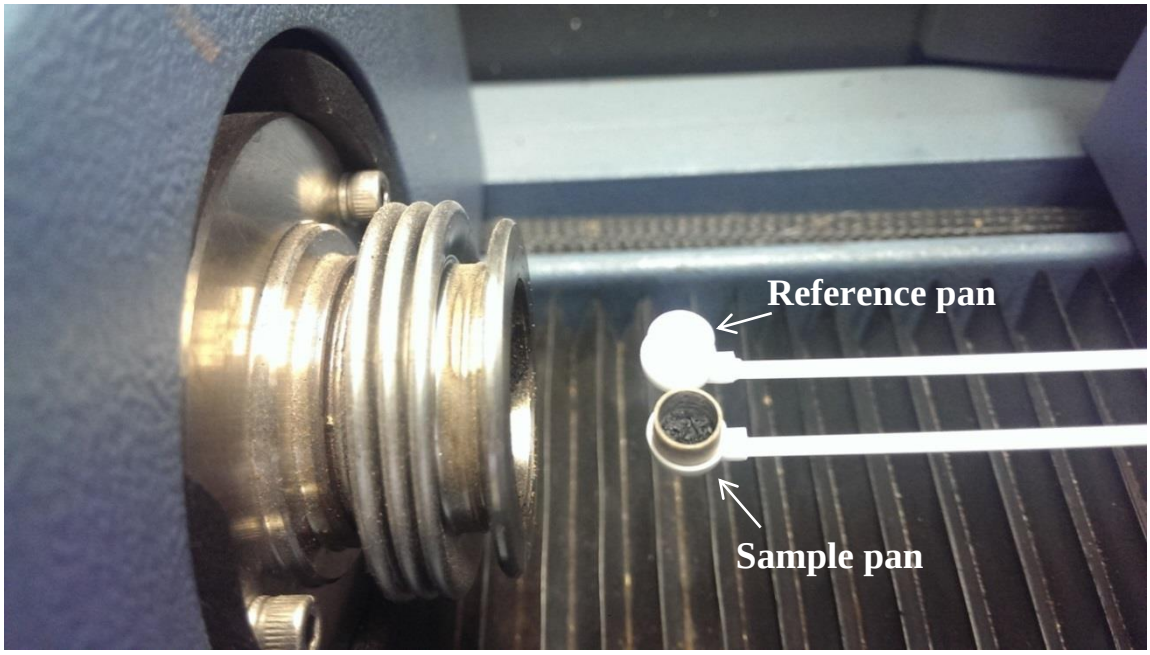

Fig. 6. Sample pan and reference pan assembly in the TGA.

TGA unit was also used to study the torrefaction of woody biomass. Torrefaction studies on the raw samples were performed using N_2 and CO_2. 10 mg of biomass sample was used for this study. The biomass was heated at a constant rate of 20˚C per minute from room temperature to desired torrefaction temperature (200-300˚C) and the temperature was maintained at the torrefaction temperature for a specified time period which can be between 15 minutes and 2 hours. After the isothermal stage, the samples were heated again up to 900˚C at a heating rate of 20˚C per minute. Different torrefaction mediums studied were N_2 and CO_2. Further details on the procedure for the torrefaction using TGA unit is available elsewhere [51].

Table 7 shows the comparison between the different units in Coal and biomass energy lab which can be used for the pyrolysis and torrefaction studies.

Table 7. Experimental units in Coal and Biomass lab to study sample pyrolysis and torrefaction.

	TGA-DTA	**Muffle furnace**	**Batch torrefaction reactor**
Sample mass	10 mg	5 g	500 g
Tmax	1500˚C	1200˚C	300˚C
dT/dt	0.1 to 100˚C per minute	40˚C per minute	20˚C per minute (estimated)
particle size	500-800 μm	all sizes	2-6 mm
medium flow rate	100 ml/min	9.44 l/min	9.44 l/min

4.5.Maximum volatile release (MVR) method

The mass loss data obtained from the TGA studies was used to extract the kinetics for the raw and torrefied samples. The kinetic constants for the three components in the biomass can also be determined using MVR method from the pyrolysis data of individual components. MVR method is based on single reaction model in which it is assumed that the heating of samples releases only volatile matter under an overall activation energy unlike parallel reaction model in which the volatiles are released over a range of activation energies [37]. Hence the overall activation energy and the pre-exponential factor for the pyrolysis process can be determined from the MVR technique. From Eq. (7), for the case of biomass which includes all the components, it can be seen that liberation rate ≈ 0 at low temperatures. At low temperatures, $E/RT \rightarrow \infty$ and thus $\exp(-E/RT) \rightarrow 0$. At high temperatures, there would not be any volatile matter left in the sample which makes the liberation rate $\rightarrow 0$. Hence, volatile release rate shows a maximum at a particular maximum temperature (T_{max}). Considering Eq. (7), the maximum volatile release rate of volatiles and corresponding temperature T_{max} can also be determined by differentiating Eq. (7) and setting to 0.

$$\frac{d^2\alpha}{dT^2} = -\frac{d^2F}{dT^2} = \frac{B}{\beta}(1-\alpha)\frac{d}{dT}\left\{\exp\left(\frac{-E}{\bar{R}T}\right)\right\} - \frac{B}{\beta}\frac{d\alpha}{dT}\left\{\exp\left(\frac{-E}{\bar{R}T}\right)\right\} = 0 \tag{11}$$

Upon simplification of Eq. (11)

$$B = \left(\frac{E \cdot \beta}{\bar{R} \cdot T_{\max}^{\ 2}}\right) \cdot \exp\left(\frac{E}{\bar{R} \cdot T_{\max}}\right) \tag{12}$$

From Eq. (7) and Eq. (12),

$$\left(\frac{d\alpha}{dT}\right)_{\max} = -\left(\frac{dF}{dT}\right)_{\max} = \frac{E}{R \cdot T_{\max}^{\ 2}} \exp\left[-\left(\frac{BE}{R^2 \cdot T_{\max}^{\ 2}}\right)\left(\frac{E_2(X_0)}{X_0} - \frac{E_2(X_{\max})}{X_{\max}}\right)\right] \tag{13}$$

If the experimental data on T_{max} and $(d\alpha/dT)_{max}$ are available, then the two unknowns: activation energy (E) and pre-exponential factor (B) can be solved from two equations Eq. (12) and Eq. (13). Eq. (11) to Eq. (13) assume that the reaction to be of single order.

If order of pyrolysis is equal to "n" then the unknowns can also be estimated from the MVR method. Modifying Eq. (5) for a reaction of order n for biomass pyrolysis,

$$B = -\left(\frac{\beta}{F^n}\right) \exp\left(\frac{E}{RT_{max}}\right)\left(\frac{dF}{dT}\right)_{max} \quad (14)$$

Hence, at the point of maximum volatile release (refer to Appendix A),

$$n = -\frac{\left\{F_{v,\,max}\left(\frac{E}{RT_{max}^2}\right)\right\}}{\left|\left(\frac{dF_v}{dT}\right)_{max}\right|} \quad (15)$$

Eq. (15) can be used to determine the order of volatile release during the pyrolysis of samples.

4.6.Zero dimensional model for cofiring biomass with coal

Combustion of solid fuels within a steam generator equipped with swirl vanes results in the development of three dimensional time dependent precessing vortex core structures which are instable [90]. Modeling such instabilities to predict the behavior of the fuels and combustion reactions are difficult. A simple zero-dimensional model which takes into account the recirculation zones developed within the burner was used to model the combustion of fuels. Similar simplified one dimensional chemical reaction model was used by He et al. [91] to model the effect of high temperature air on NOx reduction.

A simple schematic of the model is shown in Fig. 7. As the stream of coal and biomass is injected (Stream I, Fig. 7) into the burner, the model takes into account the

different sizes of the fuel from the fuel size data and tracks the change in mass of each size fraction along the burner on a Lagrangian frame of reference.

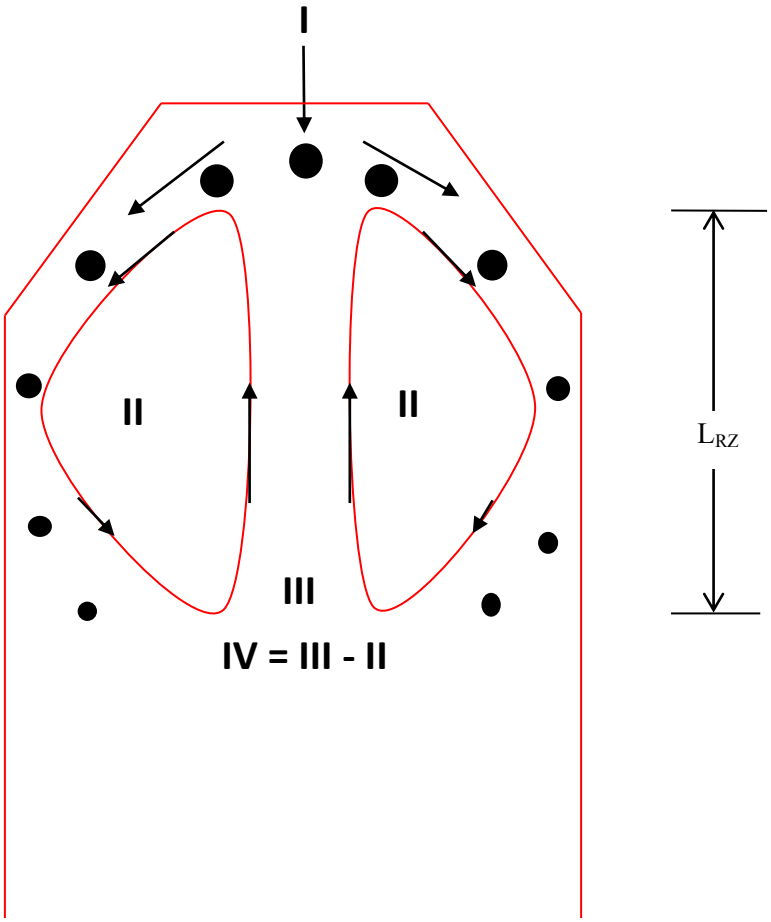

Fig. 7. Schematic of the zero dimensional combustion model.

The mass of the particle, the gases produced, temperature of the particle and gas are tracked at each time step. The residence time of the gas within the burner was determined to be 0.85 seconds using the temperature data obtained from the experiments

and ideal gas assumption [92]. The amount of fuel and air entering the burner is determined according the burner rating which is 30 kW for the current study and the equivalence ratio (ER) used.

The secondary air enters the burner through a swirler which swirls the air resulting in a generation of recirculation zone caused due to the swirl and presence of a quarl in the burner. The length of the recirculation zone (L_{RZ}, Fig. 7) and the amount of gases recirculated (stream II, Fig. 7) are determined using the experimental data provided by Lawn [93] and Syred and Beer [94]. Recirculated gases with no unburnt particles are assumed to have the same composition for all equivalence ratios (69.2% N_2, 10.9% CO_2, 10.7% H_2O, 9.2% O_2 and negligible percentages of other gas species). The composition of the recirculated gas was estimated from the gas composition at the end point of the recirculation zone. The particle seizes to see the recirculated gases at a gas residence time of 205 milli seconds from the point of fuel entry into the burner. The particles entering the burner are heated by the hot recirculating gases and hot walls of the burner though radiation and convection. The energy transfer is assumed to occur in a quasi-steady state. The hot recirculating gases are assumed to mix exponentially and isenthalpically with the incoming air and fuel particles. The energy balance and heat transfer equations used in determining the temperature of the different size fractions are available elsewhere [92]. The temperature at each time step is determined using explicit method. The model used for reburning solid fuels was modified to study the co-combustion of biomass with coal. Global reaction kinetics were used for modelling the homogenous and heterogeneous reactions occurring within the burner.

As soon as the coal and biomass mixture enters the burner, the volatiles are released and the reactions are diffusion limited. The gases released from the particle are assumed to mix with the free stream instantaneously at each temporal time step (0.000017 s). The pyrolysis of the fuel is assumed to occur according to first order single reaction scheme. The kinetic constants for pyrolysis process for coal and biomass were obtained from literature. All chemical reactions are described using simplified kinetics (Table 8 and Table 9). The global homogenous reactions which are considered and their corresponding kinetics are tabulated in Table 8. $\dot{w}_i$ is the reaction rate of species i, R is the universal gas constant (8.314 kJ/kmol K), T_g is the gas temperature, T_p is the particle temperature, Xi is the mole fraction of the gas species i, Yi is the mass fraction of gas species, p is the pressure within the burner, ρ_g is the gas density, [i] represent the molal concentration of gas species 'i' in kmol/m^3 and m_p and m_N represent the mass of the particle and nitrogen in the particle respectively. Seven heterogeneous reactions were used to model the reaction of the gases with the fixed carbon and nitrogen in the char. The heterogeneous reactions which are taken into account in the model are presented in Table 9.

Table 8. Global homogenous reactions used in the zero dimensional model.

S.no	Reaction	Reaction rate (kmol/ m^3 s)	Reference
1	$NH_3 + O_2 \rightarrow NO + H_2O + 0.5\ H_2$	$\dot{w}_{NH_3} = \frac{-3.48*10^{20} * \exp\left(\frac{-418400}{RT_g}\right) * X_{NH_3} * X_{O_2}}{\left(1+\left(6.9*10^{-6} * \exp\left(\frac{175728}{RT_g}\right) * X_{O_2}\right)\right) * \frac{p}{1000*RT_g}}$	[95]
2	$NH_3+NO \rightarrow N_2+H_2O+0.5*H_2$	$\dot{w}_{NH_3} = -6.22*10^{14} * \exp\left(\frac{-230120}{RT_g}\right) * X_{NH_3} * X_{NO} * \frac{p}{1000*RT_g}$	[95]
3	$HCN+O_2 \rightarrow NO+CO+0.5H_2$	$\dot{w}_{NH_3} = -10^{11} * X_{HCN} * X_{O_2}^{b} * \frac{p}{RT_g} * \exp\left(\frac{-33700}{T_g}\right)$ $b = \begin{cases} 0; if\ \ln X_{O_2} > -3 \\ 2.33 * \exp\left(\frac{28}{0.5+\ln X_{O_2}}\right); if\ -5.67 < \ln X_{O_2} < -3 \\ 1; if\ \ln X_{O_2} < -5.67 \end{cases}$	[91]
4	$HCN+NO \rightarrow N_2+CO+0.5*H_2$	$\dot{w}_{NH_3} = -3*10^{12} * X_{HCN} * X_{NO} * \frac{p}{RT_g} * \exp\left(\frac{-30200}{T_g}\right)$	[91]
5	$CO + 0.5\ O_2 \rightarrow CO_2$	$\dot{w}_{CO} = -1.3*10^{17} * [CO][O_2]^{0.5}[H_2O]^{0.5} * \exp\left(\frac{-125580}{RT_g}\right)$	[96]
6	$H_2+0.5O_2 \rightarrow H_2O$	$\dot{w}_{H_2} = -0.68*10^{29} * \left(\frac{Y_{H_2}}{2}\right)^{0.25} * \left(\frac{Y_{O_2}}{32}\right)^{1.5} * \rho_g^{1.75} * \exp\left(\frac{-20130}{RT_g}\right)$	[97]
7	$CH_4+2O_2 \rightarrow CO_2+2H_2O$	$\dot{w}_{CH_4} = -5.74*10^{10} * [CH_4]^{-0.5}[O_2]^{1.5} * \exp\left(\frac{-60000}{RT_g}\right)$	[98]

Table 9. Heterogeneous reactions used in the model.

S.No	Reaction	Reaction rate (m/s)	Reference
8	$C+O_2 \rightarrow CO_2$	$\dot{w}_{C,1} = 1.6*10^5 * \exp\left(\frac{-20000}{T_p}\right)$	[99]
9	$C+0.5O_2 \rightarrow CO$	$\dot{w}_{C,2} = 1.22*T_p * \exp\left(\frac{-10300}{T_p}\right)$	[100]
10	$C+CO_2 \rightarrow 2CO$	$\dot{w}_{C,3} = 3.42*T_p * \exp\left(\frac{-15600}{T_p}\right)$	[100]
11	$C+H_2O \rightarrow CO+H_2$	$\dot{w}_{C,4} = 1.67*\dot{w}_{C,3}$	[101]
12	$C + 2H_2 \rightarrow CH_4$	$\dot{w}_{C,5} = 10^{-3} * \dot{w}_{C,3}$	[100]
13	$C+NO \rightarrow CO+0.5N_2$	$\dot{w}_{C,6} = 1.57*10^5 * \exp\left(\frac{-17100}{T_p}\right)$	[95]
14	$N+0.5O_2 \rightarrow NO$	$\dot{w}_N = \dot{w}_{C,13} * \frac{m_N}{m_p}$	[95]

4.7.Cofiring torrefied biomass with coal

A 29 kWt (100,000 BTU/h) facility was used to study the effect of cofiring torrefied biomass with coal and fouling on heat exchanger tubes. The schematic of the facility used for the cofiring study is shown in Fig. 8. The fuel nozzle for cofiring experiments consist of two concentric tubes with the fuel carried by the primary air flowing through the central tube and the secondary air swirled by vanes welded to the outer surface of the central tube flowing through the outer tube. The angle of the vanes

which was used for swirling the air was 45˚ which resulted in a swirl number of 0.7. The formula to determine the swirl number is available elsewhere [93]. The burner section consisted of a 6 in (15.24 cm) diameter, 84 in (213.36 cm) long vertically down-fired combustor with a quarl at the top of the burner to aid the formation of recirculation zone. The combustor was made with a steel frame containing a 2 inch layer of insulation and a 2 inch section of refractory. In the cofiring mode, the coal or blended fuel was fired with primary air (about 100 SLPM) and secondary air was given a swirl motion. Along the walls of the boiler burner were temperature measurement ports at spaced intervals of 6 in (15.24 cm) below the burner nozzle. The gas stream was cooled down by a jet of water in the quenching area. The exhaust gas was vented out through an exhaust system.

Three single-pass heat exchanger (HEX) tubes were mounted in the boiler. The dimensions of HEX tubes were 2.7 cm (1.06 in) O.D., 2.1 cm (0.83 in) I.D. and 15.24 cm (6 in) long. Three HEX tubes whose surfaces were clean and dry were laid perpendicular to the downward flow of hot flue gases. The HEX tubes were located below the main burner nozzle at three locations : between 30 in (76.2 cm) and 36 in (91.44 cm), between 54 in (137.16 cm) and 60 in (152.44 cm), and between 66 in (167.64 cm) and 72 in (182.88 cm), respectively [8].

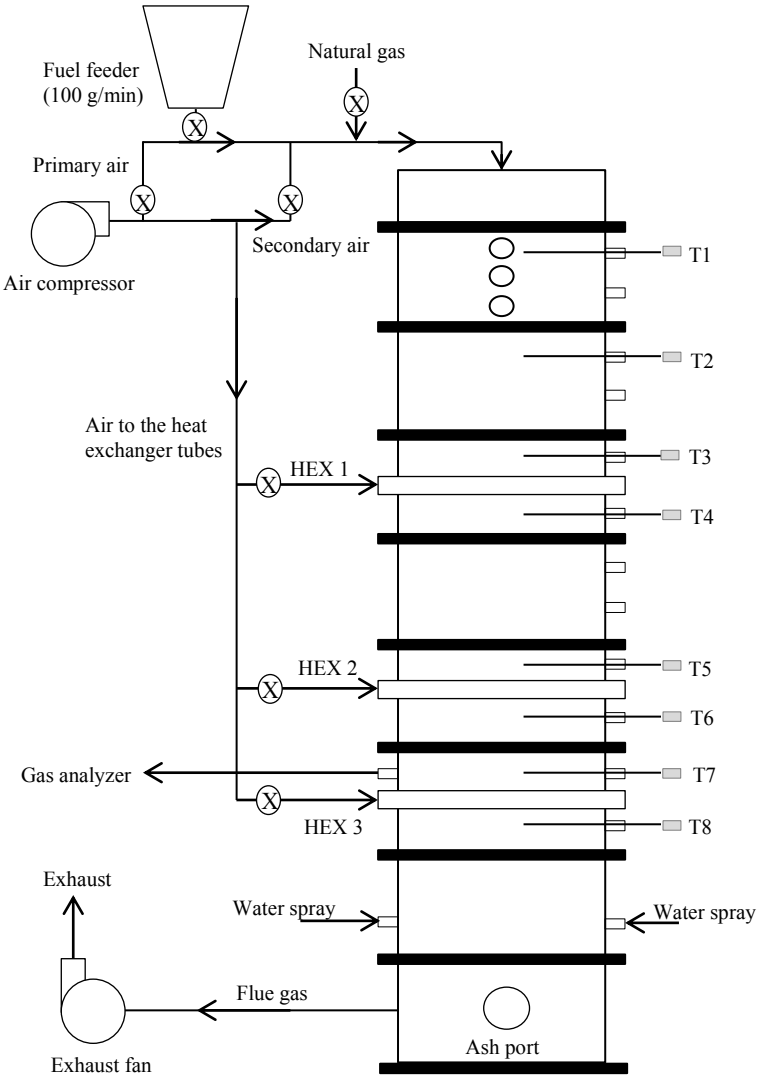

Fig. 8. Schematic of the 30 kW downfired burner at Texas A&M University; HEX: Heat exchangers; T: Thermocouples.

A typical cofiring experiment was started by preheating the burner to 1200˚C using natural gas. Once the temperature inside the burner reached the desired range, flow of natural gas was stopped and experiments were carried out for pure coal, coal and biomass blends which included raw mesquite, raw juniper, torrefied mesquite and

torrefied juniper. For the case of biomass blends, 10% of ground biomass was blended with coal on a mass basis. All the experiments were carried out for a constant thermal output of 30 kW by adjusting the fuel flow rate. Temperature profiles within the burner facility and the temperature of air entering and leaving the HEX tubes were acquired using a data (temperature) acquisition system. The gas composition at the burner exit was measured using E-instruments E8500 electrochemical gas analyzer. Gas analyzer was calibrated to ensure accurate measurements of the flue gases. Equivalence ratio (ER) is defined as the ratio of the stoichiometric amount of air needed for complete combustion of fuel to the actual air supplied for the combustion studies (Eq. (16)) [102].

$$\text{Equivalence ratio (ER)} = \phi = \frac{\left(\frac{A}{F}\right)_{stoich}}{\left(\frac{A}{F}\right)_{actual}} \tag{16}$$

where (A/F) stand for air fuel ratio. It should be noted that the ER is the inverse of the stoichiometric ratio which is commonly used in Europe. Hence ER less than one will indicate lean combustion and fuel rich combustion will have an ER greater than unity. Combustion experiments were carried out for 90 minutes in the lean region (ER between 0.85 and 0.95) which will be representative of conditions used in commercial power generation facilities. The results thus presented are transient and is not representative of steady state conditions within the burner as reaching steady state takes a long time.

Limited studies were done using raw biomass due to difficulty in size reduction caused because of its fibrous nature.

The heat transfer from the hot flue gases to the air which was used as the heat transfer fluid can be determined using Eq. (17). Eq. (18) was used to calculate the log mean temperature difference from the measured temperature data.

$$\dot{Q} = UA\Delta T_{LMTD} \tag{17}$$

$$\Delta T_{LMTD} = F\frac{\Delta T_1 - \Delta T_2}{\ln\left(\frac{\Delta T_1}{\Delta T_2}\right)} \tag{18}$$

$$\Delta T_1 = T_{h,i} - T_{c,e} \tag{19}$$

$$\Delta T_2 = T_{h,e} - T_{c,i} \tag{20}$$

where $T_{h,i}$, $T_{h,e}$, $T_{c,i}$ and $T_{c,e}$ represent the temperature of the hot flue gas above the HEX tube, below the HEX, temperature of the cold air entering the HEX and leaving the HEX respectively. Since there was negligible change in the temperature of the hot flue gas transferring the heat to the HEX fluid, the value of F was obtained to be unity for present study [103]. The overall heat transfer coefficient was determined using Eq. (21).

$$U = \frac{\dot{m}_{air} c_{p,air} \left(T_e - T_i\right)_{air}}{A \Delta T_{LMTD}} \quad (21)$$

where m_{air} is the mass flow of air within the HEX, $c_{p,air}$ is the specific heat of air, A is the surface area of the HEX, T_e and T_i are the exit and inlet temperature of air into the HEX. OHTC determined using Eq. (21) includes the different resistances to transfer of heat to the fluid within the HEX.

4.7.1. Measurement and accuracy

Dwyer Flow meters which were used to monitor the flow of air for the combustion experiments had an accuracy of 1.5% the full scale value. Dwyer variable area flow meters used to regulate the flow of the torrefaction medium for the torrefaction experiments and for the heat transfer studies within the burner had an accuracy of 3% the full scale reading of the respective flow controllers. K type thermocouples used to measure the temperature along the axis of the burner and the heat exchanger inlet and exit had an accuracy of 0.75% whenever the temperature measured is greater than 2.2˚C.

Table 10 and Table 11 show the resolution and accuracy of the different gases which are analyzed using E8500 electrochemical gas analyzer.

Table 10. Resolution and accuracy of electrochemical emission sensor, adapted from [104].

Sensor		**Range**	**Resolution**	**Accuracy**
Carbon Monoxide (CO)	Low range	0-8000 ppm	1 ppm	<300ppm, 10ppm to 8000 ppm, 4%
Carbon Monoxide (CO)	Dilution Auto-Range	4000-20000 ppm	1 ppm	>2000ppm, 10%
Nitric Oxide (NO)	Std. Range	0-4000 ppm	1 ppm	<100 ppm, 5 ppm to 4000 ppm, 4%
Nitrogen Dioxide (NO_2)	Std. Range	0-1000 ppm	1 ppm	<100 ppm, 5 ppm to 1000 ppm, 4%
Sulfur Dioxide (SO_2)	Std. Range	0-4000 ppm	1 ppm	<100 ppm, 5 ppm to 4000 ppm, 4%
Hydrogen Sulphide (H_2S)	Std. Range	0-500 ppm	1 ppm	<100 ppm, 5 ppm to 500 ppm, 4%
Oxygen (O_2)	Std. Range	0-25%	0.1%	0.1% Vol.

Table 11. Resolution and accuracy of Non-dispersive infrared (NDIR) sensors, adapted from [104].

Sensor	**Range**	**Resolution**	**Accuracy**
Hydrocarbons (C_xH_y)	0-0.40 %	0.01%	3% of Rdg + 0.01%
	0.40 - 1.00 %		5% of Rdg
	1.00% - 3.00 %		8% of Rdg
Carbon Monoxide (CO)	High Range	0.01%	
	0% - 10.00 %		0.02% or 3% Rdg
	10.01% - 15%		5% of Rdg
Carbon Dioxide (CO_2)	0.0% - 16.0%	0.10%	0.3% or 3% Rdg
	16.0% - 20.0%		5% of Rdg

The uncertainty in experimental results was determined using the method outlined by Kline and McClintock. [105].

4.8.Respiratory quotient and its applications

Biomass and other renewable fuels are considered to be carbon neutral. Typically, the amount of carbon dioxide released due to the combustion of renewable

fuels is not accounted for in carbon footprint. However this approach has been challenged by many studies. Land use change, energy conversion efficiency and productivity of forest land impacts the decision on carbon neutrality of biomass based fuels [106]. The Carbon emitted during the combustion of fossil fuels is automatically accounted into the carbon footprint. Irrespective of whether the fuel is renewable or non-renewable, each fuel has its own share to the global warming due to anthropogenic activities.

For fixed power generation in MW for engineering systems, heat input in MW is fixed and O_2 consumption is fixed for most fuels. Hence fuels with higher RQ ratio emit more CO_2 for same power output since RQ is defined as the ratio of moles of CO_2 produced to stoichiometric O_2 moles consumed. RQ factor enables the estimation of global warming potential (GWP) of different fuels and even for new fuels brought into the market for combustion applications. RQ factor of the new fuel can be compared to the conventional fossil fuels in order to determine its emission potential.

Two methods for estimating the RQ factor for different fuels are presented in the current dissertation: i). using standard formulas from combustion literature for known fuel composition and ii) using the exhaust gas analyses for unknown fuels (e.g. metabolism in human body).

4.8.1. Higher heating values based on stoichiometric oxygen

Ultimate and proximate analyses can be used to determine the chemical composition of fuels. Different correlations have been developed to estimate the heating

value of a fuel from its chemical composition. The gross or higher heating values for coals can be empirically obtained by using the Dulong equation (Eq. (22)) [102].

$$HHV(kJ/kg) = 33800*Y_C + 144153*Y_H - 18019*Y_O + 9412*Y_S \quad (22)$$

where Y_C, Y_H, Y_O and Y_S are mass fractions of carbon (C), hydrogen (H), oxygen (O) and sulphur (S) respectively. Another relation (Eq. (23)) derived by Mott and Spooner [107] for estimating the heating value is :

$$\begin{aligned} HHV(\text{kJ/dry kg}) &= 33610*Y_C + 141830*Y_H + 9420*Y_S - 14510*Y_O(organic), \text{when O} < 15\% \\ HHV(\text{kJ/dry kg}) &= 33610*Y_C + 141830*Y_H + 9420*Y_S - \left(15320 - 7200*\frac{Y_O}{(100-Y_A)}\right)*Y_O, \text{when O} > 15\% \end{aligned} \quad (23)$$

Channiwala and Parikh. [108] studied a number of different fuels including biomass and fitted the following equation to the data:

$$HHV(\text{kJ/dry kg}) = 34910*Y_C + 117830*Y_H - 10340*Y_O - 2110*Y_A + 10050*Y_S - 1510*Y_N \quad (24)$$

where Y_C, Y_H, Y_O, Y_A, Y_S and Y_N represents dry mass fractions of C, H, O, Ash, S and nitrogen (N) respectively. The heating value predicted by the above correlation had an error of about 1.5% when compared to that of measured heating values [108]. Boie empirical equation for estimating the HHV of any fuel $C_CH_HN_NO_OS_S$ is given in Eq. (25) [102].

$$HHV(kJ/kmol) = 422272*C + 117387*H - 155371*O + 100480*N + 335508*S \qquad (25)$$

where C, H, O, N and S are the number of carbon, hydrogen, oxygen, nitrogen and sulphur atoms respectively in the fuel. Channiwala [108] and Sheng et al. [109] studied the accuracy of these correlations in estimating the heating values of different fuels and biomass fuels respectively. These correlations can be applied to study the variation of fuel HHV with respect to fuel chemical composition. The HHV predicted by Boie equation had a minimum deviation from the measured HHV for both the biomass fuels and fossil fuels [109, 110]. For a fuel with given number of C, H, N, O, S atoms for carbon, hydrogen, nitrogen, oxygen and sulphur, one can estimate the heating values and the stoichiometric amount of oxygen (ν_{O_2} kg/kg of fuel) needed for complete combustion using standard atom balance [102]. The formula to determine the stoichiometric amount of oxygen is given below.

$$\nu_{O_2}(\text{kg of oxygen/kg of fuel}) = \frac{32*\left(C + \frac{H}{4} - \frac{O}{2} + S\right)}{M_{fuel}} = \frac{32*C*\left(1 + \frac{H}{4C} - \frac{O}{2C} + \frac{S}{C}\right)}{M_{fuel}} \qquad (26)$$

Based on the Boie equation, heating value per unit stoichiometric oxygen can be determined using Eq. (27).

$$HHV_{O_2} = \frac{HHV}{\nu_{O_2}} = \frac{\left\{422272 + 117387 * \left(\frac{H}{C}\right) - 155371 * \left(\frac{O}{C}\right) + 100480 * \left(\frac{N}{C}\right) + 335508 * \left(\frac{S}{C}\right)\right\}}{\left[32 * \left\{1 + \left(\frac{H}{4C}\right) - \left(\frac{O}{2C}\right) + \left(\frac{S}{C}\right)\right\}\right]} \quad (27)$$

4.8.2. Fuel composition method for RQ

Potential of a particular fuel towards carbon emissions is based on the chemical composition of the fuel. The RQ factor which is defined as the ratio of amount of carbon dioxide produced for every mole of oxygen consumed can be obtained by using Eq. (28). A fuel with C atoms of carbon will produce C moles of carbon dioxide. Hence from combustion literature [102], the following formula is obtained for RQ factor.

$$RQ = \frac{1}{\left\{1 + \left(\frac{H}{4C}\right) - \left(\frac{O}{2C}\right) + \left(\frac{S}{C}\right)\right\}} \quad (28)$$

4.8.3. Gas analyses method

The RQ factor for a fuel can also be determined from the exhaust gas composition of an unknown fuel. Appendix B provides a condensed derivation for RQ, Equivalence Ratio and A:F (air fuel ratio) from gas analyses. The results can be applied to any C-H-O-N-S fuel as long as NOx and SO_2 are formed in trace amounts and fuel is completely burnt. Based on the exhaust gas and inlet air composition, RQ can be defined as follows.

$$RQ = \frac{\text{CO}_2 \text{ moles produced}}{\text{O}_2 \text{ moles consumed}} = \frac{X_{CO_2,e}\left(\frac{X_{N_2,i}}{X_{N_2,e}}\right) - X_{CO_2,i}}{X_{O_2,i} - X_{O_2,e}\left(\frac{X_{N_2,i}}{X_{N_2,e}}\right)} \tag{29}$$

If desired one may replace on a dry basis $X_{N2,e}$ by 1- $X_{O2,e}$ –$X_{CO2,e}$. Moles of oxygen consumed can be given as:

$$Z = \frac{\text{O}_2 \text{ consumed dry or wet}}{\text{Inspired dry or wet air}} = X_{O_2,i} - X_{O_2,e}\left(\frac{X_{N_2,i}}{X_{N_2,e}}\right) \tag{30}$$

Equivalence ratio (ϕ) is defined as the ratio of stoichiometric air flow to the actual air flow for the particular combustion process. Based on the exhaust gas analysis, ϕ can be reduces as follows:

$$\varphi = 1 - \left(\frac{X_{N_2,i}}{X_{N_2,e}}\right)\left(\frac{X_{O_2,e}}{X_{O_2,i}}\right) \tag{31}$$

The air fuel ratio on a mole basis for carbon atom normalized fuel is given according to Eq. (31).

$$\left(A:F\right)_{\text{emp Fuel}} = \frac{1}{\left(RQ * \varphi * X_{O_2,i}\right)}, \text{C atom normalized fuel } \text{CH}_\text{x}\text{O}_\text{y} \tag{32}$$

where X_{N2}, X_{CO2} and X_{O2} are the mole fractions of nitrogen, carbon dioxide and oxygen which could be either on dry or wet basis and subscripts i and e refer to inlet and exit of combustion chamber respectively. For a C atom normalized fuel CHxOy, x=H/C and y=O/C. The RQ must not depend upon excess air % and as such the variation of CO_2% and O_2% in exhaust with excess air % must be such that RQ values should remain constant when combustion is complete. Thus the accuracy of measured values can also be checked.

The CO_2 produced will reach a maximum value when excess air percentage is zero or $\phi = 1$. Thus $X_{O2,e} = 0$ at $\phi=1$. From Eq. (29), with $X_{CO2,i} = 0$ (i.e. pure dry air inlet), yields

$$X_{CO_2,\max} = \frac{RQ}{\left(\frac{1-X_{O_2,i}}{X_{O_2,i}}\right)+RQ} \tag{33}$$

5. RESULTS AND DISCUSSION*

5.1. Harvesting, collection and processing

Biomass fuels used for the current study, mesquite and juniper, were harvested from the rangelands in north central Texas near Vernon. Both mesquite and juniper are scattered over a large area which is estimated to be 200,000 ha. It should be noted that the species is not concentrated throughout the entire area but dispersed with a spacing of around 1 km. After the fuel is harvested using a chain saw, a chipper is used to reduce the particle size from trunk and branches. It also includes the bark. It was observed that, when a freshly harvested biomass (moisture content around 45%) was sent into the chipper for reducing the particle size, the chips produced after the chipping process had a lower moisture percentage of between 10 to 20%. This might be because of the drying of the woodchips within the chipper using the heat produced as a result of the chipping process. Vermeer wood chippers were used for processing the biomass. Further details on the preparation of the samples are available elsewhere [31]. Previous small scale study on mesquite and juniper of particle size between 540 – 800 microns showed lower mass loss for juniper when compared to mesquite in TGA [51]. In order to study for the effect of particle size on torrefaction of softwood and hardwood, smaller softwood juniper wood chips of size 2-4mm and comparatively larger mesquite wood chips of 4-6 mm were used for the current torrefaction study.

*Reproduced in part with permission from Thanapal SS, Chen W, Annamalai K, Carlin N, Ansley RJ, Ranjan D. Carbon Dioxide torrefaction of woody biomass. Energy Fuels 2014; 28:1147–57. Copyright 2014 American Chemical Society.

Table 12. Properties of mesquite, juniper and coal. ar: as received, daf: dry ash free, VM: volatile matter, FC: Fixed carbon, HHV: Higher heating value. Uncertainty in the presented numbers is 0.5%.

	Raw Biomass		Coal
	Mesquite	**Juniper**	**PRB**
Moisture (ar)	15.53	5.85	32.88
Volatile Matter (ar)	66.09	77.99	28.49
Fixed Carbon (ar)	16.71	14.25	32.99
Ash (ar)	1.67	1.91	5.64
Carbon (ar)	43.60	49.27	46.52
Oxygen (ar)	33.57	37.00	11.29
Hydrogen (ar)	4.98	5.68	2.73
Nitrogen (ar)	0.62	0.28	0.66
Sulfur (ar)	0.03	0.01	0.27
VM (daf)	79.8	84.6	46.3
FC (daf)	20.2	15.4	53.7
HHV (kJ/kg)	16666	18987	18193
HHV_{dry} (kJ/kg)	19730	20167	27105
HHV_{DAF} (kJ/kg)	20128	20584	29597
VM HHV_{DAF} (kJ/kg)	16923	18351	25880
$HHV_{Boie,DAF}$ (kJ/kg)	21059	21509	29847
HHV (kJ/kg st O_2)	13652	13632	13521
A/F_{st} (kg/kg_{ar} fuel)	5.24	5.98	5.78
A/F_{st} (kg/kg_{daf} fuel)	6.33	6.48	9.40
$T_{adiabatic\ flame,open}$ (K)	1374	1470	1427
N loading (kg/GJ)	0.3720	0.1475	0.3628
S loading (kg/GJ)	0.0180	0.0053	0.1481
ash loading (kg/GJ)	0.8438	0.9460	2.0195
Rosin Rammler size distribution, obtained from equation[+]			
n	1.3108	1.4193	1.1400
b	0.0003	0.0010	0.0112
SMD (micron)	1071.47	469.82	49.23
Empirical Formula	$CH_{1.37}O_{0.58}N_{0.0122}S_{0.0003}$	$CH_{1.38}O_{0.56}N_{0.0049}S_{0.0001}$	$CH_{0.70}O_{0.18}N_{0.0122}S_{0.0022}$
Reference	[111]	[111]	[18]
[+]$R=100*\exp(-bx^n)$			

Powder basin sub-bituminous coal was obtained from local utilities. Received coal was ground using a vortec mill to a size such that 75% of the ground coal passes the 200 mesh (75 micron). Raw biomass was ground using an in-house vibro energy grinding mill to the desired size range for the co-firing experiments.

5.2.Properties of coal and raw biomass

The ultimate and proximate analyses of the fuel samples were obtained from Hazen labs, Golden, Colorado and are shown in Table 12. The other derived properties (e.g. dry ash free basis, average heating values of VM, A/F, etc) are presented in Table 12. It can be observed from Table 12 that the volatile matter and oxygen content in the biomass samples are much higher than the coal sample which has higher amount of fixed carbon. Hence on a dry ash free basis, heating value of PRB coal was estimated to be around 30,000 kJ/kg when compared to 20,000 kJ/kg for biomass samples. It should also be noted that mesquite is a nitrogen fixing legume with higher percentages of nitrogen (Table 12) comparable to nitrogen content in the PRB coal. The nitrogen loading numbers for both coal and mesquite was 0.37 kg/GJ and juniper had a much lower value of 0.15 kg/GJ. Lower sulfur content in the biomass resulted in lower sulfur loading (kg/GJ) numbers for both mesquite and juniper. In addition other properties derived from the ultimate, proximate and heating value analysis are shown in Table 12.

Size distribution of ground coal and raw biomass ground for 20 minutes in the grinding mill is shown below in Fig. 9. Rosin Rammler plot determined using the following equation is shown in Fig. 10.

$$R = 100 * e^{-bx^n} \tag{34}$$

where R represents the fraction of particles which are collected in the sieve (1-R, the fraction passing through), x is the particle size, b and n are constants. n is the measure of the drop sizes and b is related to the fineness of the particles.

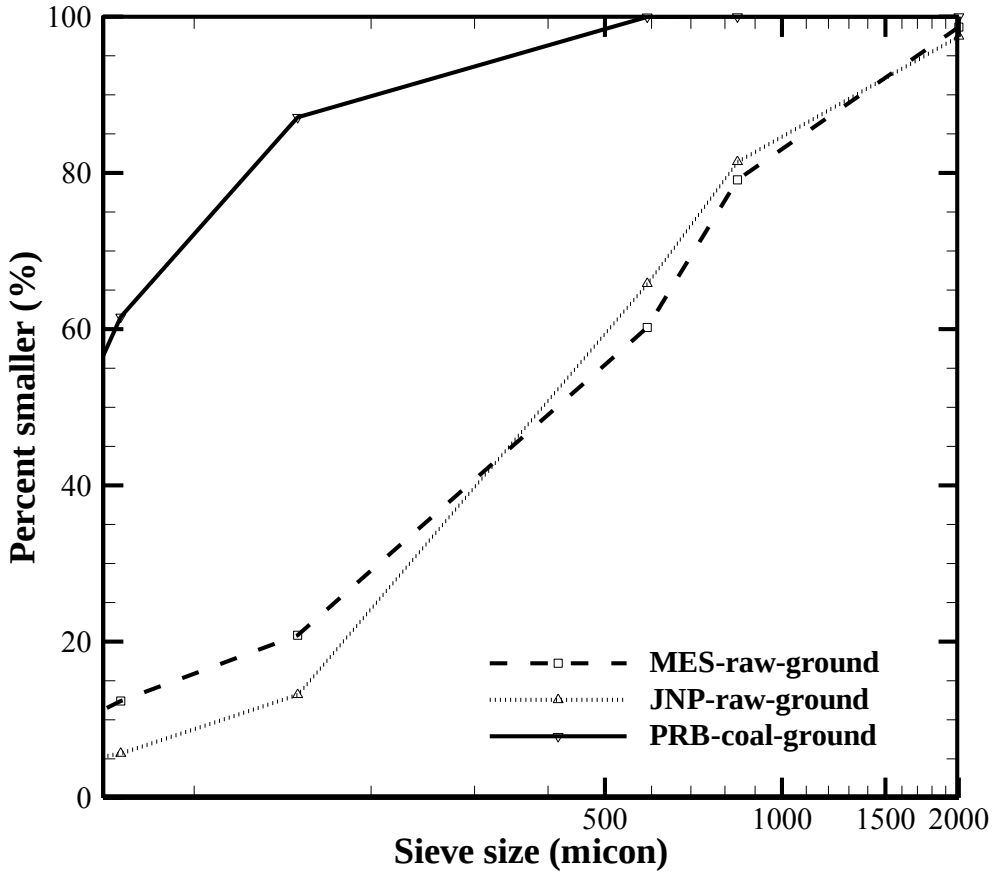

Fig. 9. Size distribution of raw mesquite and juniper and ground coal.

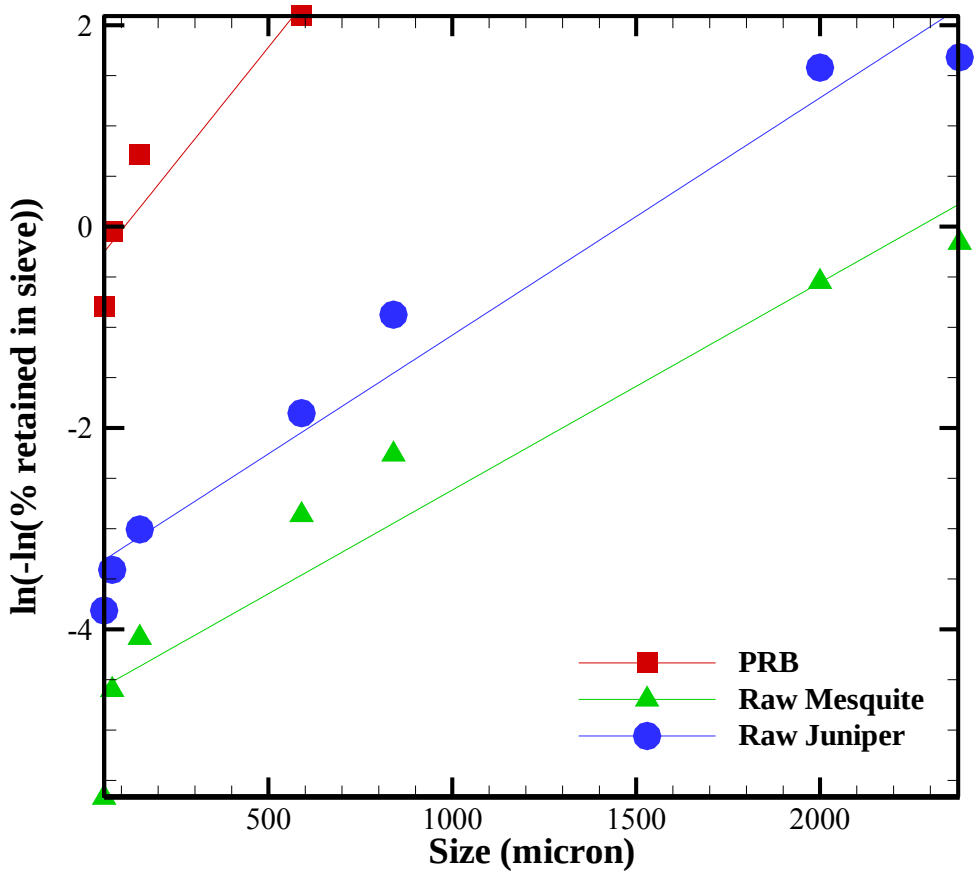

Fig. 10. Rosin Rammler plot of PRB coal, raw mesquite and raw juniper samples.

Fibrous nature of the raw woody biomass results in poor grindability of the biomass material in comparison to coal. It can be observed from Fig. 9 that around 70% of the coal passes through the 100 micron sieve in comparison to less than 20% for the case of raw mesquite and juniper. Sauter mean diameter numbers calculated from the sieve analysis shows that the biomass samples have a very high SMD which has to be reduced considerably for the suspension fired applications. In order to model the

decomposition of raw biomass during torrefaction and pyrolysis process, properties of the three basic components/constituents, their respective amounts in different biomass types along with their kinetics should be known. Chemical composition (ultimate and proximate analysis) of the biomass components hemicellulose and lignin was obtained from the literature (Table 13). The composition of lignin was then determined from the fuel composition and the data for hemicellulose and cellulose from Eq. (1) (Section 4.1).

Table 13. Ultimate and proximate analysis of biomass components [112, 113].

	Hemicellulose	**Cellulose**
Volatile matter (db)	74.11	91.64
Fixed carbon (db)	21.94	8.36
Volatile matter (daf)	77.16	91.64
Fixed carbon (daf)	22.84	8.36
Ash (db)	3.95	0
C (daf)	43.77	43.58
H (daf)	5.91	6.09
O (daf)	50.26	50.27
N (daf)	0.05	0.05
S (daf)	0.02	0.01
Heating value (kJ/daf kg)	15920	17870

Based on the pyrolysis tests carried out on the three components, 32%, 2.5% and 40% was left over as char from hemicellulose, cellulose and lignin respectively on a dry ash free basis [114]. The percentage of fixed carbon in the three components was used as a reference to determine the amount of volatile matter released from the components during the torrefaction process. Amount of these three components depends on the type of biomass. Hardwood was found to contain higher percentage of hemicellulose (lower

lignin) when compared to softwood. Percentage of the different components in hardwood, softwood and fibrous biomass were obtained from Liu et al. [115]. Table 14 shows the percentage of the three components. Major difference which can be observed from Table 14 was the percentage of lignin in softwood. Softwood had the highest lignin content and lowest hemicellulose.

Table 14. Composition of hard wood and softwood [115].

	Hemicellulose (%)	**Cellulose (%)**	**Lignin (%)**
Softwood	12.27	53.26	26.66
Hardwood	28.97	53.95	9.43
Rice Straw	29.53	41.11	5.07

Effect of pyrolysis of the three components have been studied elsewhere earlier using Thermogravimetric analyzer to extract the respective kinetics [116-118].

5.3.Three component modeling results

Activation energy and pre-exponential factors for the three components hemicellulose, cellulose and lignin of woody biomass were obtained from literature. First order single reaction assumption was used for each component and the kinetic constants were derived based on minimizing the least square errors between the calculated and experimentally obtained values for each component. It should be mentioned here that there are other methods where the mass loss was obtained versus temperature and hemicellulose, cellulose and lignin are assumed to be released within certain temperature ranges. Minimization of least squares technique was used to extract

the kinetics [117]. Table 15 shows the numbers presented in the literature for the three components, hemicellulose, cellulose and lignin.

Table 15. Kinetic parameters of the three components estimated by minimizing the least square errors.

	Hemicellulose	**Cellulose**	**Lignin**
B (1/min)	6.66E+08	6.83E+16	1000
E (kJ/kmol)	103200	201000	65000
Reference	[116]	[117]	[118]

Percentages of the three components, the kinetic constants and the composition of the hemicellulose and cellulose were used to model the torrefaction of the biomass. The three components were assumed to decompose independently according to a three independent parallel reaction mechanism during the torrefaction process. Eq. (1) to Eq. (10) (Section 4.1) were used to model the heat up of the samples to the desired torrefaction temperature and then undergo torrefaction at the given temperature for the desired time period. The conversion of all the three components in addition to the overall conversion was determined. It was assumed that the composition of the volatiles leaving the components remains constant and the conversion varies with increased release of the volatile matter from the samples. Effect of the wood type, heating rate to the torrefaction temperature, torrefaction temperature and residence time for torrefaction was studied using the TCM. Fig. 11 plots the variation in conversion for the three components in addition to overall conversion for the case of torrefaction of mesquite for 60 minutes at 240˚C with a heating rate of 20˚C per minute to the torrefaction temperature.

At the end of 60 minutes, the loss of volatiles from the three components was predicted to be 71.5%, 1.39% and 1.46% for hemicellulose, cellulose and lignin respectively on a dry ash free basis. The overall dry ash free mass loss from the biomass sample was 18.1%. Lower activation energy for hemicellulose resulted in higher loss of this component during mild torrefaction when compared to the other two remaining components. Since mesquite is a hardwood with comparatively higher percentages of hemicellulose, the overall mass loss is higher. The effect of torrefying juniper under the same conditions (240˚C for 1 hour) with an initial heating rate of 20˚C per minute upto the torrefaction temperature yielded a lower overall mass loss due to variations in composition of the three components (Fig. 12). Higher percentages of lignin (Table 14) in softwood types resulted in higher mass retention at 240˚C. The overall mass loss for the torrefaction of juniper was 8.32% on a dry ash free basis.

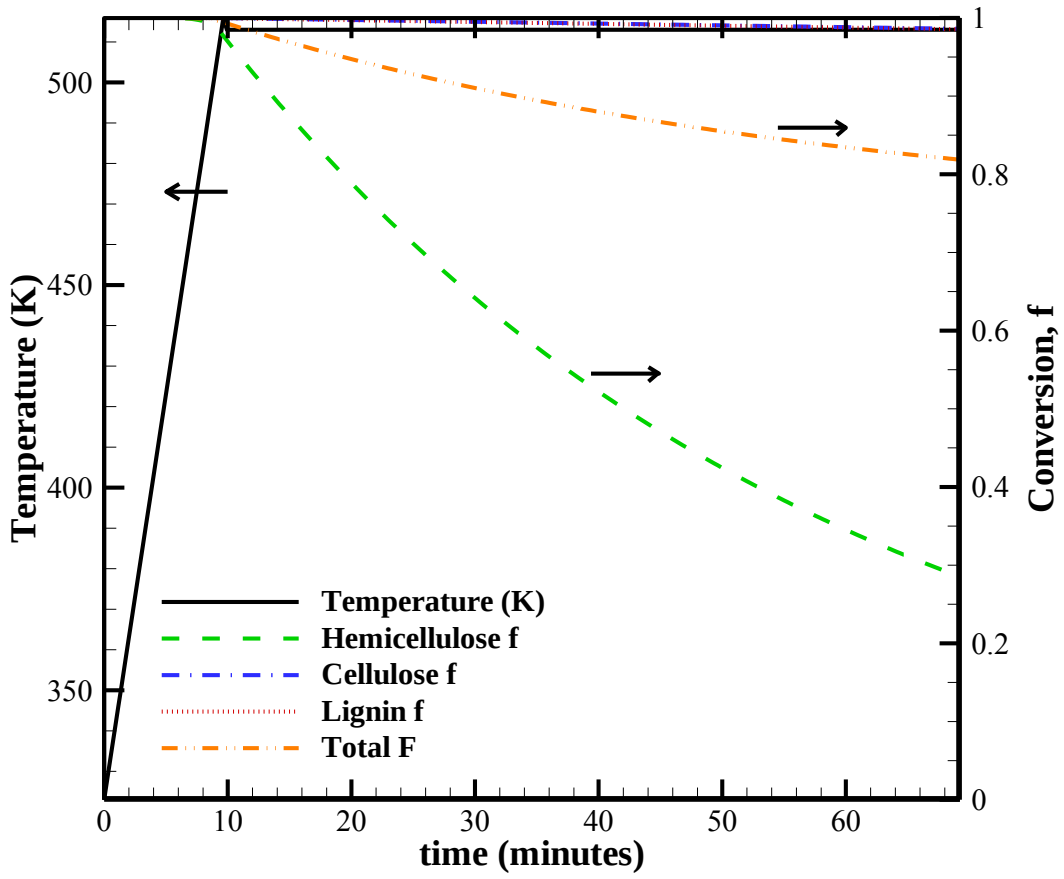

Fig. 11. Torrefaction of mesquite at 240˚C for 60 minutes; initial heating rate 20˚C/minute; results predicted by TCM.

Higher torrefaction temperatures will result in much higher losses due to volatilization of cellulose at higher temperatures.

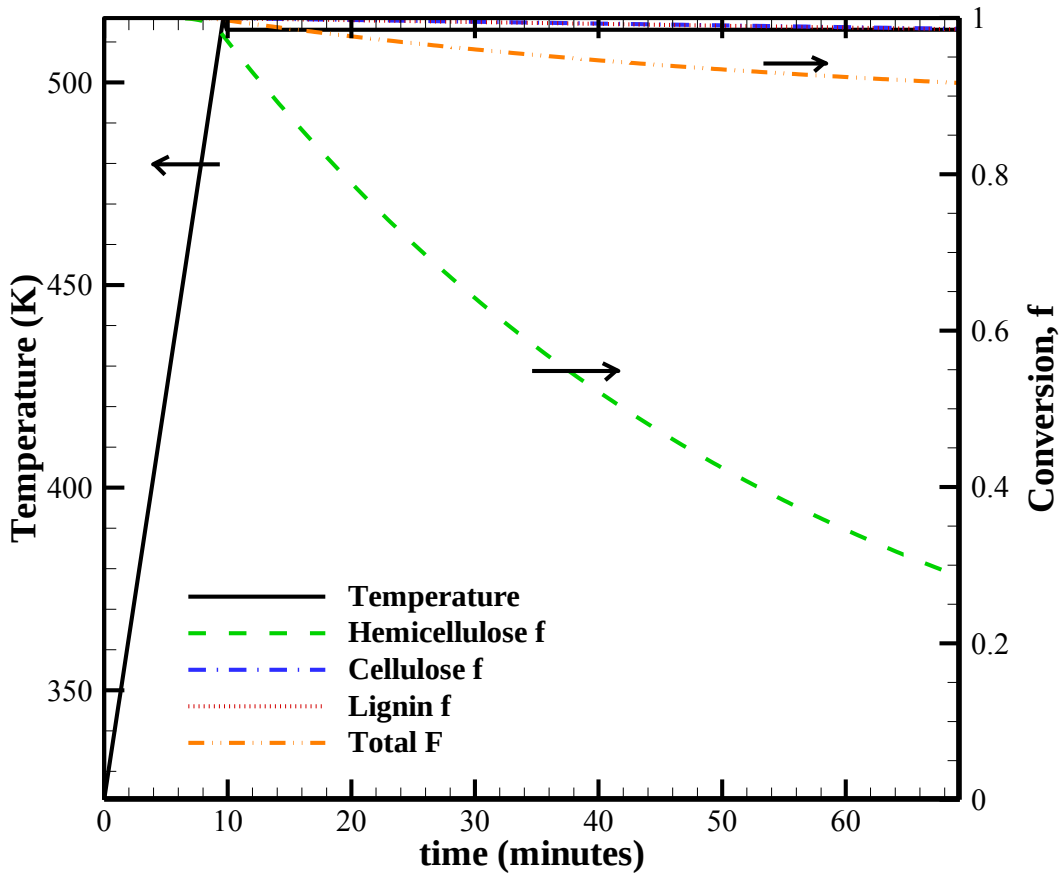

Fig. 12. Torrefaction of juniper at 240˚C for 60 minutes; initial heating rate 20˚C/minute; results predicted by TCM.

Fig. 13 shows the variation in conversion of the three components during torrefaction of mesquite at 280˚C for 60 minutes with an initial heating rate of 20˚C per minute from room temperature to the torrefaction temperature.

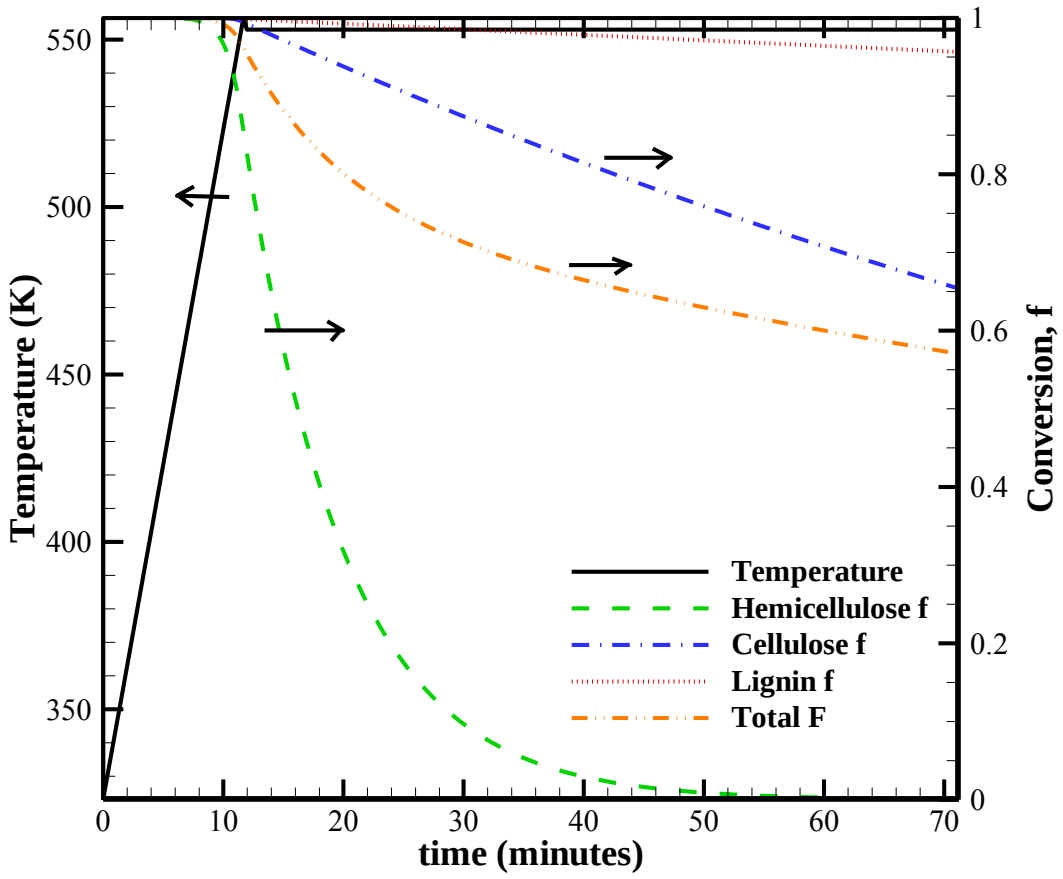

Fig. 13. Torrefaction of mesquite at 280˚C for 60 minutes; initial heating rate 20˚C/minute; results predicted by TCM.

About 99.93%, 34.62% and 4.35% of the DAF volatile matter in hemicellulose, cellulose and lignin respectively has been liberated resulting in an overall DAF mass loss of 42.95% during torrefaction of mesquite at 280˚C. Under similar conditions juniper lost 29.3% of mass on a DAF basis (Fig. 14).

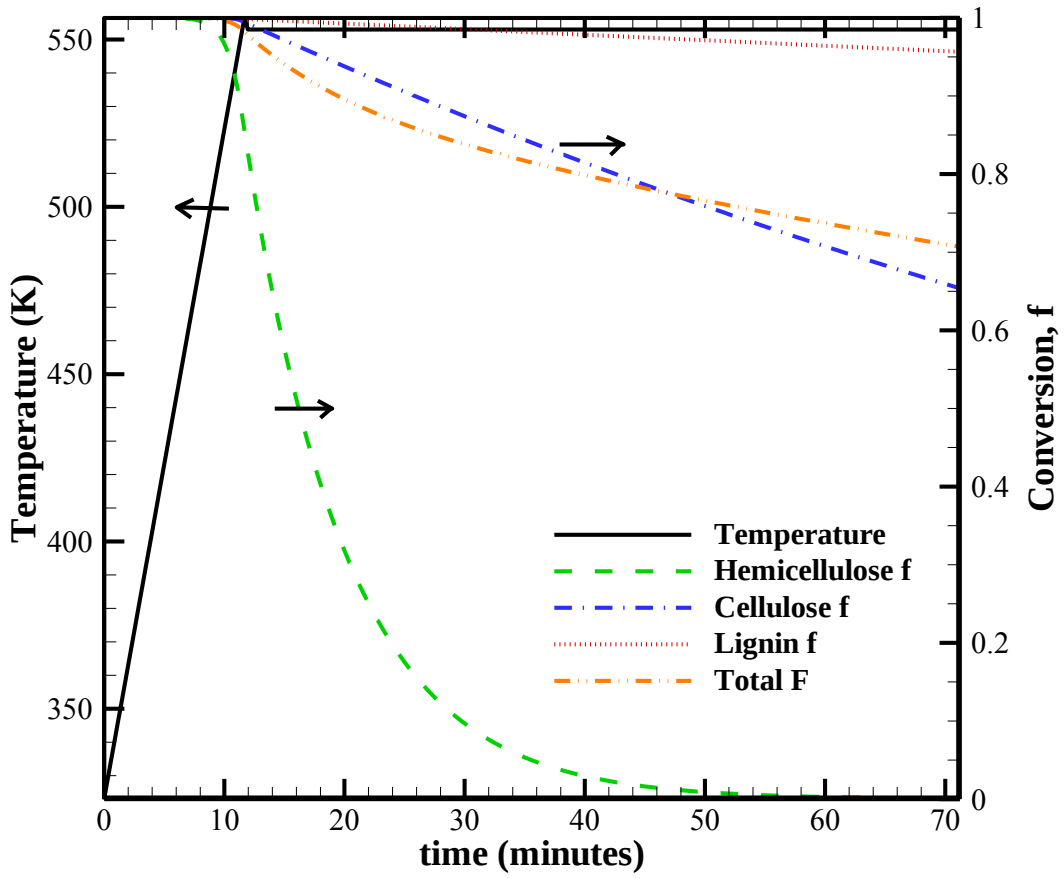

Fig. 14. Torrefaction of juniper at 280˚C for 60 minutes; initial heating rate 20˚C/minute; results predicted by TCM.

The results predicted by the TCM were compared with the results obtained from experiments conducted on mesquite and juniper samples (10 mg) in a TGA unit. Experimental results are tabulated in Table 16 [51].

Table 16. Results from TGA torrefaction experiments carried out using nitrogen as an inert medium. Mass remaining in the torrefied woody biomass given on a dry ash free basis [51]. Mass of sample: 10 mg.

Temperature (˚C)	**Mesquite (%)**	**Juniper (%)**
200	93.6	98.0
220	88.8	94.4
240	80.7	88.0
260	71.6	79.5
280	56.2	65.9
300	40.2	47.9

Fig. 15 compares the TCM results with the experimental results for a residence time of 60 minutes for both mesquite and juniper samples. The model results compare well with the experimental results except at the upper temperature limit. At temperature of 300˚C, TCM over predicts the mass loss from the woody biomass. The kinetic constants of cellulose used to model the torrefaction process resulted in increased losses of cellulose at higher temperatures in the TCM. Also, the mass loss predicted by the model for juniper is lower than the experimentally observed values. It should be noted that the percentage of the three components were not determined experimentally and it was assumed to have the same composition as that of hardwood and softwood which was reported in literature (Table 14). Accurate determination of the three component composition would have enabled better mass loss prediction from both mesquite and juniper. These plots lead to the determination of HHV_{DAF} versus T and the plots could be used to determine desired torrefaction temperature.

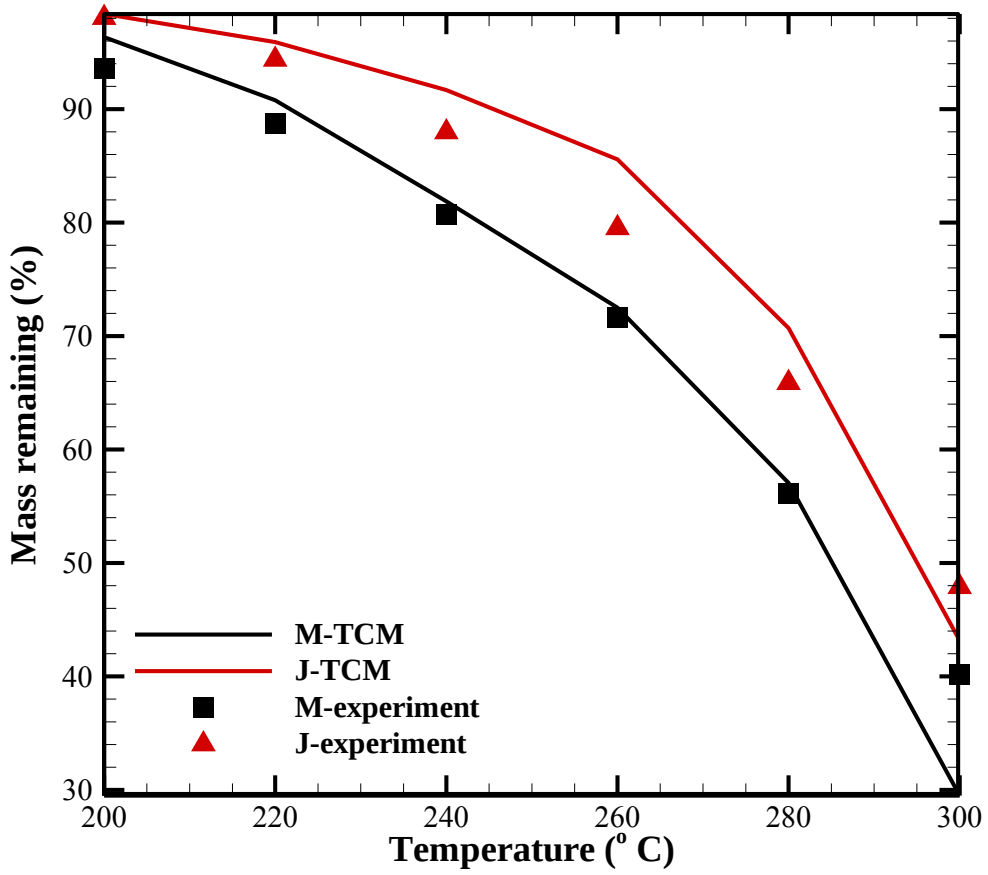

Fig. 15. Effect of temperature on the loss of volatile matter from the samples. Results from the model are compared with experimental results of Eseltine et al. [51] using N_2 gas. M: Mesquite; J: Juniper; TCM: Three component model (Uncertainty in TGA experiment results were 1%).

Fig. 16 shows the plot of mass loss from mesquite and juniper determined using TCM and TGA on a logarithmic scale. The slope of the line will be $(E/R)_{global}$ for the bulk sample.

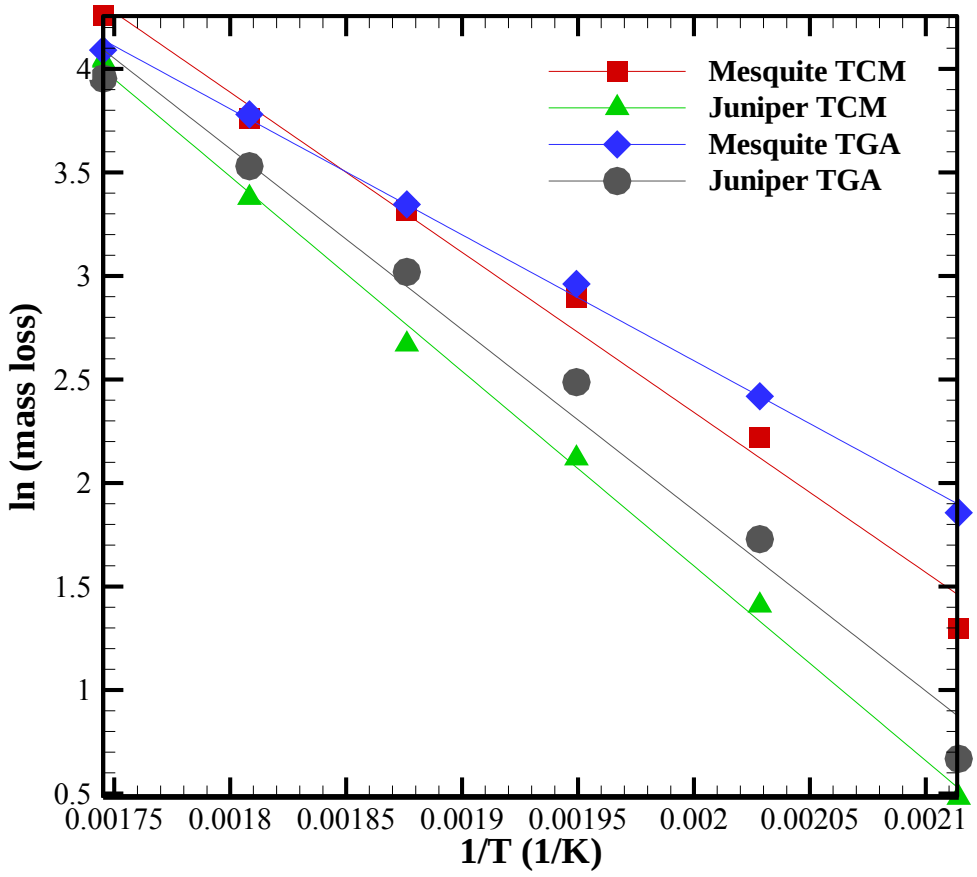

Fig. 16. Mass loss from the samples expressed on a natural logarithmic scale versus (1/T). The slope of the trend line will be (E/R) of the bulk biomass sample.

From the graph, $(E/R)_{TCM,juniper}$ was 9407 K and $(E/R)_{TCM,mesquite}$ was 7731 K. Since $(E/R)_{juniper}$ is higher than that of mesquite, it indicates lower mass loss from the juniper sample due to higher activation energy. It is noted that the mass loss rate varies as complex function of temperature during heat up period but the loss rate is a linear

function of time at constant temperature. The variation in mass loss with increase in residence time for an initial heating rate of 20˚C/min is plotted in Fig. 17.

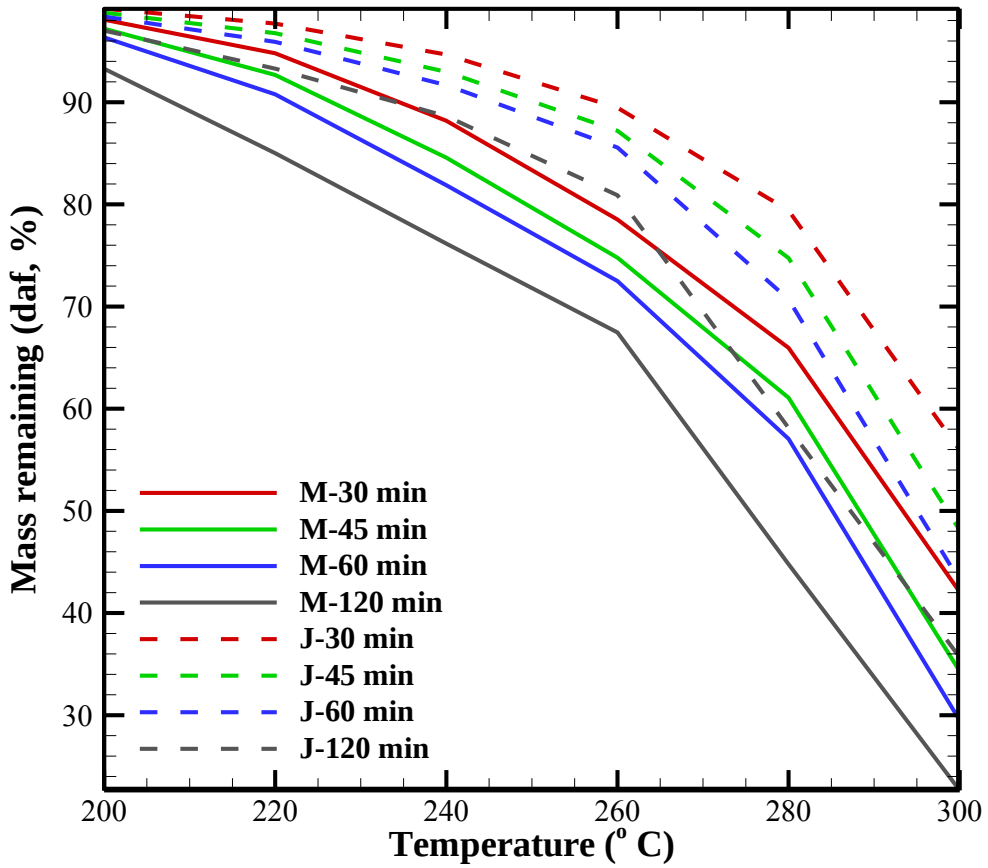

Fig. 17. Variation in mass loss with increase in torrefaction temperature and residence times. M: Mesquite; J: Juniper.

Following residence times were studied: 30 minutes, 45 minutes, 60 minutes and 120 minutes. Effect of higher residence time on mass loss was negligible at lower

torrefaction temperatures while an increase in temperature resulted in increased mass loss due to higher time and energy available for the volatilization of cellulose and lignin present in the biomass. Higher amount of cellulose was released from the sample resulting in higher mass loss. The effect of heating rate on the torrefaction of woody biomass using TCM showed a comparatively higher retention (negligible difference) of mass at higher temperatures when compared to the lower heating rates. The results predicted by TCM at different heating rates and residence time is presented in Appendix C. Higher heating rates do not allow sufficient time for the volatiles to escape out from the biomass which causes lower mass loss during the initial heat up period. Hence higher heating rates are preferred to reduce the loss of combustible volatile matter from the torrefaction of biomass at higher temperatures.

The heating value and the chemical composition of the three components were used to monitor the change in heating value of the torrefied biomass with reference to the raw samples. Energy conversion ratio which is defined as the ratio of the energy content of the torrefied sample to the energy content of the raw biomass and the ratio of the heating value of the torrefied biomass to raw biomass was also determined. Fig. 18 shows the variation of heating value and energy conversion ratio with respect to torrefaction temperatures. As can be observed from Fig. 18, heating value of the torrefied sample increases with increase in torrefaction temperature as the hemicellulose and cellulose volatizes and the sample become rich in char and lignin which have higher heating value. The ration of the heating value of the torrefied samples to the raw biomass samples from the experiments at 240˚C for a residence time of 60 minutes was 1.06 and

1.05 for mesquite and juniper samples respectively. The ratio of the heating values predicted by the model was lower. In the case of TCM, the composition of volatile matter released from the sample is assumed to remain constant and it also includes carbon and hydrogen along with oxygen. Hence lower ratios were predicted by the model when compared to that of experiments.

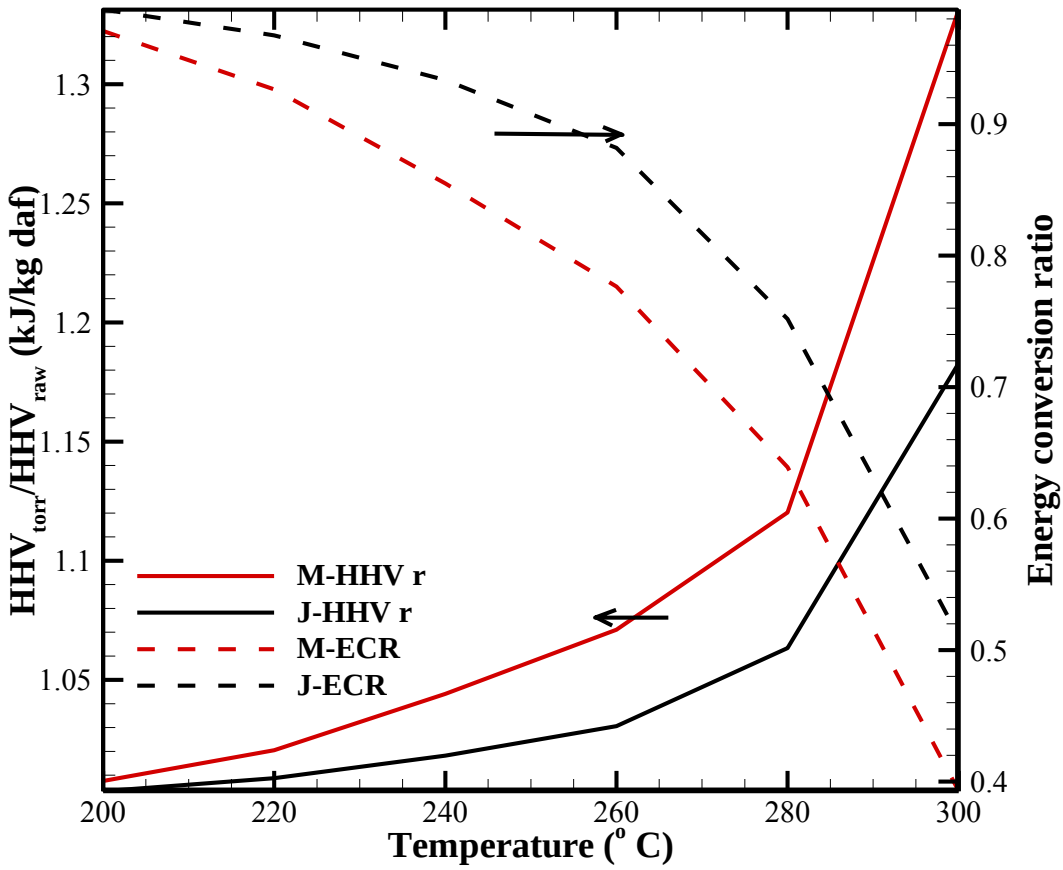

Fig. 18. Variation in heating value and ECR with increase in temperature. M: Mesquite; J: Juniper; HHV r: Heating value ratio; ECR: Energy conversion ratio.

The energy conversion ratio (ECR) of the torrefied samples decreases due to loss of combustible volatile matter. As the energy content of the sample decreases with increase in temperature, ECR decrease. It is seen that ECR decreases rapidly after about 260˚C due to higher loss of cellulose. Thus T_{torr} must be limited to T_{torr}<260˚C. However on a unit mass basis, heating value of the torrefied sample is higher than the raw biomass. Hence the three component model is a simple model to predict the mass loss from the biomass samples undergoing torrefaction. Such a model can also be applied to the fibrous biomass torrefaction. It should be noted here that the order of reaction for the volatization of the three components are assumed to be one. The TCM can also be applied for non-unity order based on the extraction of kinetic parameters from the MVR.

5.4.Torrefaction in batch reactor for bigger batch

Torrefaction studies were done for temperatures from 200˚C to 300˚C in steps of 20˚C for mesquite (M) and juniper (J) using biomass of 500g in a torrefaction reactor. The temperatures selected were below the temperature of maximum volatile release rate. Two pretreatment mediums in form of N_2(N) and CO_2(C) were used. Samples torrefied will be represented by the following nomenclature: temperature-biomass-pretreatment medium used. For example, 200-M-C will represent mesquite pretreated with CO_2 at 200˚C. A few of the tests were repeated to check for repeatability of experiments. In total, 24 samples were obtained from the torrefaction of two woody biomass using two different mediums for the six temperatures studied.

5.4.1. Torrefied biomass properties

Proximate analysis was done on the torrefied samples. Moisture, volatile matter and ash were determined using ASTM standards E871, E872 and E1755 respectively. The remaining mass in the sample is fixed carbon (Fixed carbon was estimated from the difference). Gross heating values of the samples were determined using a bomb calorimeter according to ASTM test method E711. Table 17 shows the results obtained for the proximate analysis of the samples. The values for the volatile matter (VM), fixed carbon (FC) and higher heating value (HHV) or gross heat value obtained on a dry basis and dry ash free basis (DAF) are also presented in Table 17.

It can be observed from Table 17 that the ash percentage of the samples treated using CO_2 and N_2 are higher than the raw biomass samples. Though the ash percentage shows some minor deviations it may be attributed to the non-uniform distribution of ash within the samples. Assuming there is no loss in the ash components during torrefaction, using ash balance [60].

$$\left(m_0 - m_{loss}\right) * y_{ash} = m_0 * y_{ash,0} \tag{35}$$

$$y_{ash} * \left(1 - \frac{m_{loss}}{m_0}\right) = y_{ash,0} \tag{36}$$

Table 17. Proximate analysis of the torrefied samples [60]. Uncertainty in the presented numbers is 0.5%

Sample	Moisture, ar (%)	Ash, ar (%)	VM, ar (%)	FC, ar (%)	HHV, ar (kJ/kg)	Ash, dry (%)	VM, dry (%)	FC, dry (%)	HHV, dry (kJ/kg)	VM, DAF (%)	FC, DAF (%)	HHV, DAF (kJ/kg)
Mesqutie-Raw	15.5	1.67	66.1	16.7	16700	1.98	78.2	19.8	20169	79.8	20.2	20169
Juniper-Raw	5.85	1.91	78.0	14.3	19000	2.03	82.8	15.1	20598	84.6	15.4	20598
200-M-C	3.64	2.56	67.5	26.3	19298	2.66	70.0	27.3	20026	72.0	28.0	20573
220-M-C	3.50	2.33	66.9	27.3	19658	2.41	69.3	28.3	20371	71.0	29.0	20874
240-M-C	3.10	2.74	66.7	27.5	20785	2.82	68.8	28.3	21450	70.8	29.2	22074
260-M-C	3.32	1.59	62.9	32.2	20661	1.64	65.1	33.3	21371	66.2	33.8	21727
280-M-C	2.29	3.22	58.2	36.3	22274	3.29	59.5	37.2	22796	61.6	38.4	23572
300-M-C	2.88	4.05	52.0	41.1	23101	4.17	53.5	42.3	23786	55.9	44.1	24821
200-M-N	4.94	1.92	67.5	25.7	19125	2.02	71.0	27.0	20119	72.4	27.6	20535
220-M-N	4.27	1.72	67.2	26.8	19416	1.79	70.2	28.0	20283	71.5	28.5	20653
240-M-N	3.58	2.55	66.4	27.5	19869	2.64	68.9	28.5	20606	70.7	29.3	21166
260-M-N	2.87	2.26	65.0	29.8	20621	2.32	67.0	30.7	21230	68.6	31.4	21735
280-M-N	2.22	2.43	61.3	34.1	21971	2.48	62.7	34.9	22469	64.3	35.7	23042
300-M-N	2.04	2.60	57.9	37.5	22733	2.66	59.1	38.3	23206	60.7	39.3	23839
200-J-C	5.03	1.41	68.5	25.1	19372	1.48	72.1	26.4	20398	73.2	26.8	20705
220-J-C	3.99	2.25	69.9	23.9	19602	2.34	72.8	24.9	20417	74.5	25.5	20906
240-J-C	3.42	2.31	68.5	25.8	20242	2.39	70.9	26.7	20959	72.6	27.4	21472
260-J-C	2.97	1.55	67.9	27.6	20418	1.60	70.0	28.4	21043	71.1	28.9	21385
280-J-C	1.78	1.83	64.5	31.9	22905	1.87	65.6	32.5	23320	66.9	33.1	23764
300-J-C	2.10	1.22	57.9	38.8	24206	1.25	59.2	39.6	24725	59.9	40.1	25038

Table 17. Continued

Sample	Moisture, ar (%)	Ash, ar (%)	VM, ar (%)	FC, ar (%)	HHV, ar (kJ/kg)	Ash, dry (%)	VM, dry (%)	FC, dry (%)	HHV, dry (kJ/kg)	VM, DAF (%)	FC, DAF (%)	HHV, DAF (kJ/kg)
200-J-N	3.48	1.96	69.2	25.4	19909	2.03	71.7	26.3	20626	73.2	26.8	21054
220-J-N	4.04	2.88	70.5	22.6	19492	3.00	73.5	23.5	20313	75.8	24.2	20941
240-J-N	4.53	2.13	69.1	24.3	20906	2.23	72.4	25.4	21898	74.0	26.0	22397
260-J-N	3.09	1.45	68.9	26.6	21577	1.49	71.1	27.4	22265	72.2	27.8	22602
280-J-N	3.04	1.81	65.3	29.8	21829	1.87	67.4	30.8	22513	68.6	31.4	22941
300-J-N	2.66	1.27	63.8	32.2	23390	1.30	65.6	33.1	24029	66.4	33.6	24347

ar: as received basis; dry: dry basis; DAF: dry ash free basis; M: Mesquite; J: Juniper; C: Carbon dioxide; N: Nitrogen

where m_o, m_{loss}, y_{ash} and $y_{ash,0}$ stands for mass of the raw biomass samples, mass lost during torrefaction from the biomass samples, mass fraction of the ash in the torrefied sample and the initial percentage of ash in the raw biomass sample respectively. From the above equations (Eq. (35) and Eq. (36)), the product of remaining dry ash mass fraction and remaining mass fraction of fuel [$= (m/m_0) = (m_0-m_{loss})/m_0$] should remain constant. Using the data obtained from the torrefied samples, following plot (Fig. 19) is obtained for torrefied mesquite and juniper. With increase in temperature the ash percentage fluctuated.

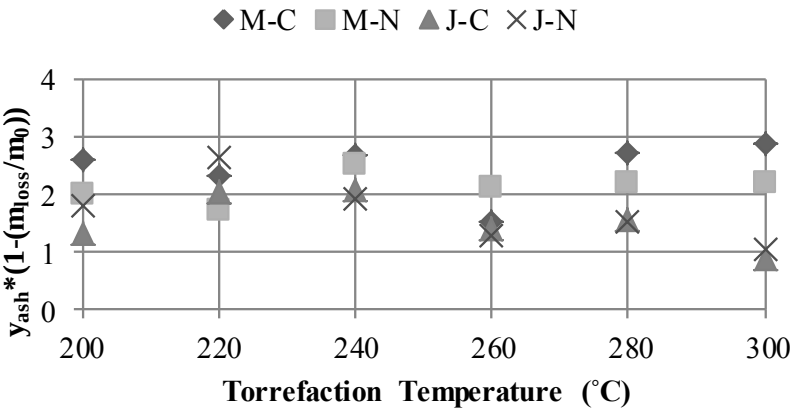

Fig. 19. Ash tracer technique to show the ash balance in the raw and torrefied samples. M: Mesqutie; C: Carbon dioxide; J: Juniper; N: Nitrogen [60].

From the above plot it can be seen that product approximately remains constant (around 2% on a dry basis) and the ash tracer technique is valid for the torrefied samples. The melting and boiling points of the different constituents in the biomass ash were

obtained from the literature [102]. It was observed that the boiling points of the ash constituents vary between 1373 K for potassium oxide to 3873 K for magnesium oxide. The partial pressures of the different inorganics in the ash were determined according to formula presented in Alcock et al. [119] and the partial pressures of the metals at the temperature range used for the torrefaction condition was found to be very low (in the order of 10^{-5} to 10^{-36} atm) indicating much higher temperature would be needed to volatize and remove the inorganics. Hence torrefaction process will not result in loss in ash constituents. Further work should be done to determine the mineral content in the raw biomass ash and the torrefied biomass ash.

5.4.2. Mass yield

Mass yield after torrefaction is defined according to Eq. (37) as the ratio of the amount of mass left after pretreatment to the original mass of the raw biomass.

$$\text{Mass yield} = \frac{m_{TB}}{m_{RB}} * 100 \tag{37}$$

where m_{TB} and m_{RB} represent the mass of the torrefied biomass and raw biomass respectively. Variation in mass yield under two environments, CO_2(C) and N_2 (N) is shown below in Fig. 20 for mesquite (M) and juniper (J) on a dry ash free (DAF) basis. It can be seen that the mass loss was comparatively higher when using CO_2 as the pretreatment medium for the hardwood species mesquite which has a higher moisture

and hemicellulose content when compared to juniper. Juniper with lower moisture and hemicellulose content showed similar mass losses under two torrefaction conditions at temperatures below 280˚C. At higher temperatures, the mass loss was much higher for both the species under study on using CO_2 as the torrefaction medium.

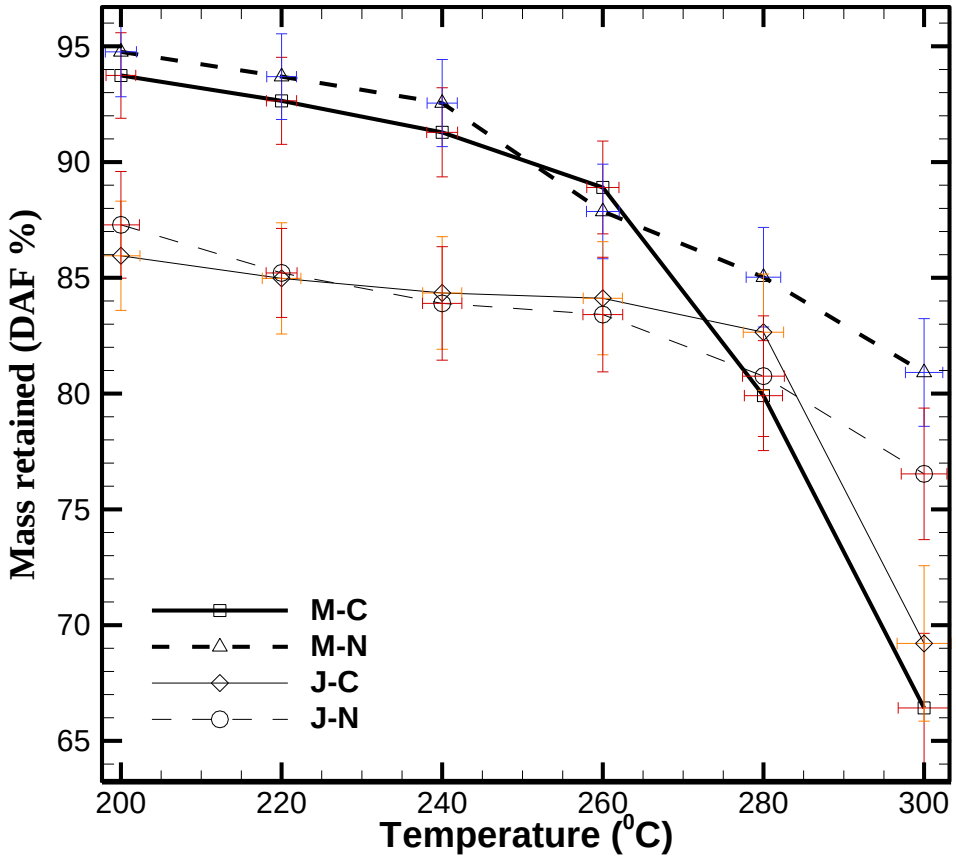

Fig. 20. Mass retained after pretreatment in CO_2 and N_2. Graphs are presented for the dry ash free (DAF) case. Mesquite size: 4-6 mm; Juniper size: 2-4 mm; 500 g sample [60].

In addition to temperature, mass loss rate is affected by i) type of wood (hardwood or softwood), ii) batch size in grams, iii) particle size and iv) torrefaction medium used (CO_2 or N_2). Juniper with lower particle size showed higher VM loss when compared to mesquite. Studies conducted on similar particle sizes (589-840 μm) for both the woody biomass (mesquite and juniper) using a TGA showed increased mass losses for mesquite samples when compared to juniper during the torrefaction process [51]. Softwood species (juniper) with lower hemicellulose content showed higher mass loss rate than mesquite which is a hardwood with higher hemicellulose. Hence, the effect of particle size on the mass loss behavior of the lignocellulosic samples was compared in the current study to understand the torrefaction process on different wood types. In the batch torrefaction reactor, the torrefaction medium permeates the samples. Thus batch size may not lead to temperature gradients. However the larger particle size will reduce the mass loss rate and hence will lead to higher mass retained for mesquite sample (4-6 mm).

CO_2 had a minor effect on the softwood species when temperature was lower than 280 °C compared to that of mesquite. Different phenomenon which can be accounted for such behavior of biomass under these pretreatment mediums include, a) higher specific heat of carbon dioxide when compared to that of nitrogen which results in some heat being removed by the pretreatment mediums during the heating process, b) reaction of the pretreatment medium (CO_2) with the biomass fuels, c) effect of ash contents in biomass which can catalyze the reaction between pretreatment medium CO_2 with biomass and d) effect of particle size of the biomass. From the results obtained it

can be concluded that the particle size can be altered in addition to using different torrefaction mediums to obtain desired mass loss from the samples.

The behavior of hemicellulose, cellulose and lignin content in both juniper and mesquite can be predicted from the TGA-DTA trace. A biomass sample which has higher percentage of hemicellulose will exhibit a hump at lower temperatures of around 200-300˚C during pyrolysis process [27, 88, 89, 116]. TGA-DTG (Thermogravimetric and Differential thermograms) curves obtained for mesquite and juniper pyrolysis under nitrogen environment is available elsewhere [51]. Lower amount of hemicelluloses in the softwood species juniper is evident from the smaller hump in the DTG curve (dotted line) when compared to that of mesquite. Since lower particle size of juniper was used in the current study, more hemicellulose is lost at the temperature range of torrefaction for juniper when compared to that of larger mesquite fuel particles. Though mesquite has larger amount of hemicelluloses, larger particle size has restricted the passage for the hemicelluloses at the center of the particle to escape. Studies conducted on similar particle sizes (589-840 μm) for both the woody biomass (mesquite and juniper) using a TGA showed increased mass losses for mesquite samples when compared to juniper during the torrefaction process due to difference in hemicellulose content [51].

Based on equilibrium concepts for reaction $C+CO_2 \rightarrow 2CO$, it has been shown that the Boudouard reaction is thermodynamically favorable only at temperatures above 710˚C [58] i.e $\Delta G < 0$ at $T > 710$˚C; called transition temperature which leads to an equilibrium constant value which is greater than 1. A higher value for the equilibrium constant indicates that the mole fraction of CO will be much higher than the mole

fraction of CO_2 at temperatures above 710˚C. The effect of CO_2 reacting with fixed carbon in the biomass at temperatures used for the present study was considered to be negligible. In order to validate the temperature and time dependence, the Boudouard reaction kinetics was obtained from the literature [99, 120]. Assuming CO_2 reacts with the carbon in the biomass, the mass loss rate can be given by,

$$\frac{dW}{dt} = k_0 p_s^m S_m W \exp\left(\frac{-E}{RT}\right) \tag{38}$$

where p_s is the partial pressure of species, S_m is the specific surface area of the particle and W is the weight of the particle. The values of the constants m, k_0 and E in the above expression are available elsewhere [99]. The effect of the Boudouard reaction at lower temperatures and increased residence times (60 minutes) was studied. Curves obtained for the percent mass loss for different temperatures with respect to residence time shows an increasing trend in mass loss with increased residence times. Fig. 21 shows the results obtained from the Boudouard reaction kinetics for the case of coal char. Higher mass loss was observed when the temperatures were increased beyond the temperature range used for the current torrefaction studies indicating temperature and time dependent mass loss. It should be noted that the value of the constants used in Eq. (38) were derived for coal chars with higher surface area. Though the biomass undergoing torrefaction will not have a high surface area, the above model can be used as a reference to validate the time dependency of Boudouard reaction at the temperature range used for torrefaction study.

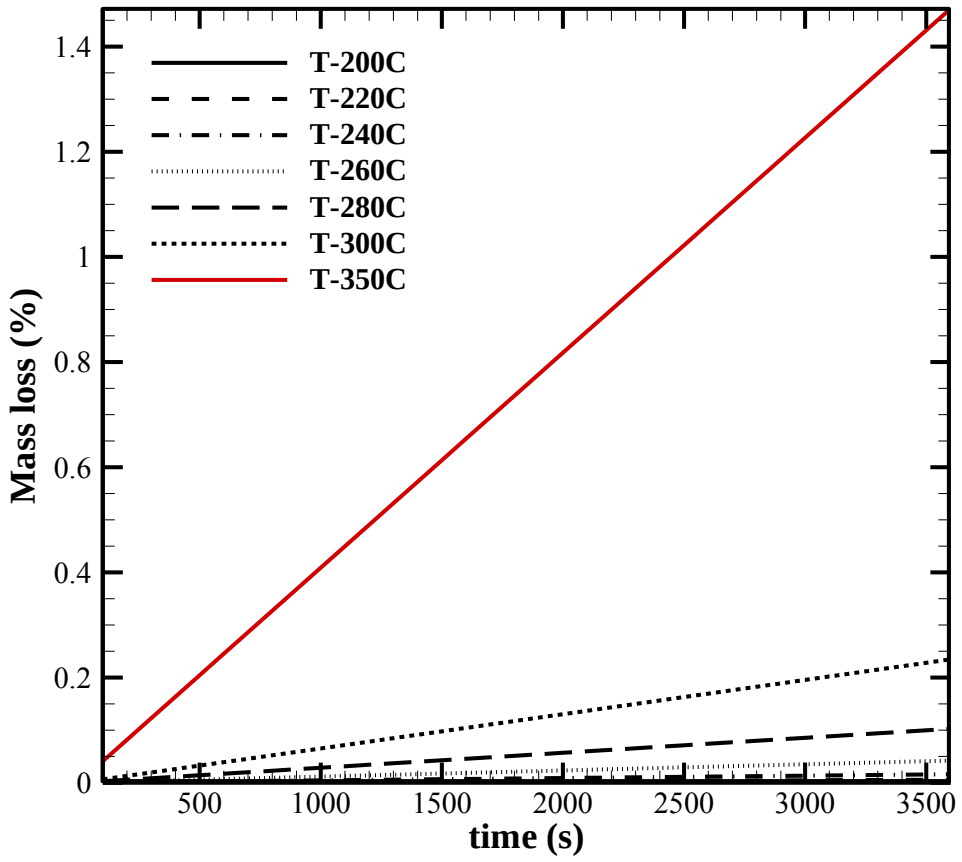

Fig. 21. Effect of residence time and temperature on the Boudouard reaction. Temperatures above 300˚C shows higher mass loss with respect to residence time.

Use of carbon dioxide as the pretreatment medium has an impact on the mass loss behavior of the biomass. A small amount of mass loss due to the reaction of carbon with carbon dioxide will cause a slight increase in the pore spaces available for the volatiles trapped within the biomass particle to leave the particle. A TGA unit was used to study the time dependency of CO_2 reacting with the biomass. 10 mg of juniper sample

of particle size 300 micron was used for this study. The biomass was heated at a constant rate of 20˚C per minute from room temperature to 240˚C and the temperature was maintained at 240˚C for three different time periods (15 minutes, 30 minutes and 60 minutes). After the isothermal stage, the samples were heated again up to 1000˚C at a heating rate of 20˚C per minute. Two different mediums (N_2 and CO_2) were used to study the mass loss behavior during the torrefaction stage (isothermal period). Fig. 22 shows the mass loss for different mediums at three different residence times.

It can be seen that lower residence time (15 minutes) did not have any impact on the mass loss upon using CO_2 as similar mass losses were observed with both mediums. However with increase in residence times (30 and 60 minutes), using CO_2 resulted in higher mass loss indicating a mild effect of the reaction of CO_2 with biomass carbon at higher residence times. Biomass treated with different mediums will have different kinetic parameters. Effect of the pretreatment mediums on the kinetic parameters of biomass will be presented later in the MVR results section.

5.4.3. Energy yield

Pretreated biomass with higher fixed carbon and lower oxygenated compounds and moisture content will have higher heating value than the raw virgin biomass. However in order to account for the mass loss associated with the pretreatment process, a term called Energy yield is used and is defined according to Eq. (39) [121].

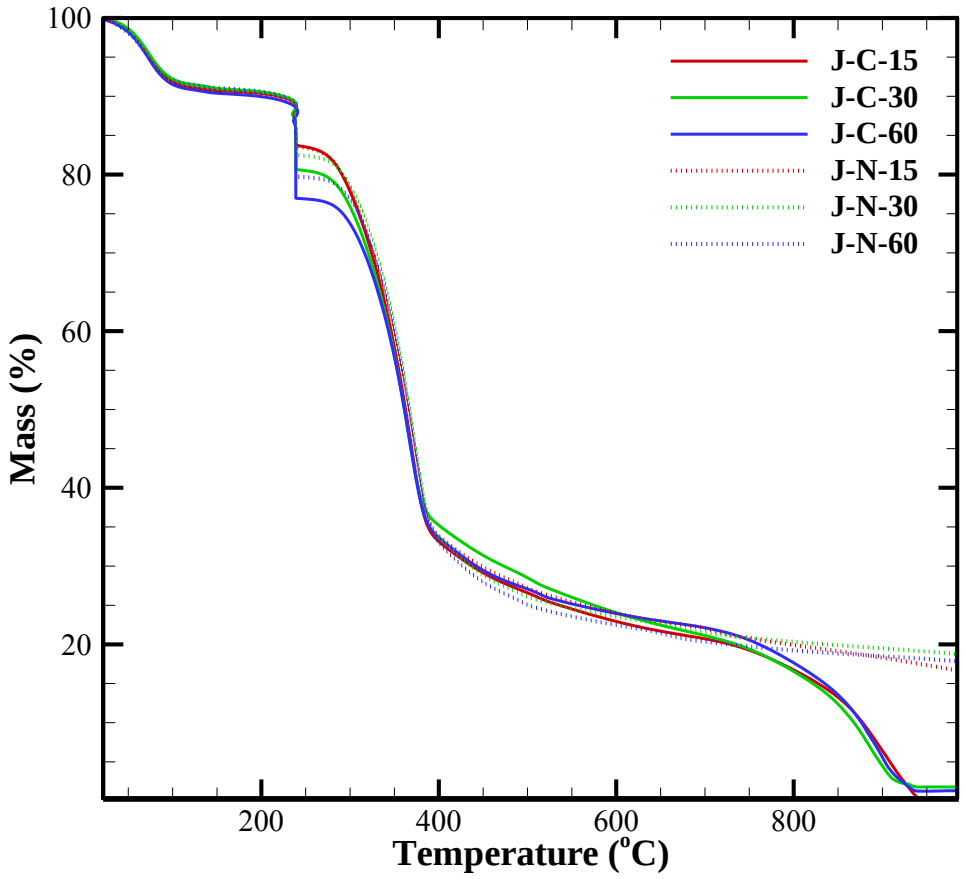

Fig. 22. Mass loss behavior of juniper samples torrefied at 240˚C for different residence times using N_2 and CO_2 as the torrefaction medium in a TA instruments SDT Q600 TGA unit. J: Juniper; C: Carbon dioxide; N: Nitrogen; 15,30 and 60 denote the isothermal time period in minutes for torrefaction.

$$\text{Energy yield} = \text{mass yield}_{DAF} * \frac{HHV_{TB,DAF}}{HHV_{Raw,DAF}} * 100 \quad (39)$$

where $HHV_{TB,DAF}$ and $HHV_{Raw,DAF}$ are the dry ash free higher heating values of the torrefied biomass and raw biomass respectively. Heating value of the volatile matter of

the biomass can be estimated on a dry ash free basis according to approximate Eq. (40) [102, 122] which ignores heat of pyrolysis.

$$HHV_{fuel,DAF} = VM * HHV_{VM} + (1 - VM) * HV_{FC} \quad (40)$$

where $HHV_{fuel,DAF}$ is the average dry ash free heating value of the biomass, VM is the fraction of volatile matter in the biomass, HHV_{VM} is the heating value of the volatile matter and HV_{FC} is the heating value of fixed carbon. Using Eq. (40) the average heating value of the VM for mesquite and juniper are estimated to be 17,000 kJ/kg and 18,400 kJ/kg on a dry ash free basis. As a first approximation, Eq. (40) can be used to estimate the increase in heating value of the treated biomass with respect to the raw biomass when some of the volatiles are released during pretreatment. Fig. 23 is a plot of the results from the model and experiments. In the model, it was assumed that the heating value of the volatile matter remains constant and does not change throughout the pyrolysis process.

However it can be seen that the variation of heating value with respect to the amount of volatile matter released was much higher in the experiments than the model value due to the variation in VM heating value i.e. the approximate model presumes that HV of volatiles remain constant. As the oxygenated compounds are released the heating value of the remaining volatile matter in the biomass will have a higher value than the initial heating value of the biomass VM. It can also be observed from Fig. 23 that juniper

with lower particle size shows a higher VM release at lower temperatures resulting in higher heating values of the torrefied biomass.

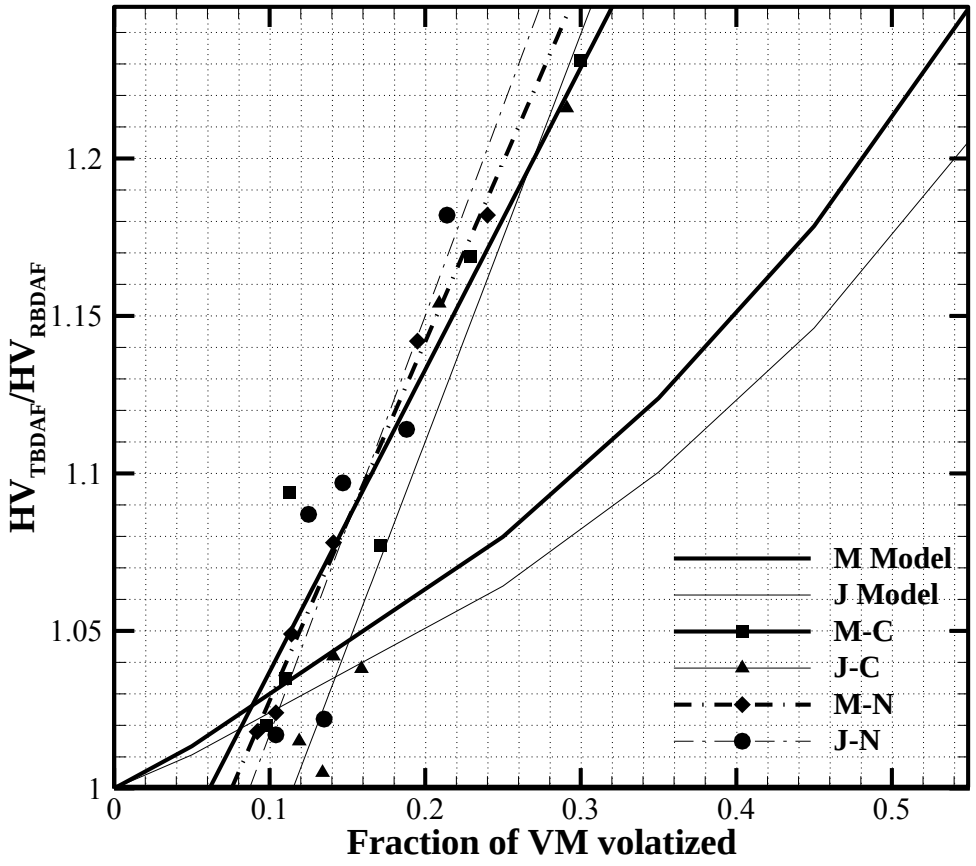

Fig. 23. Variation of biomass heating value with release of VM from the biomass. M model and J model represents the modeled increase in the heating value of mesquite and juniper respectively with release of VM.

Both the pretreatment mediums showed comparatively similar loss in volatile matter at temperatures below 250 °C and higher mass loss at higher temperatures for the mesquite samples. However juniper shows a higher release in VM when pretreated with CO_2.

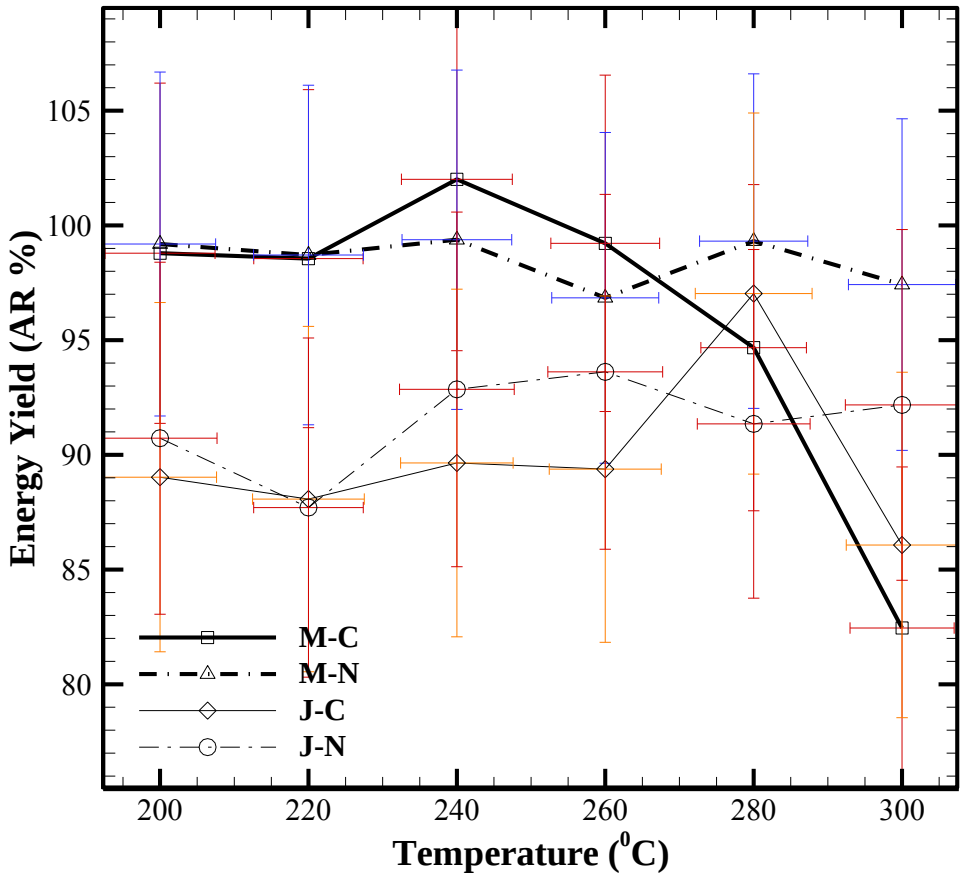

Fig. 24. Variation in the energy yield for both mesquite and juniper samples. Uncertainty for all the measurements was around 7%.

The energy yield of the torrefied samples obtained using Eq. (38) is presented in Fig. 24. A rise in the energy yield value indicates an increase in heating value and lower mass loss behavior at that particular temperature. Both mesquite and juniper showed an increase in energy yield at temperatures around 250˚C which suggested that this is the optimum temperature for torrefaction of these woody biomass samples. Though further increase in temperature shows an increase in energy yield for juniper samples, it will result in higher loss in combustible volatile matter from the biomass. Typical temperatures at which maximum volatile release rate occurs is 710 K or 437˚C for coal; 604 K or 331˚C for dairy biomass, 651 K or 378˚C for juniper and 628 K or 355˚C for Mesquite [123]. All values obtained are at heating rate of 20˚C/min. Torrefaction at these temperatures will lead to very rapid volatile loss. If heating rate is raised to 100˚C/min, these temperatures raise from 25 to 50˚C. This is because of lower residence time available for the release of the volatile matter from the biomass. Some volatile matter will remain within the samples which shifts the peak volatile release point to higher temperatures. The recommended temperature of 250˚C is much below these temperature values. Though mesquite has an energy yield which is greater than the heat content of the raw biomass it can be attributed primarily to the loss of oxygenated compounds in the volatile matter and there is also an uncertainty associated with the measured heating values.

5.4.4. ANOVA of the experimental results

The results obtained from the torrefaction experiments were tested for statistical significance using ANOVA. A P-value less than 0.05 will indicate that the results obtained are not due to random effects and are significant [124]. Two factor (temperature and sample type) ANOVA was done for the mass yield and energy yield results. Table 18 shows the two factor ANOVA results for the mesquite and juniper samples.

Table 18. Two factor ANOVA for mass and energy yield of mesquite and juniper.

Sample	Between temperature P-value	Between treatment medium P-value
Mesquite-mass yield	1.07E-02	1.73E-01
Juniper-mass yield	7.23E-03	5.32E-01
Mesquite-energy yield	9.23E-05	1.82E-02
Juniper-energy yield	8.10E-03	8.67E-01

The P-value obtained for the mass yield and energy yield was below 0.05 for the between temperatures values indicating that the temperature affects the mass loss and energy yield significantly. However the difference between the treatment mediums was not significant as the P-values were more than 0.05 for mesquite and juniper mass yield. This indicates that similar mass losses were observed for both the mesquite and juniper samples when different torrefaction mediums were used for torrefaction. The treatment medium did have a significant effect for the case of mesquite energy yield as the P-value was 1.82E-02. Juniper did not show significant differences with respect to treatment

mediums used for torrefaction at lower temperatures and hence the P-value for juniper was 0.867.

5.4.5. DTA analysis of the samples

Mesquite and juniper samples were torrefied in the TGA instrument using nitrogen and CO_2. DTA traces were obtained along with the weight loss trace during the torrefaction period. Fig. 25 shows the DTA plot and weight % for juniper sample torrefied at 240˚C for 30 minutes. DTA is plotted with respect to time and TGA trace (Fig. 26) is plotted with respect to temperature. The use of CO_2 as the pretreatment medium causes an increased mass loss. DTA trace gives the difference in sample temperature during torrefaction in CO_2 and N_2. Torrefaction is known to be slightly exothermic, although many times moisture evaporation (endothermic) usually dwarfs the heat released from torrefaction.

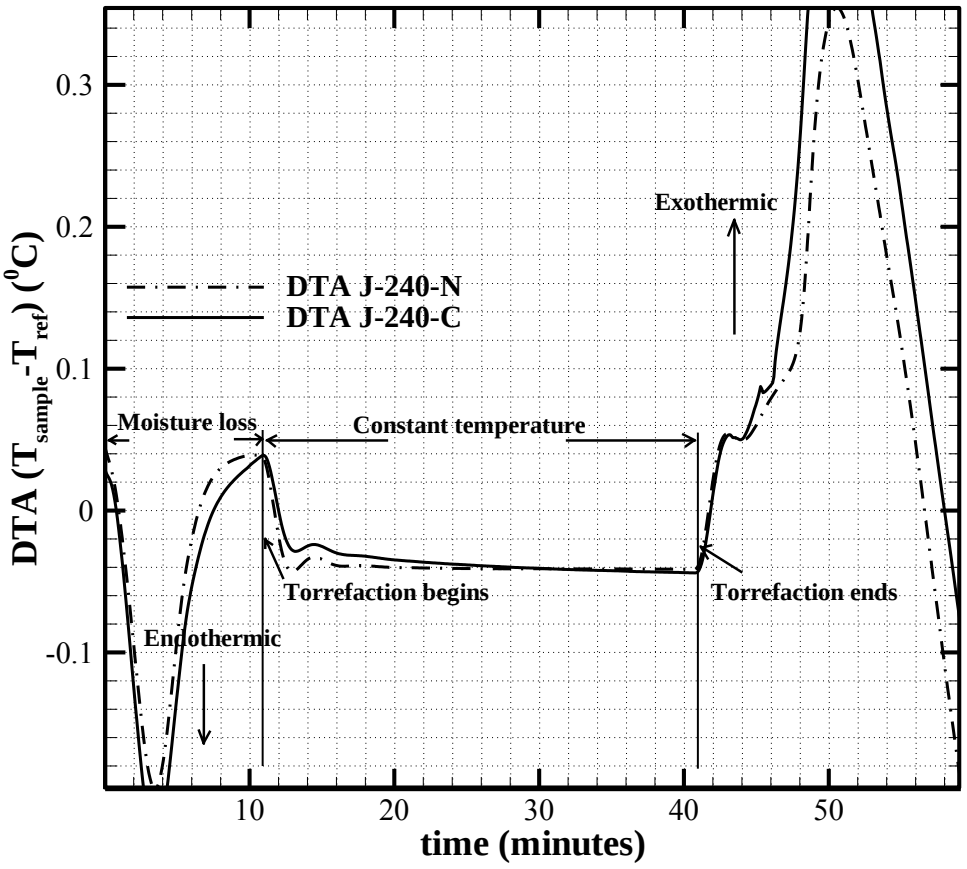

Fig. 25. DTA trace for torrefaction of juniper at 240˚C using nitrogen and carbon dioxide. DTA trace shows the differential thermal analysis with respect to time.

A slight endothermic reaction was observed when CO_2 was used as the torrefaction medium after 15 minutes indicating the time dependence of endothermic Boudouard reaction.

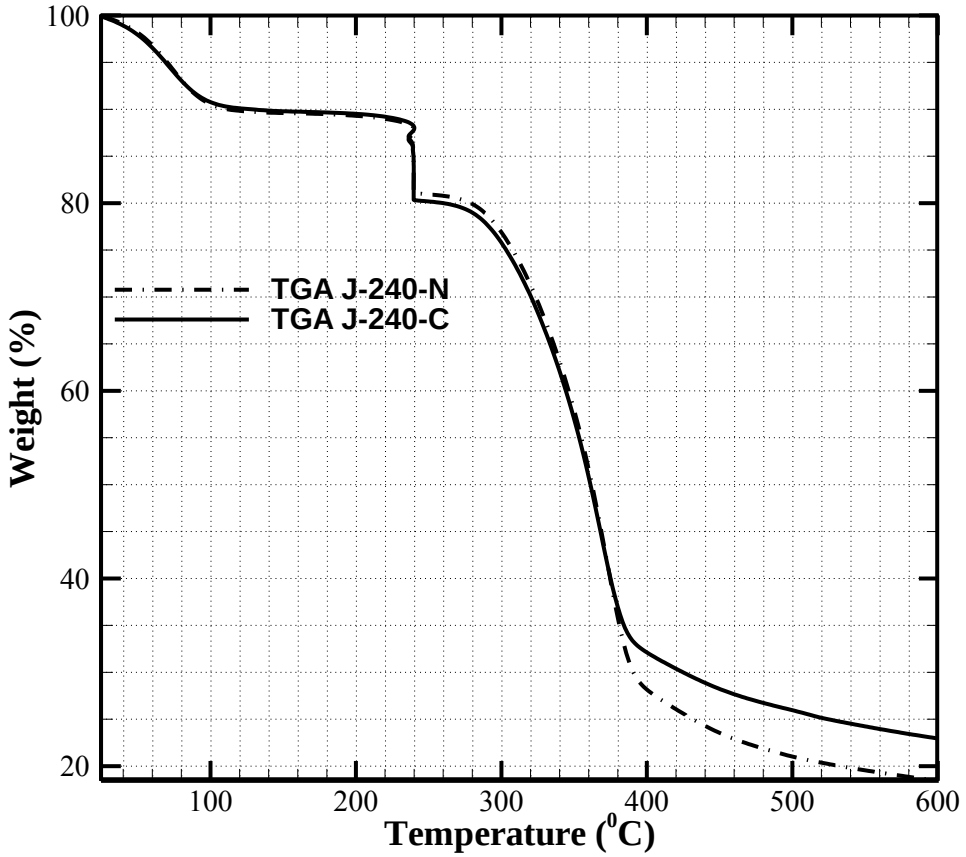

Fig. 26. TGA trace for torrefaction of juniper at 240˚C using two different mediums. TGA trace shows the weight loss with respect to temperature.

5.5.Grindability of torrefied samples

Torrefaction has been proved to improve the grindability of biomass resulting from breakdown of fibres and increased porosity of the pretreated biomass [125, 126]. In the present study, samples treated in nitrogen and CO_2 are ground for a constant time period (20 minutes) in a grinding mill. The total energy consumed by the Grinding mill

for grinding the samples for 20 minutes was estimated to be 0.8 MJ. Size distribution of the ground samples was studied. Fig. 27 and Fig. 28 shows the size distribution of mesquite samples pretreated in CO_2 and N_2 respectively. Size distribution of a sub-bituminous powder river basin (PRB) coal ground in a vortec mill and raw mesquite ground for 20 minutes in the grinding mill is also presented for comparison. It should be noted that the PRB coal was ground in a vortec mill for a sufficient time so that 70% of particles are less than 75 micron. However the torrefied biomass was ground only for 20 minutes to study improvement in grindability. Results obtained from the size distribution of torrefied juniper ground in the grinding mill for 20 minutes exhibited a trend similar to mesquite on using CO_2 and N_2. Appendix D has the results on size distribution obtained from the grinding studies on torrefied juniper.

It can be observed from Fig. 27 and Fig. 28 that the use of CO_2 as the pretreatment medium improves the grindability of the biomass. Higher percent of ground samples pass through the smaller sieves indicating better size reduction. Analysis of Sauter Mean Diameter (SMD) defined according to Eq. (41) [102] will give a better understanding on the grindability of pretreated biomass.

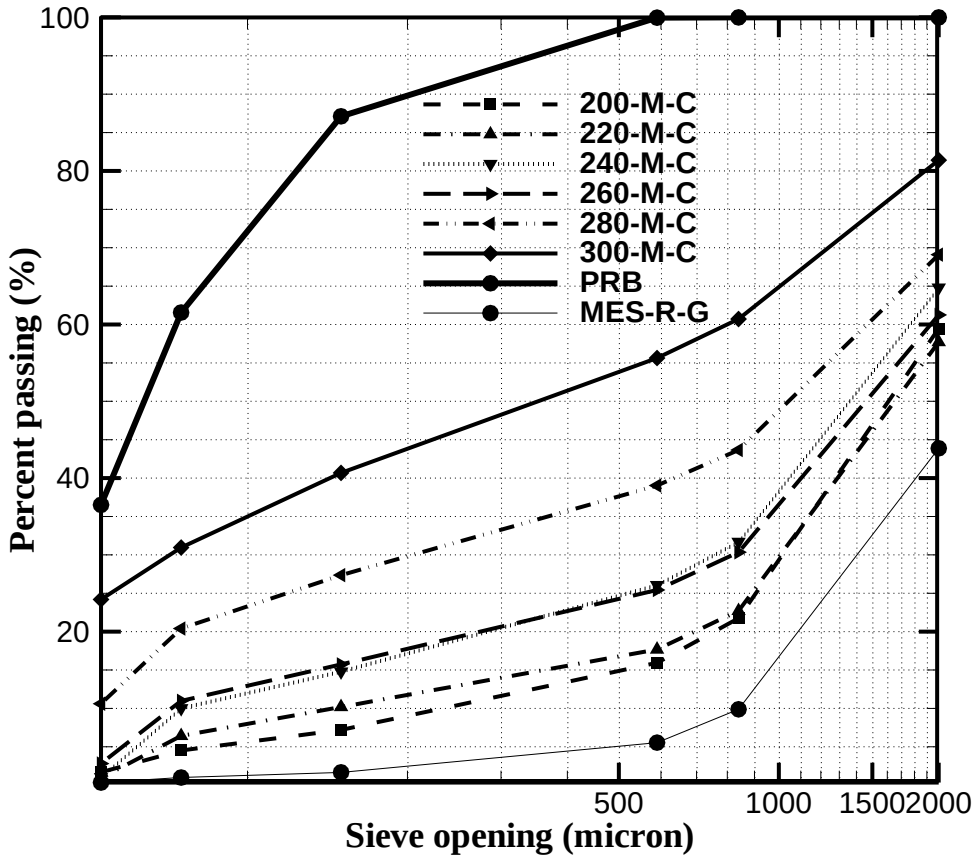

Fig. 27. Comparison of grindbility of the CO_2 pretreated mesquite expressed according to the percent biomass passing the sieves of different sizes. MES-R-G refers to raw mesquite samples ground for 20 minutes in the grinding mill.

$$\text{Sauter Mean Diameter (SMD)} = \frac{\sum N_i d_{pi}^3}{\sum N_i d_{pi}^2} \tag{41}$$

Where dp is the diameter of the particle collected in each sieve and N is the number of particles in each size group.

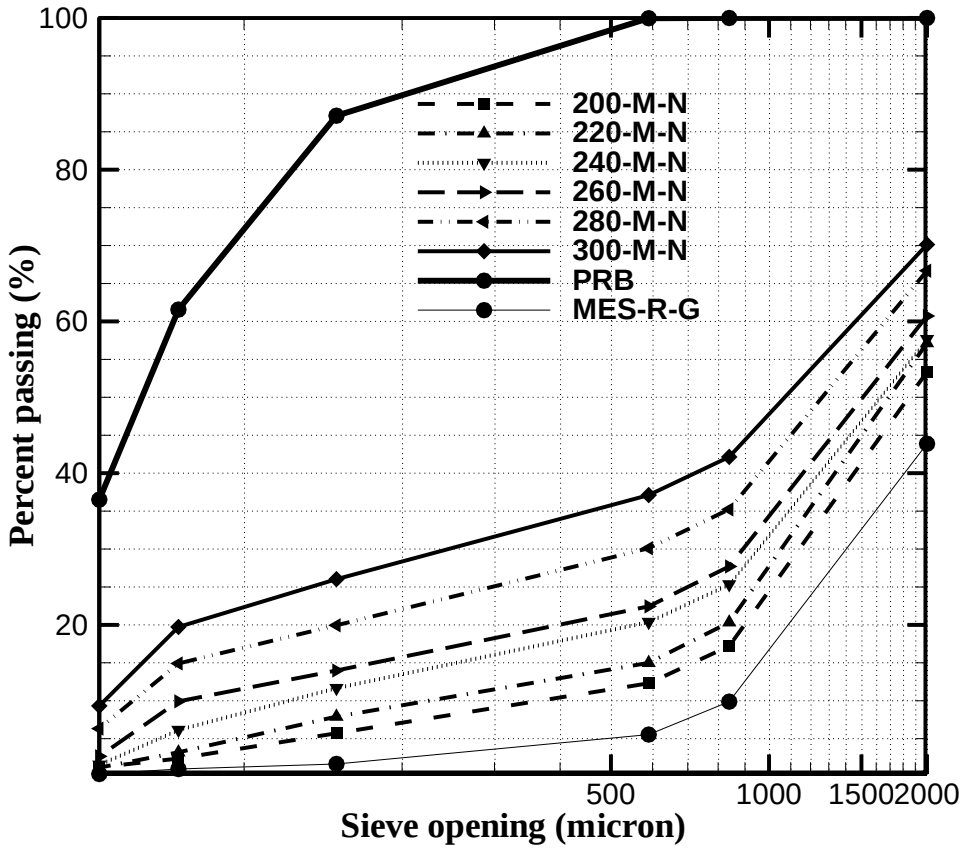

Fig. 28. Grindability of Mesqutie torrefied in Nitrogen.

Fig. 29 shows the variation in Sauter Mean Diameter (SMD) of the samples torrefied in CO_2 and N_2. The SMD values obtained showed a decrease in the mean diameter of the samples torrefied in CO_2 for both mesquite and juniper indicating improved grindability. Rosin rammler plot obtained for the ground samples showed an improvement in the fineness of the particles torrefied in CO_2 in comparison to N_2

torrefaction. Eq. (34) [127] (Section 5.2) was used to get the values for rosin rammler plot which are used commonly to study the size distribution of ground coal particles.

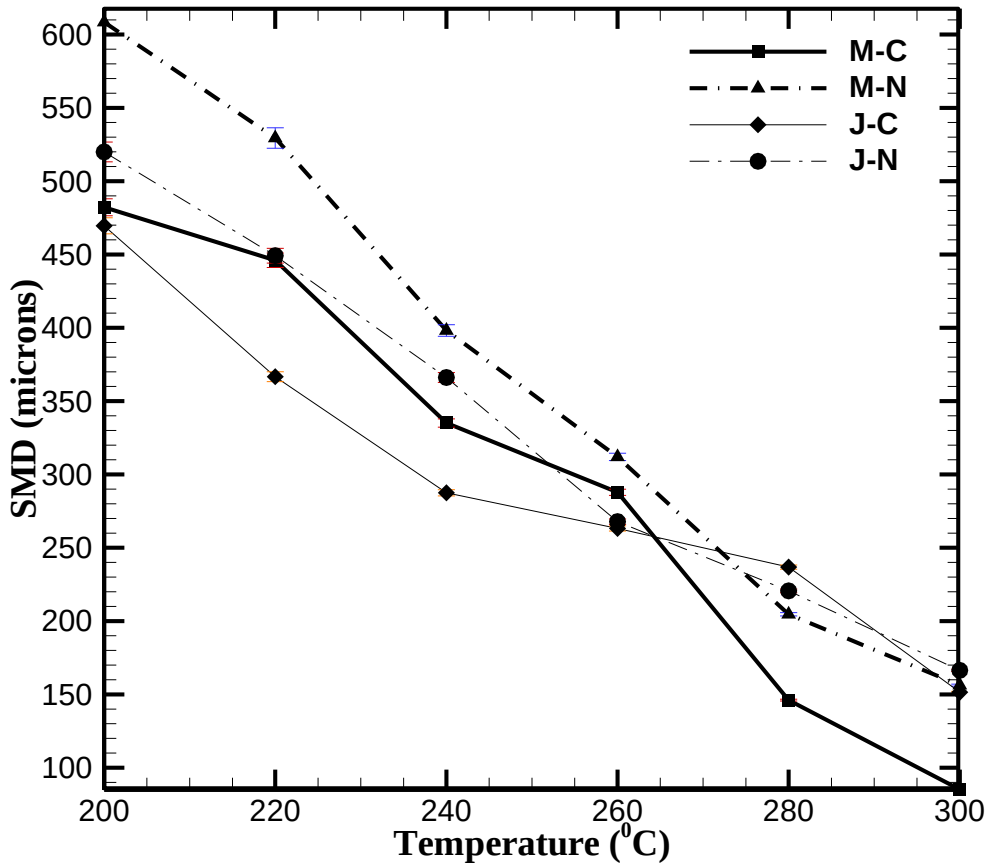

Fig. 29. Variation of SMD of the ground torrefied samples of mesquite and Juniper.

An increase in the value of b indicates an increase in the fineness of the particles. For the current set of data obtained, application of Eq. (34) yielded an increase in the value of constant b (Table 19) showing an improvement in the fineness of the ground

torrefied samples with increase in temperature and using CO_2 as the pretreatment medium.

Table 19. b values determined for the torrefied ground samples. M: Mesquite; J: Juniper; C: CO_2; N: N_2.

T (˚C)	M-C	M-N	J-C	J-N
200	0.00041	0.00036	0.00067	0.00068
220	0.00043	0.00041	0.00073	0.00068
240	0.00057	0.00044	0.00074	0.00076
260	0.00047	0.00044	0.00079	0.00073
280	0.00066	0.00054	0.00082	0.00086
300	0.00143	0.00066	0.00107	0.00098

Such an improved grindability can be linked to the increase in the number of pores or in other words increased porosity of the samples pretreated in CO_2 which is supposed to be non-reacting under the temperature range used for torrefaction. BET surface area analysis and SEM image analysis of the torrefied samples were done to study the effect of CO_2 medium on the development of pores.

5.5.1. Surface area analysis

BET analysis was performed on the torrefied samples using Quantachrome NOVA 4200e instrument. The samples tested were ground and sieved to a size of between 300 to 500 micron. The samples were initially degassed for 16 hours at 75˚C to remove any adsorbed moisture and impurities. The adsoption isotherms were then

obtained at a constant temperature of 77K using nitrogen as the medium for adsorption to determine the surface area of the torrefied samples.

Samples torrefied at 300˚C under N_2 and CO_2 were analyzed for their surface area. The tests were done thrice on each of the samples and the average of the obtained result is shown in Table 20. Adsorption isotherms obtained for the samples resembled a typical type-I isotherm [128] for samples with micropores (pores smaller than 2nm). Table 20 shows the results obtained from the BET analysis.

Table 20. BET surface area of the ground torrefied biomass [60]. The tests were repeated thrice for each of the samples.

Fuel	**Medium**	**BET surface area (m^2/g)**	**Total pore volume (cc/g)**	**Avg Pore radius (Å)**
300-J-C	**CO_2**	0.36 +/- 0.04	0.000182	10.12
300-J-N	**N_2**	0.23 +/- 0.15	0.000116	9.708
300-M-C	**CO_2**	0.75 +/- 0.35	0.000365	9.845
300-M-N	**N_2**	0.58 +/- 0.28	0.000275	9.746

It is noted that BET surface area in CO_2 is 55% more for Juniper and 29% more for mesquite. The samples pretreated with CO_2 showed a comparatively higher surface area when compared to the samples torrefied with N_2. The average pore radius obtained was much higher than the average diameter of CO_2 (3.94 Å) and N_2 (3.798 Å) molecules estimated using collision diameter values [85]. Hence the CO_2 and N_2 molecules can easily diffuse into the voids created in the biomass particles at higher residence times. Though the numbers for the surface area are much smaller, it should be noted that these are the numbers obtained for the ground samples. This is consistent with the study

conducted by Pilon and Lavoie [129] and Gray et al. [130]. Pilon and Lavoie [129] showed the BET surface area of the ground switch grass sample treated at 300˚C also to be less than 1 m^2/g. Gray et al. [130] listed the surface area of the wood char obtained from the pyrolysis of wood waste at a temperature of 330˚C in nitrogen environment to be less than 0.8 m^2/g. The effect of treatment temperature on the apparent char surface area was reported by Valenzuela-Calahorro et al. [131]. Fig. 30 shows the plot of surface area of char determined at various temperatures.

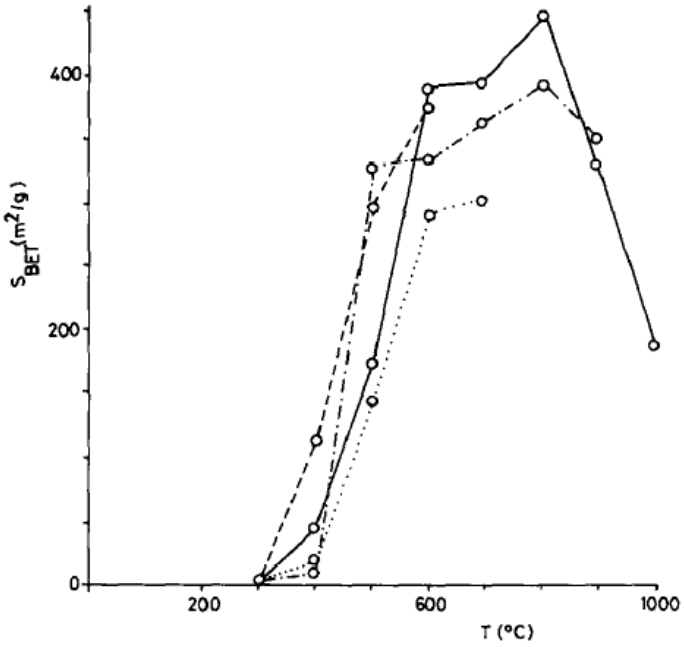

Fig. 30. Effect of temperature on the apparent surface area of char obtained from holm-oak wood. Different symbols stand for methods used to pyrolyze the char. Adapted from [131].

The surface area of the char pretreated at lower temperatures say less than 500˚C has a low surface area as evidenced from Fig. 30. Since torrefaction is carried out at

much lower temperatures, and there is only partial pyrolysis, very high surface areas will not be observed for the torrefied samples. The external surface area per unit mass of a particle can be estimated using the following Eq. (42) [102].

$$S_{ext,m} = \frac{6}{\left(d_p \rho_p\right)} \tag{42}$$

where ρ_p is the apparent particle density and d_p is the diameter of the particle. Since the diameter of the particles of mesquite and juniper used for the current study was around 2 mm, the external surface area per unit mass was estimated to be 0.075 m^2/g assuming an apparent particle density of 400 kg/m^3 for raw wood [126]. The results obtained from the BET internal surface area were around 0.750 m^2/g for the case of mesquite torrefied at 300˚C with CO_2 (Table 20). Further, internal surface area increases with increase in carbon burnout [102].

5.5.2. SEM image analysis

SEM images of the samples treated using nitrogen and CO_2 were obtained using JEOL JSM-7600 F. The images were obtained at a magnification of 2000x to identify the pores formed on the samples when using different torrefaction mediums. Fig. shows the SEM images of the raw juniper sample and torrefied juniper sample.

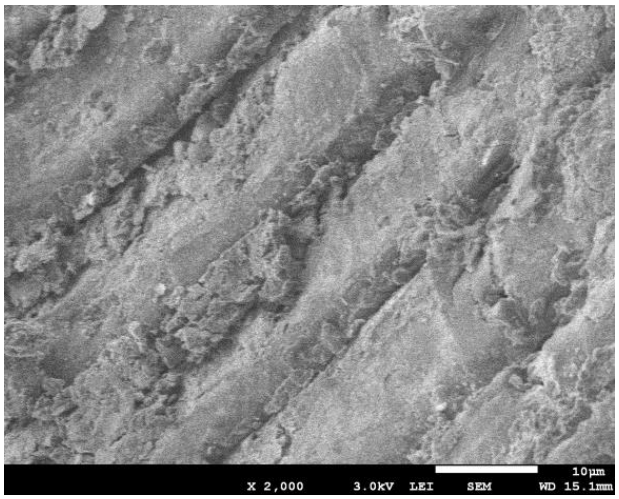

(a)

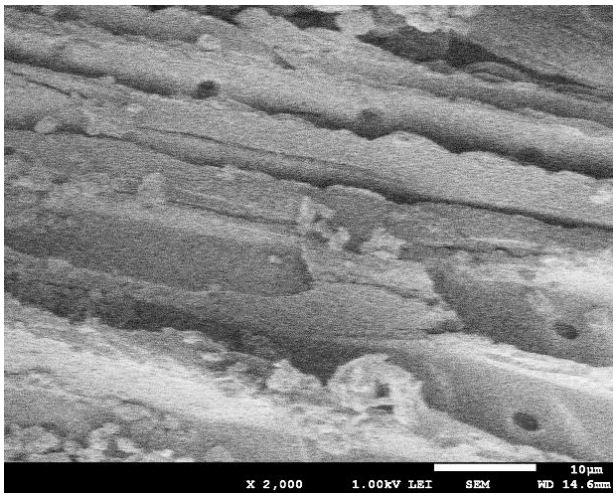

(b)

Fig. 31. SEM images. (a) Raw juniper sample, (b) Juniper sample torrefied at 300˚C with CO_2, (c) Juniper sample torrefied at 300˚C with N_2. Magnification of 2000 was used and the scale is 10 micron.

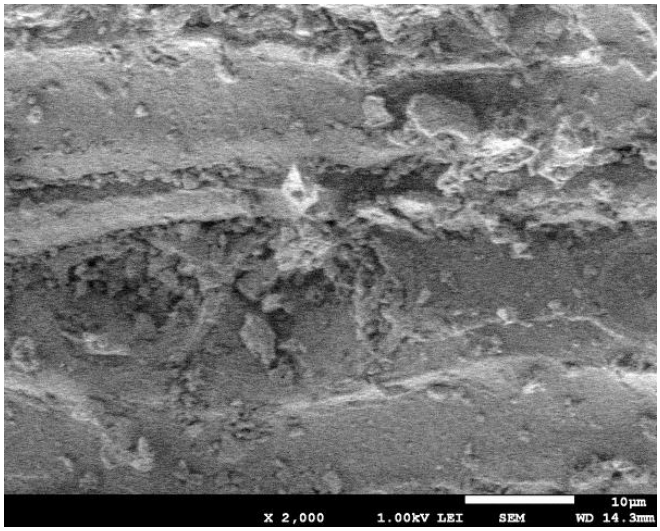

(c)

Fig. 31. Continued.

It is evident from the SEM images that more pores were visible in the samples torrefied using CO_2. It is clear from the BET analysis and SEM images that Boudouard reaction indeed has a minor effect on the torrefaction temperature range owing to increased residence times. Though not much fixed carbon reacts with the CO_2 during the pretreatment process, sufficient reaction occurs to form small voids on the surface of the biomass i.e. creating more pore space. These voids pave the way for the release of volatile matter from the biomass. Increased mass loss on using CO_2 as the torrefaction medium can be attributed to this behavior of the biomass.

The effect of increased porosity on using CO_2 as the torrefaction medium can also be observed from the proximate analysis results of the samples (Table 17). The

amount of volatile matter in the biomass treated with CO_2 on a dry ash free basis was lower than the biomass treated with N_2 indicating more volatile matter was removed from the pores. A corresponding increase in FC was observed with decrease in VM within the torrefied biomass.

5.6.TGA-DTG results of raw and torrefied samples

5.6.1. Raw biomass and coal

Raw biomass samples were initially tested in the TGA to study its mass loss characteristics in comparison to PRB coal. Fig. 32 shows the TGA curve obtained during the pyrolysis of raw mesquite, juniper and coal on a dry basis. The samples were heated at a rate of 20˚C per minute up to 900˚C. Since coal has higher percentages of fixed carbon and ash, higher mass was retained at the end of pyrolysis which is representative of the fixed carbon and ash. Biomass with higher volatile matter shows much higher mass loss. Differential thermograms (DTG) of the samples can be used to estimate the percentages of different components in the sample and study the release of volatile matter in the samples. A sample with higher hemicellulose will exhibit a hump at temperatures around 200-300˚C indicating decomposition of hemicellulose in the sample. Fig. 33 shows the DTG curves of the biomass samples and coal. Mesquite being a hardwood with higher hemicellulose content shows a hump at lower temperature. The rapid release of volatile matter from the biomass samples at temperatures around 300-500˚C can also be observed from the DTG curve. Peak of the DTG curve is higher for the case of biomass fuels than the PRB coal.

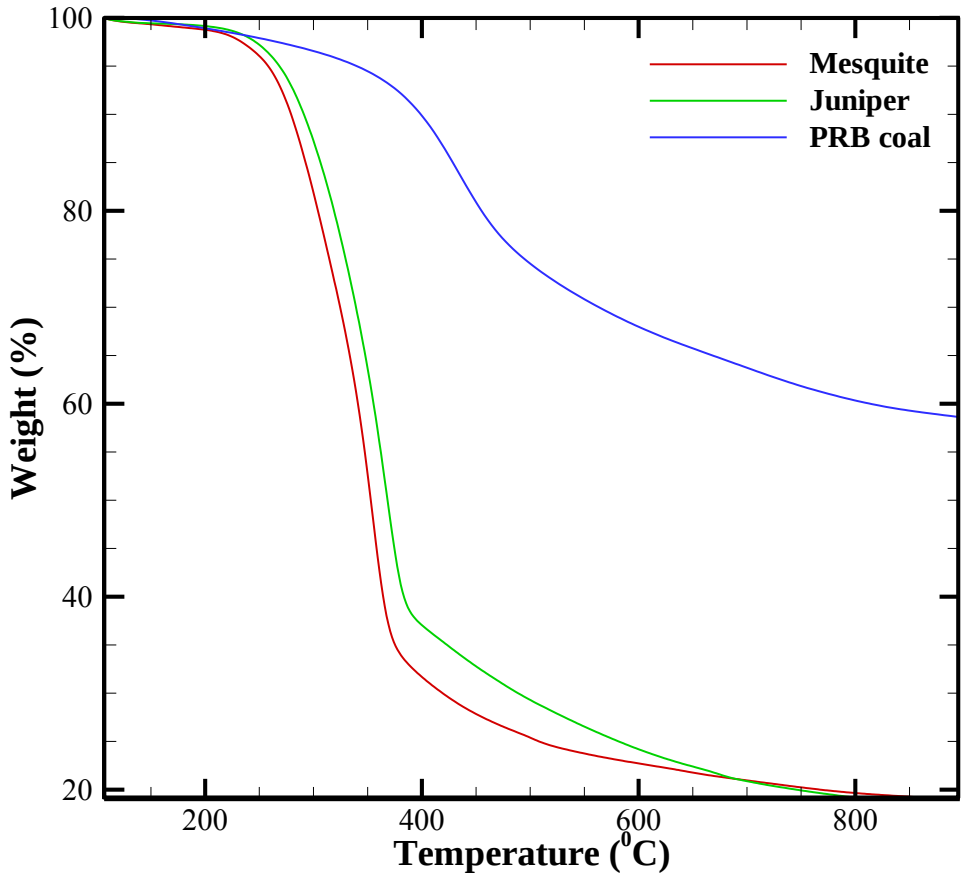

Fig. 32. TGA curves for the pyrolysis of raw mesquite, raw juniper and PRB coal at a heating rate of 20˚C per minute with nitrogen as an inert medium, d_p = 580 – 840 micron.

The peak release of volatile matter occurs between 300-350˚C for both the biomass samples. The release of volatile matter at lower temperatures from the biomass samples also indicates lower activation energy for devolatilization from the biomass when compared to coal.

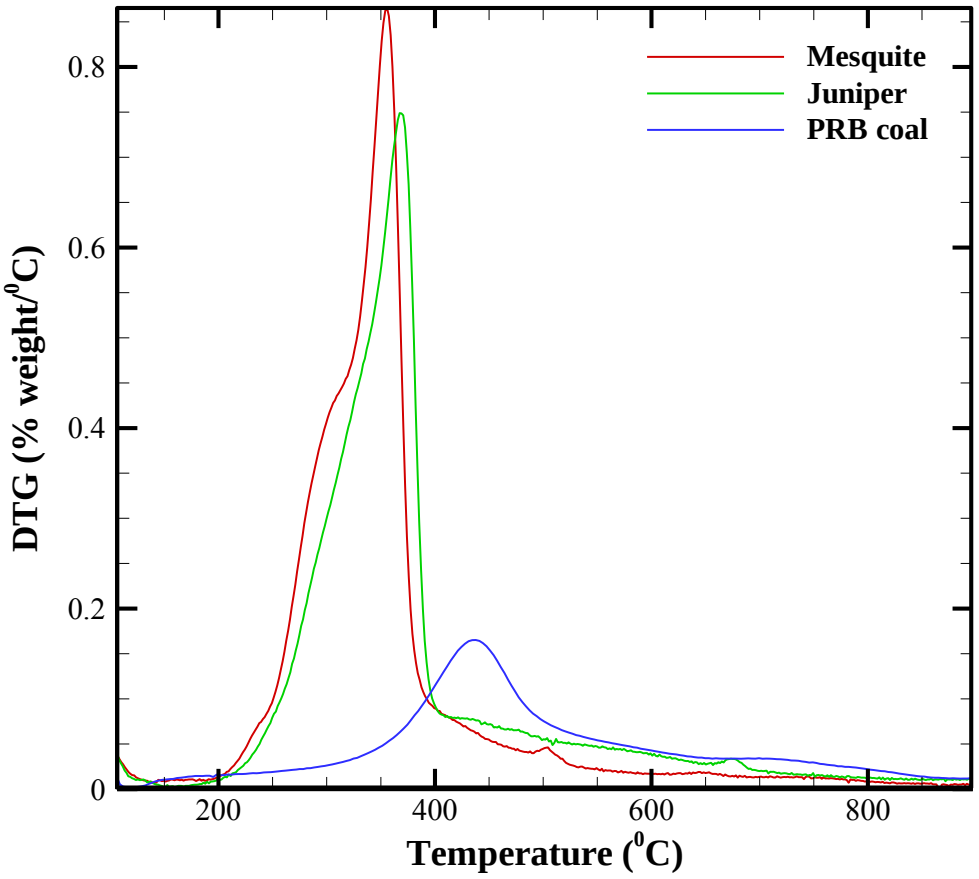

Fig. 33. DTG (% weight/˚C) curves obtained from the pyrolysis data of raw mesquite, juniper and coal. d_p = 580 – 840 mircon.

5.6.2. Torrefied biomass

The samples torrefied using different torrefaction mediums were also pyrolyzed in a nitrogen environment from room temperature to 900˚C. Fig. 34 shows the DTG curve obtained for the pyrolysis of mesquite samples torrefied in nitrogen. As it can be observed from Fig. 34, the hump which is visible at lower temperatures and for the raw

mesquite has decreased with increase in temperature. Hemicellulose which has a lower activation energy as seen in the TCM torrefaction model, is released at a faster rate when compared to the other two components.

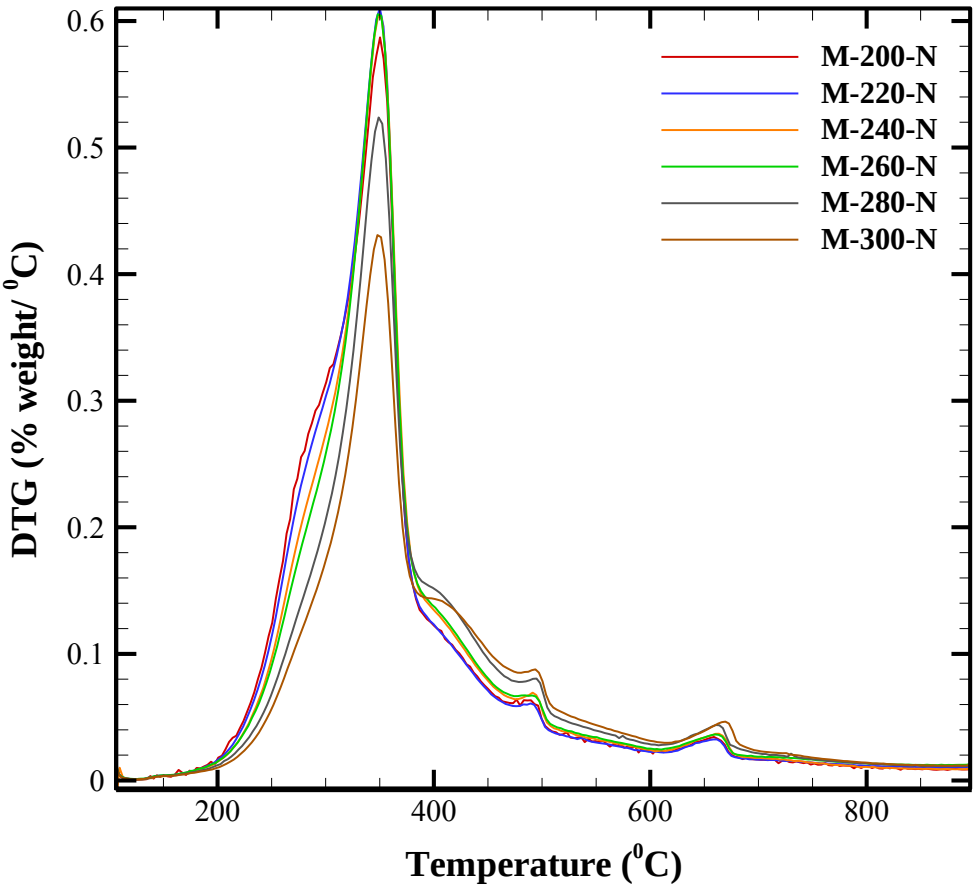

Fig. 34. DTG curves for mesquite samples torrefied in nitrogen at different pretreatment temperatures.

Also the peak observed at temperatures around 345-350˚ C in the DTG curve which indicates the peak of cellulose release in the biomass also decreases with increase

in pretreatment temperature indicating volatilization of cellulose during torrefaction process. Fig. 35 shows the DTG curves obtained from pyrolysis of mesquite torrefied in CO_2.

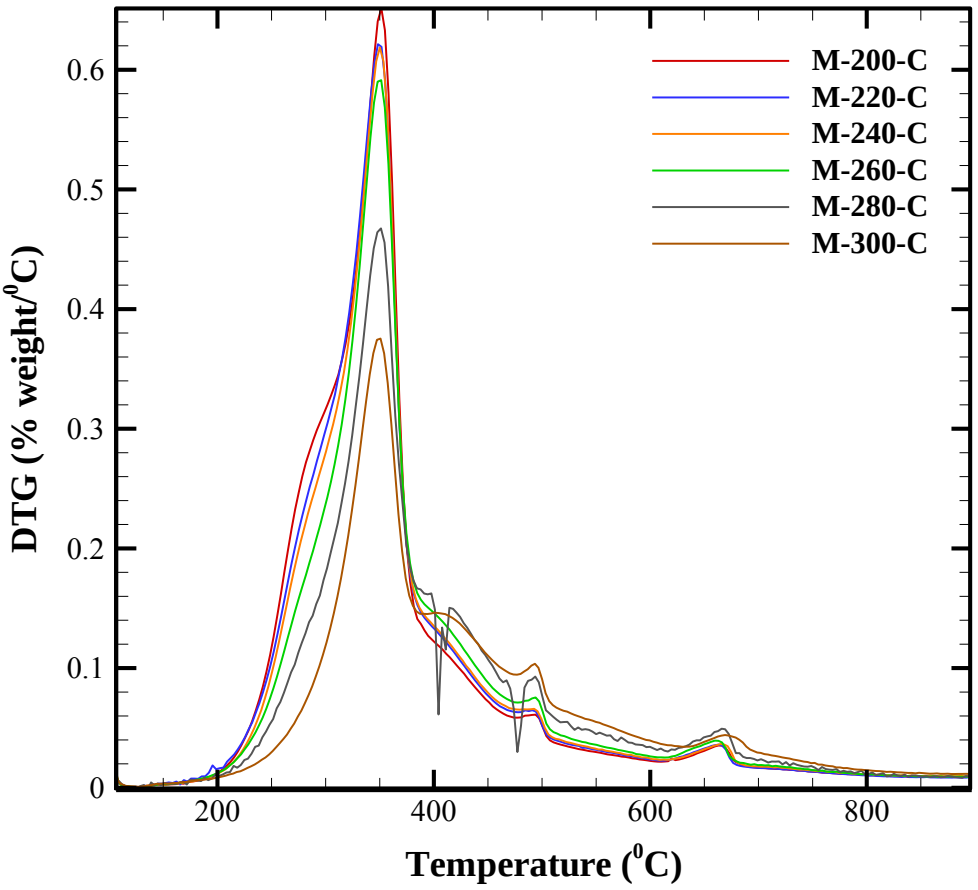

Fig. 35. DTG curves for mesquite samples torrefied in carbon dioxide at different pretreatment temperatures.

Lower cellulose content at higher torrefaction temperatures is evident from lower peak release rates (0.37 for M-300-C) when compared to the DTG curves of N_2 torrefied mesquite (0.42 for M-300-N) (Fig. 34). (Dips exhibited by the DTG curves are due to experimental noise caused by the pan vibration). Torrefied juniper samples also exhibited a comparable trend with respect to degradation of the components with increase in pretreatment temperature.

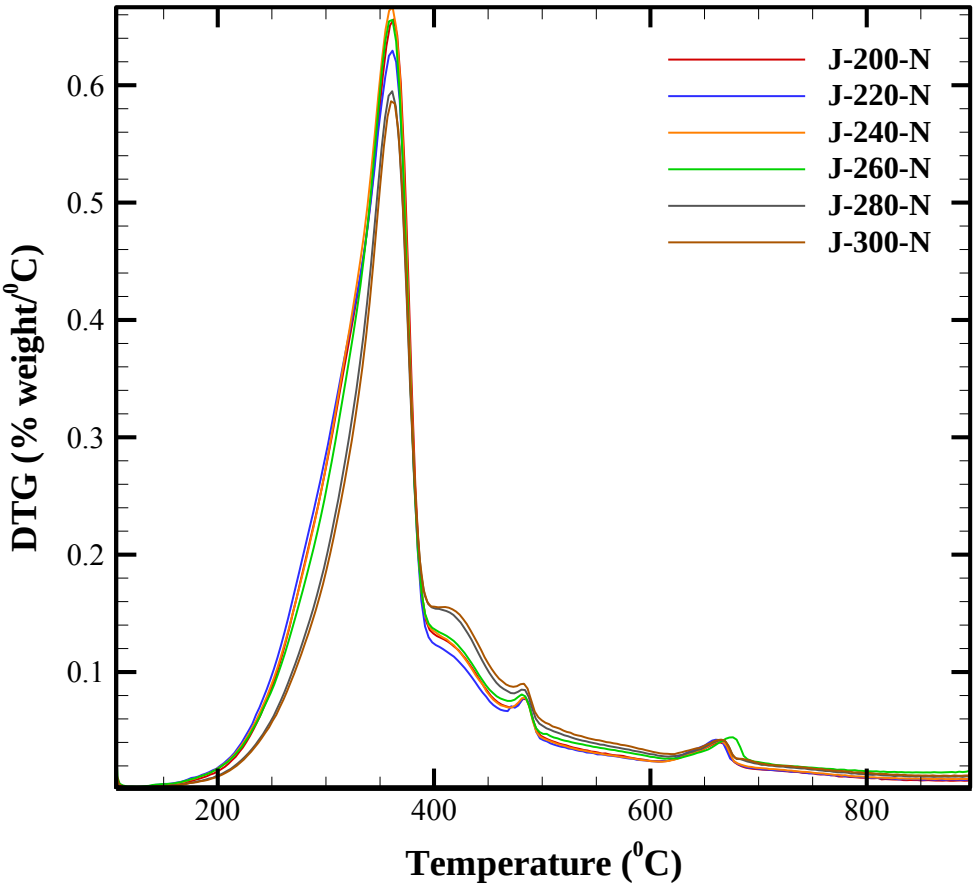

Fig. 36. DTG curves for juniper samples torrefied in nitrogen.

Fig. 36 and Fig. 37 shows the DTG curves obtained from the pyrolysis of juniper torrefied with nitrogen and carbon dioxide respectively. Similar results were observed when smaller samples of juniper and mesquite (10 mg) were torrefied and pyrolyzed in a TGA unit [51].

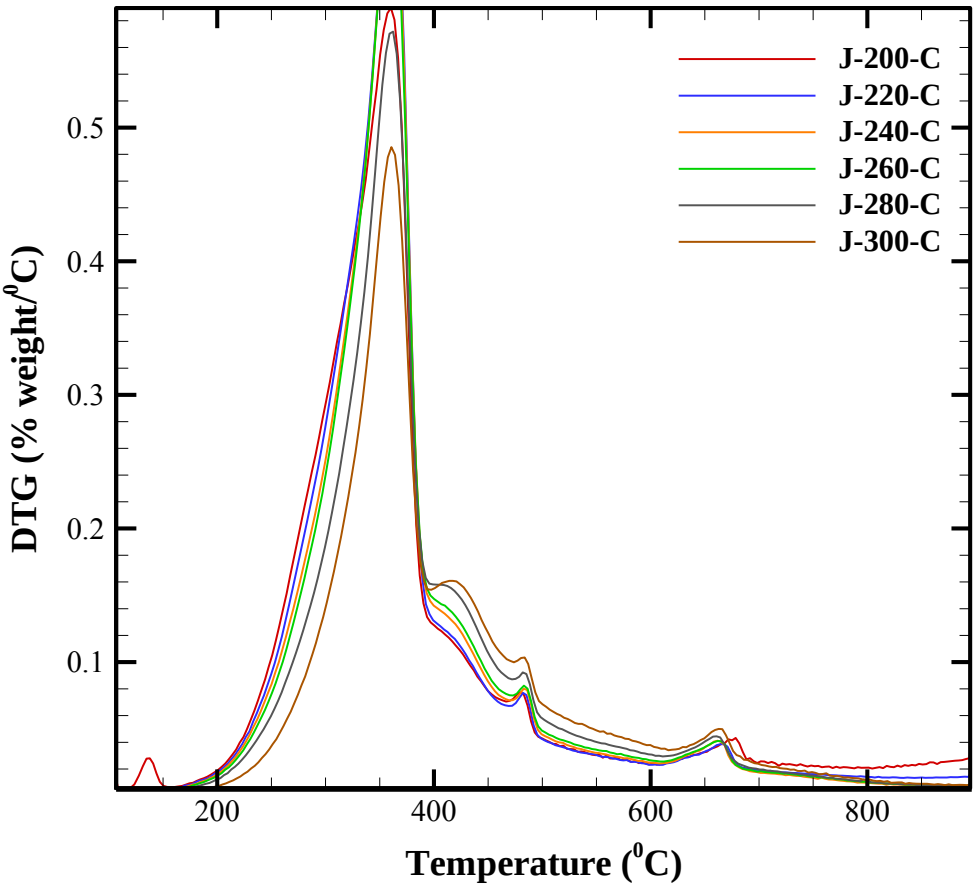

Fig. 37. DTG curves for juniper samples torrefied in carbon dioxide.

Results obtained from the pyrolysis of raw and torrefied biomass samples were used to extract the kinetics based on maximum volatile release method (MVR).

5.7.Kinetics of samples: MVR method

The maximum volatile release method can be used to determine the temperature at which the release rate of the volatile matter is the maximum. It is based on single reaction model and the overall activation energy for the single reaction can be determined. The maximum volatile release rate point $|(dm_v/dT)_{max}|$ was used to extract the kinetics of pyrolysis of biomass. At peak point, T_{max}, $|(dm_v/dT)_{max}|$ and m_v are known. Out of the three T_{max} and $|(dm_v/dT)_{max}|$ were used first to extract the kinetics by assuming first order. The third one i.e., mv at peak point is later used to extract the order of pyrolysis. Eq. (11) to Eq. (15) from section 4.5 were used to extract the overall kinetic constants using the DAF volatile matter release data from the TGA and MVR method. The activation energy obtained for juniper and mesquite upon using the maximum volatile release method was 94300 kJ/kmol and 107900 kJ/kmol respectively when the order of pyrolysis was assumed to be unity. For orders not equal to 1, the activation energy and order of pyrolysis for mesquite was 77200 kJ/kmol and 0.52 respectively.

The kinetic constant thus extracted at the maximum point was used to model the release of volatile matter from the biomass. The accuracy of the modelled release was checked by calculating the summed squared errors between the measured mass loss and the modelled mass loss by selecting a temperature range of 490 K (100% DAF volatile matter remaining in the biomass) to 750 K (5% DAF volatile matter remaining in the

sample). The summed square errors were low for non-unity orders indicating improved accuracy of the MVR method in predicting the order of reaction. The summed square error obtained when the order was assumed to be one was 0.0798 and the error reduced to 0.0424 when non unity order was used for the modelling the volatile loss for the case of raw mesquite pyrolysis. Fig. 38 shows the predicted mass loss curve for mesquite pyrolysis using the MVR method.

Further the maximum volatile release method can be extended to model the pyrolysis process in multiple steps by dividing the pyrolysis process into different reaction zones as done earlier in a number of pyrolysis studies [32-35]. Identification of the T_{max} will enable researchers in the field of torrefaction to understand the point of maximum volatile release from biomass. T_{max} will serve as the upper limit for the torrefaction process and hence temperatures should be well below this value to reduce the significant loss of combustible volatile matter from the biomass.

The peak point obtained from the differential thermograms (DTG) will be the temperature (T_{max}) at which maximum volatile matter release take place. MVR method using an order of unity and non-unity orders predicts the T_{max} accurately as the kinetic constants are extracted based on the T_{max} values. Further TCM was used to get the conversion of the bulk biomass sample by including the conversion of all the three components when the sample was pyrolyzed from room temperature to 900˚C in an inert environment. The release of dry ash free volatile matter from the biomass was used to determine the DTG curve. The DTG curves thus obtained from the TGA experiments,

MVR method with an order of one, MVR method with non-unity order, and from the TCM pyrolysis model results are shown in Fig. 39 for the case of mesquite.

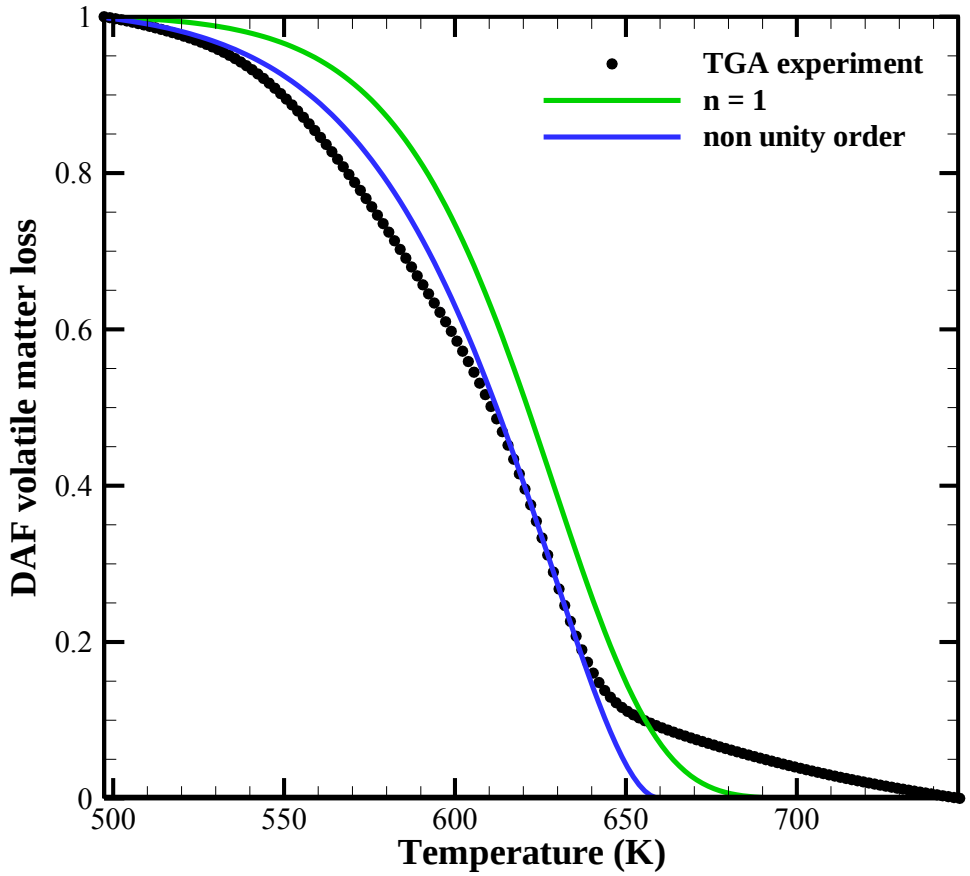

Fig. 38. Volatile matter release for the case of mesquite with increase in temperature within the TGA.

The peak mass release rate from the TGA experiment on pyrolysis of mesquite was found to occur at T_{max} of 628 K and the DTG curve determined from the TCM bulk pyrolysis data showed a maximum at 624 K (Fig. 39). Small difference between the

experimentally determined peak temperature and the peak temperature predicted from the TCM is due to the difference in composition of the three components in the mesquite sample used for TGA experiment and assumed in the TCM. This result shows that the MVR method can be used to determine the kinetics of three components.

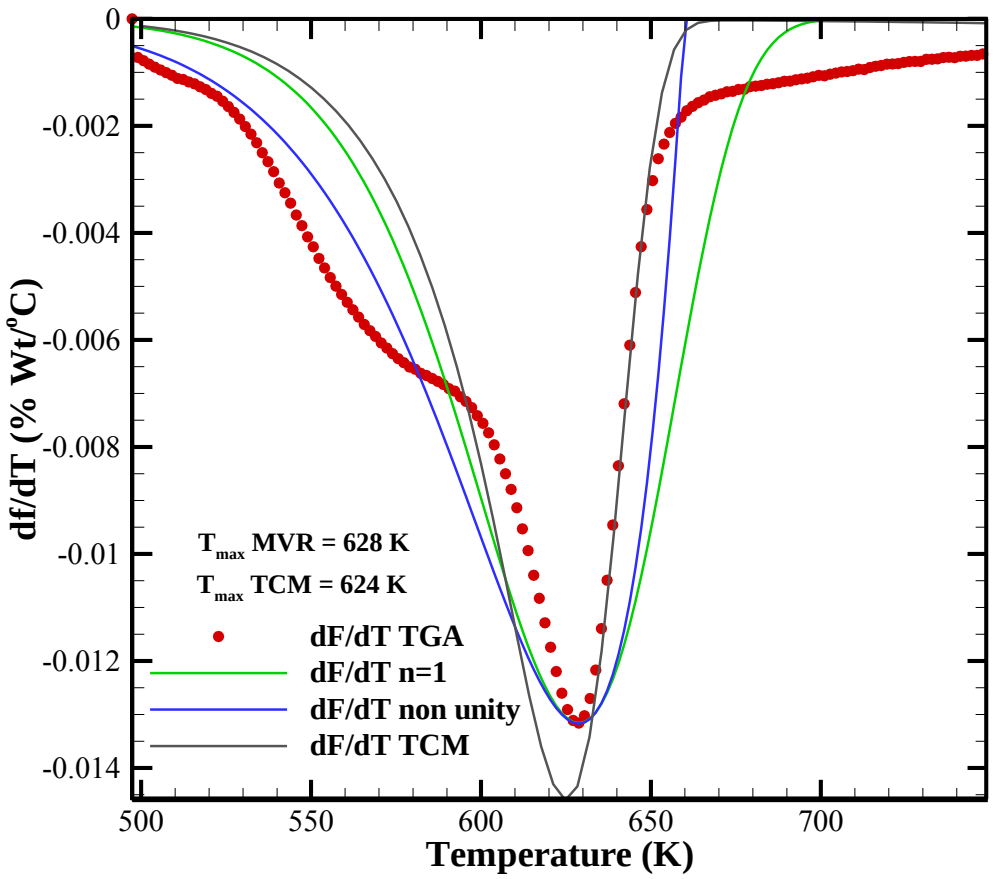

Fig. 39. DTG curves obtained from the TGA pyrolysis data of mesquite and determined using MVR method and TCM.

Determined kinetic parameters can then be utilized in modelling of torrefaction and pyrolysis of biomass. Fig. 40 plots the results obtained from the pyrolysis of juniper samples. T_{max} predicted from the TCM pyrolysis model for bulk juniper was higher than the experimentally determined values. It should be noted here that the composition of the mesquite and juniper samples were not determined experimentally and it was assumed to have the similar composition as hardwood and softwood.

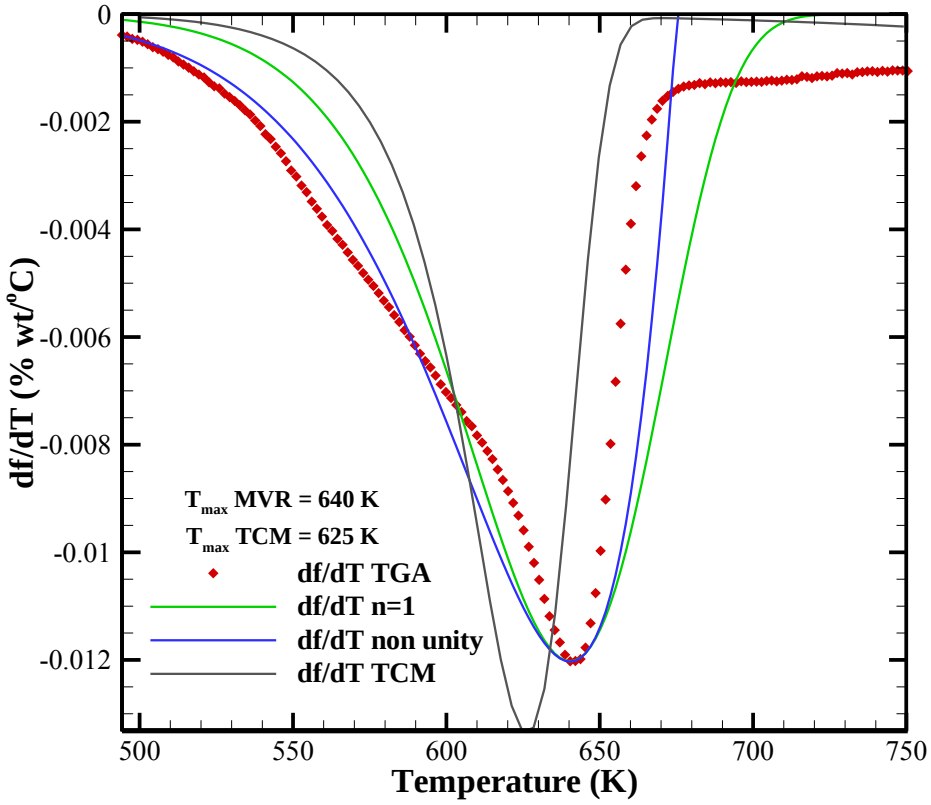

Fig. 40. DTG curves obtained from the TGA pyrolysis data of juniper and determined using MVR method and TCM.

The activation energy and pre-exponential factors determined using the MVR method for the torrefied and raw biomass samples are shown in Table 21 for cases with n = 1 and n ≠ 1. The constants obtained from pure coal pyrolysis are also shown. The activation energy for the case of n=1 for both the mesquite and juniper samples did not exhibit notable trends with pretreatment temperatures.

Table 21. Kinetic constants for the pyrolysis of torrefied and raw biomass determined using MVR. Kinetics for n=1 using T_{max} and $|dm_v/dT|_{max}$ data and kinetics for n≠1 using T_{max}, $|dm_v/dT|_{max}$ and m_v at maximum point.

	Mesquite n = 1			Juniper n = 1		
Temperature (˚C)	E (kJ/kmol)	B (1/min)	n	E (kJ/kmol)	B (1/min)	n
Raw	107861	6.E+08	1	94288	3.E+07	1
200	87278	3.91E+06	1	84526	4.45E+06	1
220	90360	8.62E+06	1	81679	2.58E+06	1
240	92116	1.04E+07	1	85120	5.15E+06	1
260	91440	1.13E+07	1	87581	5.77E+06	1
280	85056	3.45E+06	1	84705	4.79E+06	1
300	75663	6.53E+05	1	82703	3.29E+06	1
	n ≠ 1			n ≠ 1		
	E (kJ/kmol)	B (1/min)	n	E (kJ/kmol)	B (1/min)	n
Raw	77229	1.E+06	0.519	77753	1.04E+06	0.703
200	77951	6.53E+05	0.817	74711	6.30E+05	0.801
220	82751	1.98E+06	0.856	69310	2.18E+05	0.742
240	99568	4.34E+07	1.141	75024	6.87E+05	0.795
260	105042	1.56E+08	1.263	83286	2.50E+06	0.913
280	116246	1.45E+09	1.654	97654	6.27E+07	1.271
300	119428	3.50E+09	2.024	107372	4.42E+08	1.539

Powder river basin coal		
E (kJ/kmol)	B (1/min)	n
76446	1.51E+05	1.000
92211	2.53E+06	1.368

Further the summed squared errors between the predicted mass loss was much higher for reactions with n=1. Kinetic constants extracted for the non-unity order case for the torrefied samples shows an increasing trend for the activation energy with increase in torrefaction temperature. The increase in activation energy for the torrefied biomass is due to the lower amount of hemicellulose and cellulose content in the torrefied biomass. The volatile matter started releasing at higher temperatures from the samples pretreated at higher temperatures when compared to the raw biomass and biomass treated at lower temperatures. Further the kinetics of pyrolysis of powder river basin (PRB) sub-bituminous coal was also extracted using the TGA data and MVR method. The results obtained shows a comparatively higher activation energy and higher reaction order when compared to the raw biomass samples. The order of reaction of PRB coal was comparable to the samples torrefied at higher temperatures. Van Heek and Hodek [132] varied the order of reaction to model the pyrolysis of coal and concluded that increased orders favor the formation of gases from the pyrolysis of coal while lower orders favor the tar formation.

An increase in the order of reaction also indicates an increase in volatile matter release from the samples upon heating. This shows the porosity of the samples influences the release of volatile contents during pyrolysis. Coal has higher porosity when compared to the raw biomass and torrefied biomass. Porosity of biomass increases with increase in treatment temperatures. Further studies should be done to understand the mechanism behind the increasing order for the torrefied biomass samples.

5.8.Zero dimensional model

Based on the batch torrefaction studies, biomass torrefied at 240˚C was found to have the optimum mass loss. Hence both mesquite and juniper torrefied at 240˚C using CO_2 as the torrefaction medium was used for the co-firing studies to study for the effect of torrefaction on combustion and emissions. Table 22 shows the properties of biomass torrefied at 240˚C using CO_2 as torrefaction medium along with properties of raw biomass and coal. Torrefied samples have a higher percentage of fixed carbon on a dry ash free basis than the raw biomass. In addition a small decrease in the volatile matter in the biomass was observed (Table 22). Nitrogen loading for the case of torrefied mesquite is 10% higher than the raw mesquite sample. NOx formation from the fuel bound nitrogen is responsible for 80% of the total NOx generated in pulverized coal fired burners [133]. Depending on the fuel, the emission of volatile nitrogen during the pyrolysis will vary with HCN being the dominant species from coal pyrolysis [102, 134] and NH_3 being the dominant one for biomass pyrolysis [133]. Since there will be a slight increase in ash content in the torrefied samples, the numbers for ash loading are also high for the torrefied samples.

Section 4.6 presents the details of Zero dimensional model. Properties of the raw biomass, torrefied biomass and coal (ultimate analysis, proximate analysis and sieve analysis giving particle size distribution) were used as input parameters for the zero dimensional code.

Table 22. Properties of fuel samples including raw biomass, torrefied biomass and coal. ar: as received, daf: dry ash free, VM: volatile matter, FC: Fixed carbon, HHV: Higher heating value. Uncertainty in the presented numbers is 0.5%.

	Raw Biomass		**Torrefied Biomass (240°C with CO_2)**		**Coal**
	Mesquite	**Juniper**	**Mesquite**	**Juniper**	**PRB**
Moisture (ar)	15.53	5.85	4.84	5.69	32.88
Volatile Matter (ar)	66.09	77.99	69.51	74.60	28.49
Fixed Carbon (ar)	16.71	14.25	23.26	18.63	32.99
Ash (ar)	1.67	1.91	2.39	1.08	5.64
Carbon (ar)	43.60	49.27	53.41	53.55	46.52
Oxygen (ar)	33.57	37.00	33.17	34.06	11.29
Hydrogen (ar)	4.98	5.68	5.33	5.42	2.73
Nitrogen (ar)	0.62	0.28	0.81	0.19	0.66
Sulfur (ar)	0.03	0.01	0.05	0.01	0.27
VM (daf)	79.8	84.6	74.9	80.0	46.3
FC (daf)	20.2	15.4	25.1	20.0	53.7
HHV (kJ/kg)	16666	18987	19822	20099	18193
HHV_{dry} (kJ/kg)	19730	20167	20830	21312	27105

Table 22. Continued.

	Raw Biomass		Torrefied Biomass (240°C with CO_2)		Coal
	Mesquite	**Juniper**	**Mesquite**	**Juniper**	**PRB**
HHV_{DAF} (kJ/kg)	20128	20584	21367	21558	29597
VM HHV_{DAF} (kJ/kg)	16923	18351	17539	18750	25880
$HHV_{Boie,DAF}$ (kJ/kg)	21059	21509	23015	22914	29847
HHV (kJ/kg st O_2)	13652	13632	13092	13261	13521
A/F_{st} (kg/kg_{ar} fuel)	5.24	5.98	6.50	6.51	5.78
A/F_{st} (kg/kg_{daf} fuel)	6.33	6.48	7.01	6.98	9.40
$T_{adiabatic\ flame,open}$ (K)	1374	1470	1412	1442	1427
N loading (kg/GJ)	0.3720	0.1475	0.4086	0.0945	0.3628
S loading (kg/GJ)	0.0180	0.0053	0.0252	0.0050	0.1481
ash loading (kg/GJ)	0.8438	0.9460	1.1459	0.5064	2.0195
SMD (micron)	57.2600	42.6400	66.7000	43.3000	49.2300
Empirical Formula	$CH_{1.37}O_{0.58}N_{0.0122}S_{0.0003}$	$CH_{1.38}O_{0.56}N_{0.0049}S_{0.0001}$	$CH_{1.20}O_{0.47}N_{0.01307}S_{0.0004}$	$CH_{1.21}O_{0.48}N_{0.003}S_{0.0001}$	$CH_{0.70}O_{0.18}N_{0.0122}S_{0.0022}$
Reference	[111]	[111]	[51]	[51]	[18]

Table 23. Input to the zero dimensional code

Fuel	**PRB coal, PRB and biomass blend**
Percentage biomass in blend	10%
Main Burner thermal input	30 kW (100000 BTU/hr)
HHV (PRB Coal)	18193 kJ/kg
HHV (raw mesquite)	16666 kJ/kg
HHV (raw juniper)	18987 kJ/kg
HHV (torrefied mesquite)	19822 kJ/kg
HHV (torrefied juniper)	20099 kJ/kg
Mixing time (Recirculated gases)	100 ms
Inlet temperature of primary air and fuel	300 K
Inlet temperature of secondary air	450 K
Temperature of recirculated gases	1200 K
Ratio of $HCN:NH_3:N_2$ from coal	75:15:10
Ratio of $HCN:NH_3:N_2$ from biomass	30:60:10
Temporal time step	0.025 ms
Overall Equivalence Ratio	0.85, 0.90, 0.95
Total gas residence time	0.856 s

Table 23 presents the input data to the zero dimensional code. Mixing time is of particular importance here since it affects the rate at which recirculated combustion gases mix with the incoming fresh coal-air stream and hence affect burnt fraction and emission of pollutants. Temperature of recirculated gases (T_{RCZ}) was selected to be 1200 K since the highest temperature measured at a distance of about 15.24 cm (6 in) from the

nozzle exit was 1200 K. Effect of combustion of pure coal, blend of raw biomass (mesquite and juniper) and coal (10:90 on a mass basis) and blend of torrefied biomass (torrefied mesquite and torrefied juniper) and PRB coal (10:90 on a mass basis) was studied using the combustion code. Equivalence ratios studied were 0.85, 0.90 and 0.95 for pure coal and coal-biomass blends. Composition of all the gas species, the temperature of the particles, and burnt fraction are tracked for a given residence time estimated using ideal gas assumptions and axial temperature within the burner. Variation in composition of oxygen and NOx on a dry basis in the flue gases are predicted using the zero dimensional combustion model for combustion of pure PRB at an ER of 0.85 is shown below in Fig. 41. The NOx values estimated by the zero dimensional model is only the NOx produced from the fuel nitrogen. Other NOx forming routes (thermal and prompt NOx) were assumed to have negligible effects on the total NOx produced during the combustion of pulverized coal and biomass.

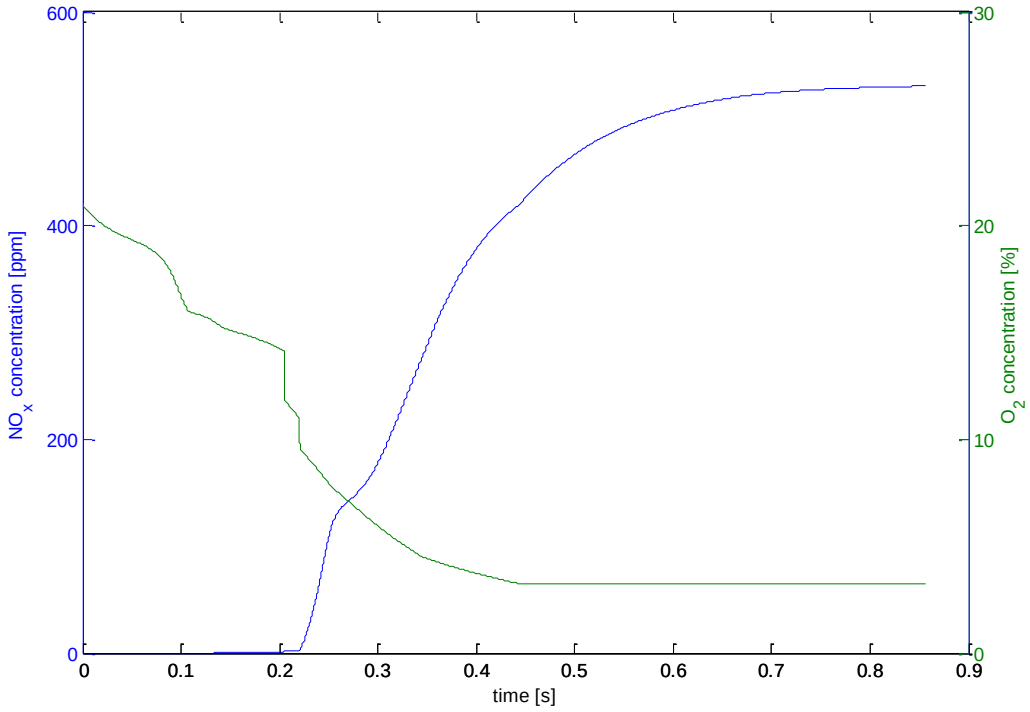

Fig. 41. Variation in oxygen and total NOx concentration along the axis of the burner for pure PRB, ER = 0.85, t_{mix}=100 ms, T_{RCZ}=1200 K.

The oxygen concentration at the burner entrance is 21% and starts to decrease as the fuel particles consume the oxygen for combustion reactions. In addition, rapid release of volatile matter from the coal near the fuel nozzle prevents the diffusion of oxygen to the fuel nitrogen and hence reducing the concentration of the NOx in the flue gas stream. In addition, it should be noted that the percentage of NOx in the recirculating gases is low and hence the dilution of NOx by the recirculating gases resulted in lower NOx numbers in the initial period. Since the combustion is lean with around 3.2% of oxygen in the flue gas stream on a dry basis, the NOx produced also stabilized at around

531 ppm for combustion of pure PRB at an ER = 0.85. With increase in ER, the percentage of oxygen in the flue gas exit and the burnt fraction will also decrease slightly. This will result in increased unburnt char with increase in ER (from lean to rich combustion region). Presence of unburnt char in the gas stream reduces the NOx in the flue stream to molecular N_2 according to reaction 13 in Table 9. Thus NOx decreases with increase in equivalence ratio. The fuel input was varied in the zero dimensional model to determine the exhaust composition for different fuel blends under various ER.

5.8.1. Oxygen percentage in exhaust

Oxygen concentration in the exit of the burner was determined on a dry basis for all fuel combinations and three ER. Result obtained from the model is plotted in Fig. 42. Percentage of oxygen in flue gas decreases with increase in ER due to lower amount of air entering the burner and due to consumption of oxygen during fuel combustion. The oxygen percentage in the exhaust is slightly higher for co-firing biomass with coal. For same thermal input, since the heating value of the biomass is lower, the number of particles per unit volume is higher which must compensate for lowered heating value. Also the recirculated gas flow was maintained constant which causes slower rate of heating of fuel particles.

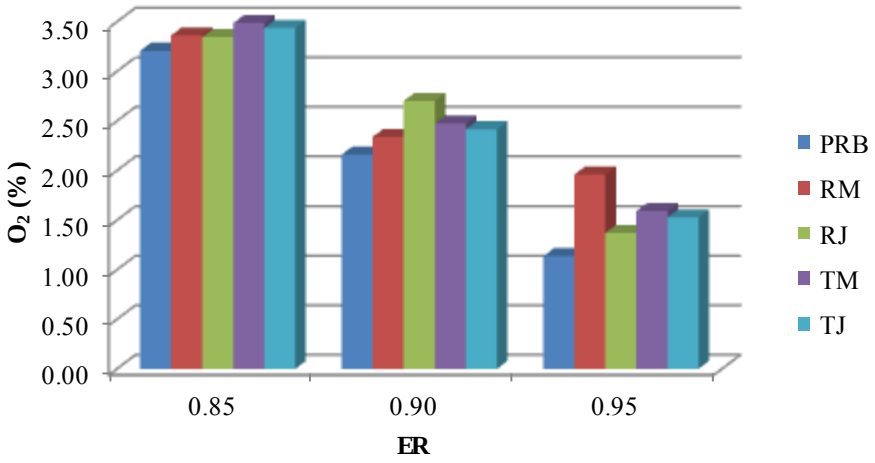

Fig. 42. Variation in oxygen concentration in the flue gas exit. PRB: PRB coal (100:0); RM: raw mesquite (90:10 with 10% being raw mesquite); RJ: raw juniper (90:10); TM: torrefied mesquite (90:10); TJ: torrefied juniper (90:10).

Higher percentage of oxygen during cofiring biomass with coal is due to the higher amounts of volatile matter in the biomass which rapidly consumed oxygen and reduced oxygen availability to char. The DTG curves obtained for the raw and torrefied biomass showed the peak release rates of volatile matter occurred at a lower temperature than PRB coal. Released volatile matter from the biomass prevents the diffusion of oxygen to the coal particles near the burner. With increased equivalence ratios, lower air will be sent in to the combustion chamber and hence the burnt fraction will also vary for rich combustion. Hence a slightly higher percentage of oxygen is detected in the flue gas during biomass co-combustion scenario. Burnt fraction results which are provided in the following section can be used to explain higher percentages of oxygen in the flue gas exit.

5.8.2. NOx concentration

The NOx emission decreases with increase in equivalence ratio for pure coal case and also for blends of biomass and coal. Increased equivalence ratio decreases the amount of oxygen entering the burner which contributes to lower probability for the reaction of fuel nitrogen with the oxygen in incoming air. In addition creation of fuel rich zone near the fuel nozzle helps to reduce the NOx produced to molecular nitrogen. Lower fuel nitrogen in the biomass (i.e lower HCN and NH_3) can also be considered to be one of the reasons behind lower NOx emission for the case of juniper. However for mesquite, which has comparable fuel nitrogen as coal synergistic effects were observed in reducing the NOx and resulting in lower numbers.

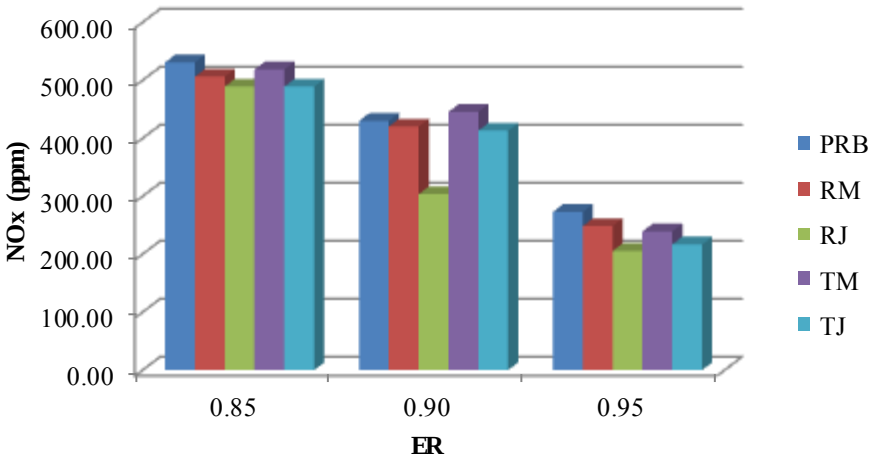

Fig. 43. Variation in NOx concentration in the flue gas exit. PRB: PRB coal ; RM: raw mesquite (90:10 with 10% being raw mesquite); RJ: raw juniper (90:10); TM: torrefied mesquite (90:10); TJ: torrefied juniper (90:10).

Torrefied mesquite which has 10% higher nitrogen loading number than the raw mesquite sample, resulted in higher NOx emission than the raw biomass at lower ER. Pyrolysis of biomass nitrogen was observed to produce more NH_3 however HCN is one of the main products of coal nitrogen pyrolysis [133]. The reduction of NO by the ammonia liberated from the biomass nitrogen can be considered to be one of the possible reasons for the reduced NOx emission from biomass co-firing conditions. Oxidation of NH_3 to NOx occurs at higher temperatures (greater than 1483 K) [135]. Hence temperatures below 1500 K will favor the reduction of NOx by the biomass ammonia.

5.8.3. Carbon dioxide and burnt fraction

Carbon dioxide composition for the different equivalence ratios studied is presented in Fig. 44. It can be seen that the percentage of carbon dioxide generated increases with an increase in equivalence ratio. As the amount of air supplied approaches the stoichiometric region (ER=0.95), higher amount of carbon dioxide is produced due to increased temperatures within the burner at near stoichiometric conditions. Blends of biomass with coal resulted in comparatively lower CO_2 levels due to lower percentage of carbon in the fuel blend since biomass has higher percentage of volatile matter and lower fixed carbon content. The burnt fraction estimated by the model is shown in Fig. 45. Burnt fraction is estimated based on the amount of combustibles (fixed carbon and volatile matter) left in the exhaust stream.

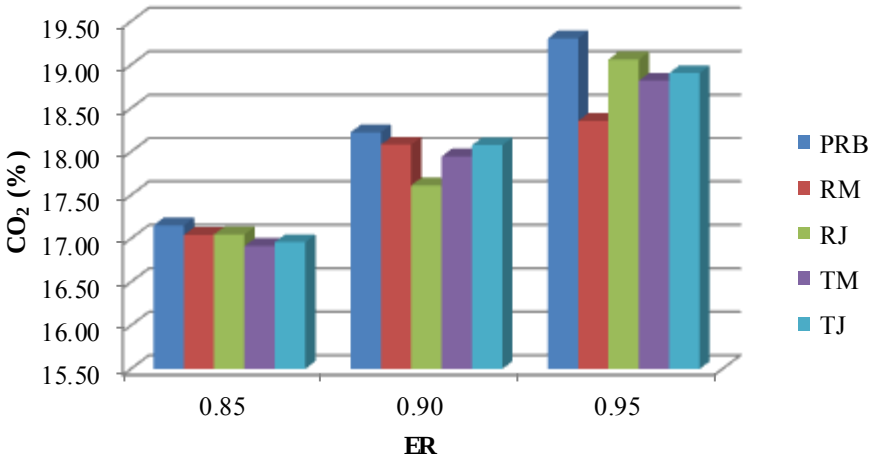

Fig. 44. Variation in CO_2 concentration in the flue gas exit. PRB: PRB coal ; RM: raw mesquite (90:10 with 10% being raw mesquite); RJ: raw juniper (90:10); TM: torrefied mesquite (90:10); TJ: torrefied juniper (90:10).

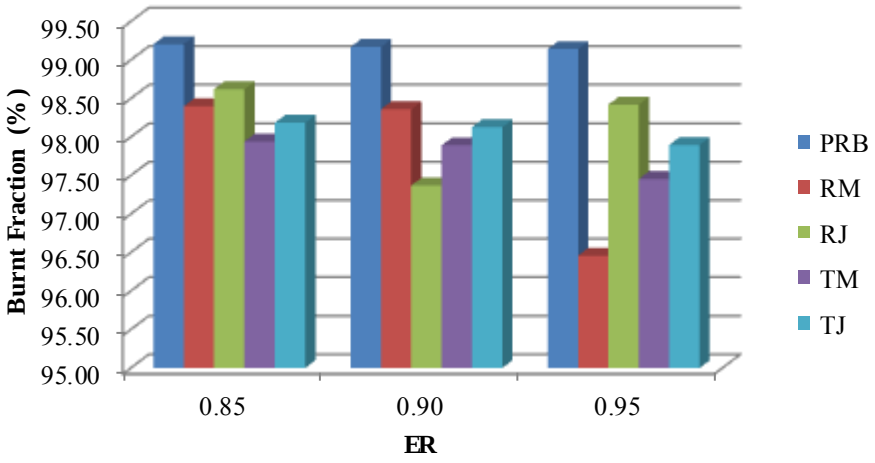

Fig. 45. Variation in particle burnt fraction. PRB: PRB coal ; RM: raw mesquite (90:10 with 10% being raw mesquite); RJ: raw juniper (90:10); TM: torrefied mesquite (90:10); TJ: torrefied juniper (90:10).

Burnt fraction showed an increasing trend for the case of coal combustion with increase in equivalence ratio. Effect of biomass blended with coal showed a lower burnt fraction as the combustion shifted from lower ER to higher ER. Lower burnt fraction at higher ER would have been due to i) higher amounts of volatile matter in the biomass which is released in the high temperature region within the burner near the fuel nozzle., ii) The released volatile matter creating a fuel rich region which causes lower diffusion of oxygen to the char particles which remain unburned and iii) lower residence time within the burner also does not allow for complete combustion of particles.

5.9.Experimental results from cofiring raw and torrefied biomass

The results from the cofiring experiments was used to validate the results predicted by the model and in turn understanding the reactions behind the formation and destruction of harmful emissions during the combustion of coal and coal-biomass blends. All the experiments were carried out in a 30 kWt downfired burner for 90 minutes.

5.9.1. Oxygen concentration and ER_{flue}

Fig. 46 plots the oxygen concentration in the exhaust for the different equivalence ratios studied for coal and coal-biomass mixtures. The oxygen concentration in the flue gas varied between 1.1% and 3.2% for the measured ER between 0.95 and 0.85 respectively.

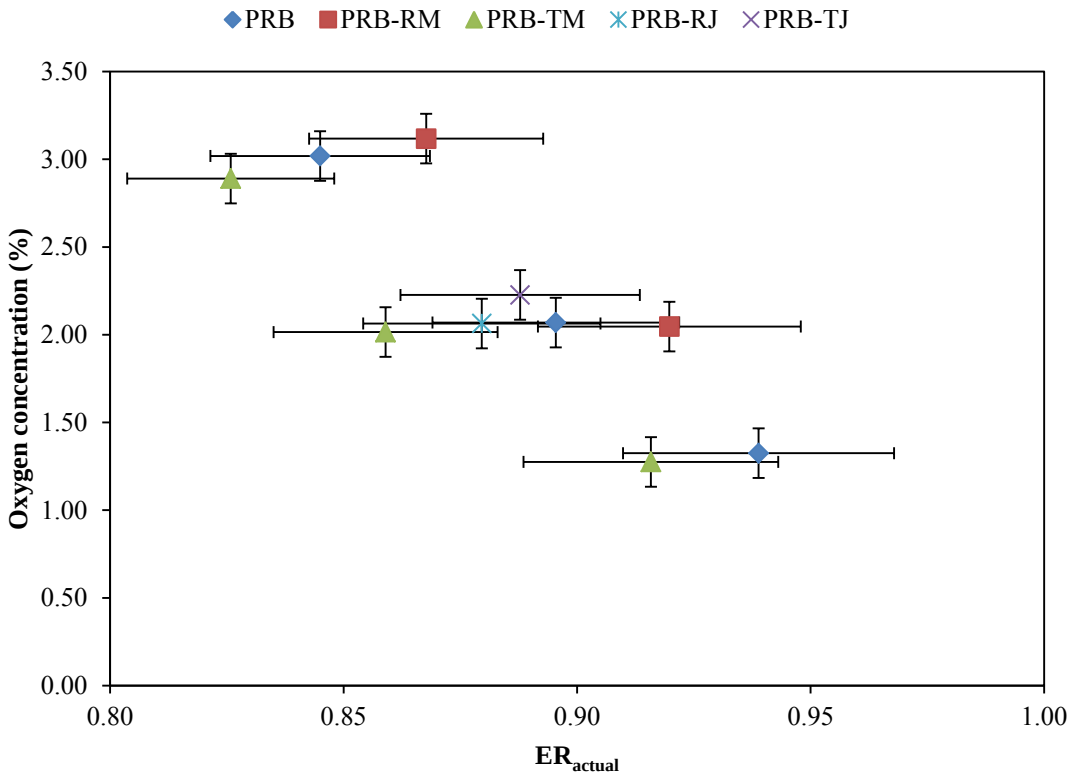

Fig. 46. Variation in oxygen percentage in the exhaust.

The concentration of oxygen or carbon dioxide in the exhaust can be used to estimate the equivalence ratio for any C-H-O fuel for lean combustion conditions using the following relation [18].

$$\phi_{flue} = 1 - \frac{x_{O_2,flue}}{x_{O_2,amb}}, \phi < 1 \qquad (43)$$

where $x_{O2,flue}$ is the mole fraction of oxygen in the flue gas and $x_{O2,amb}$ is the concentration of oxygen in the ambient air (21% on volume basis). The ER based on the

oxygen concentration in exhaust (ϕ_{flue}) is plotted against the ER from the measured air and fuel flow rates. Fig. 47 shows the variation of the measured ER vs the ER calculated from the oxygen concentration in the flue gas. It can be observed from Fig. 46 that the flue gas oxygen concentration can be used to predict the ER used for lean cases in case composition of the fuel is not known. Note that the scales are enlarged and the range is closer to the operating conditions in commercial power generating facilities.

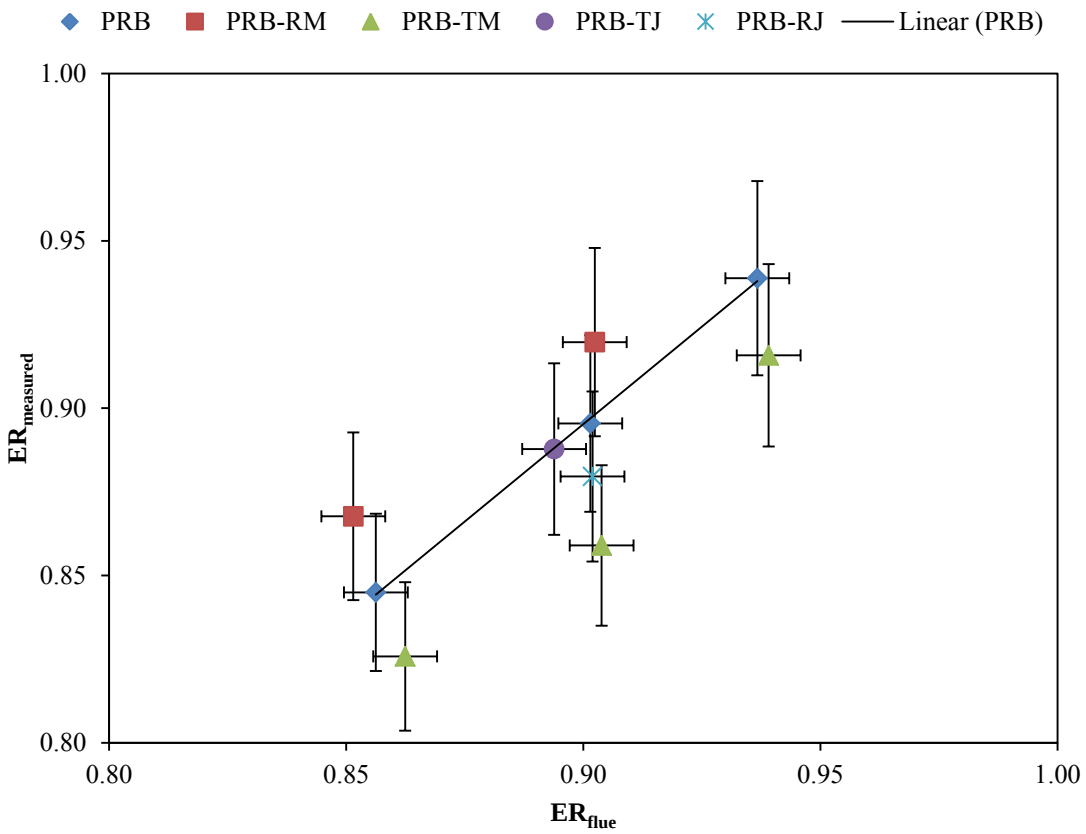

Fig. 47. ER measured vs ER flue estimated using the relation given in Eq. (43). Solid line indicates a linear fit based on mean values with a R^2=0.9992.

Burnt fraction of the fuel particles can be estimated based on the flue oxygen concentration using Eq. (44) [18]. Fig. 48 plots the burnt fraction determined for all the combustion experiments. It can be observed that the burnt fraction decreases with increase in ER due to lesser amount of oxygen available for complete fuel oxidation. The uncertainty in the ER is 0.02 and the uncertainty in the estimated burnt fraction is 0.03. The numbers obtained for the burnt fraction are higher than 1 due to the uncertainty and fluctuations. It is also one of the limitations of applying Eq. (41) for determining the burnt fraction [18].

$$BF = \frac{1}{\phi} * \left(1 - \frac{x_{O_2}}{x_{O_{2,amb}}} \right) \tag{44}$$

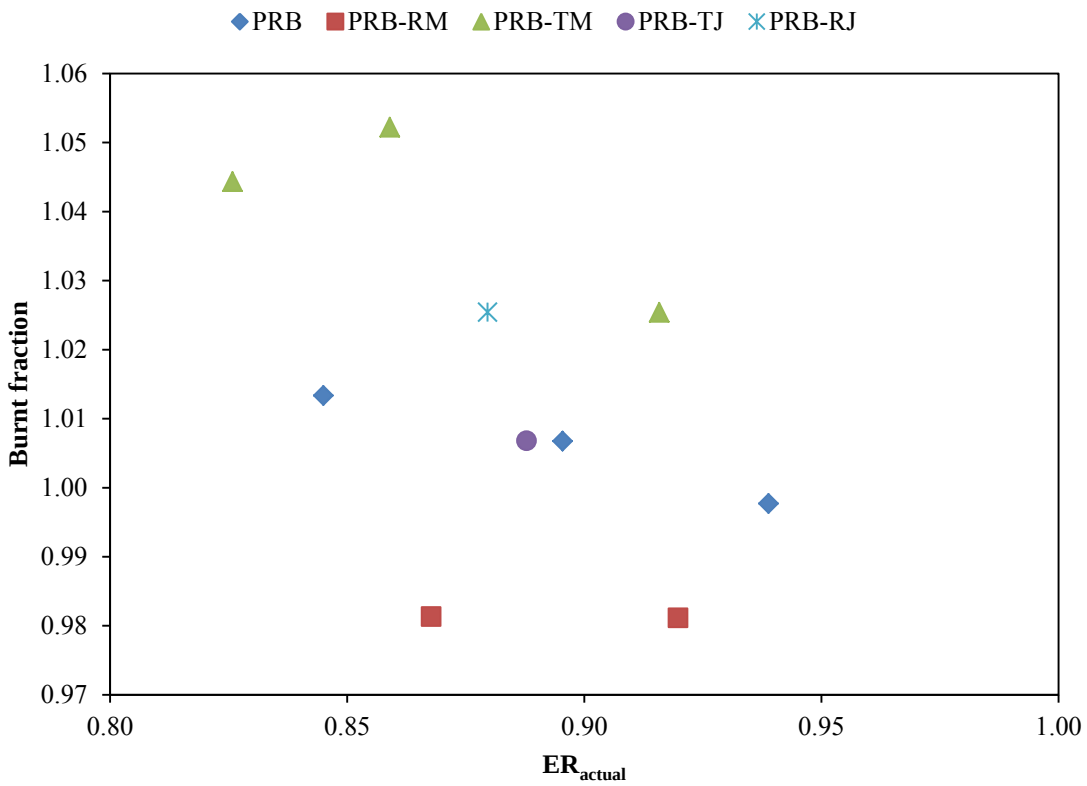

Fig. 48. Estimated burnt fraction with increase in ER (Uncertainty in the ER was 0.02 and the uncertainty in the burnt fraction was 0.03).

5.9.2. Carbon dioxide and carbon monoxide emissions

The experimental results showed an increase in the percentage of carbon dioxide in the flue gas with increase in the ER (Fig. 49). The uncertainty for all the carbon dioxide readings presented in Fig. 49 was 0.9%. The results predicted by the model were in close agreement with the experimentally obtained numbers (See section 5.8.3). Carbon dioxide percentage in the exhaust can be used to estimate the respiratory quotient (RQ) of the fuel (Section 5.10).

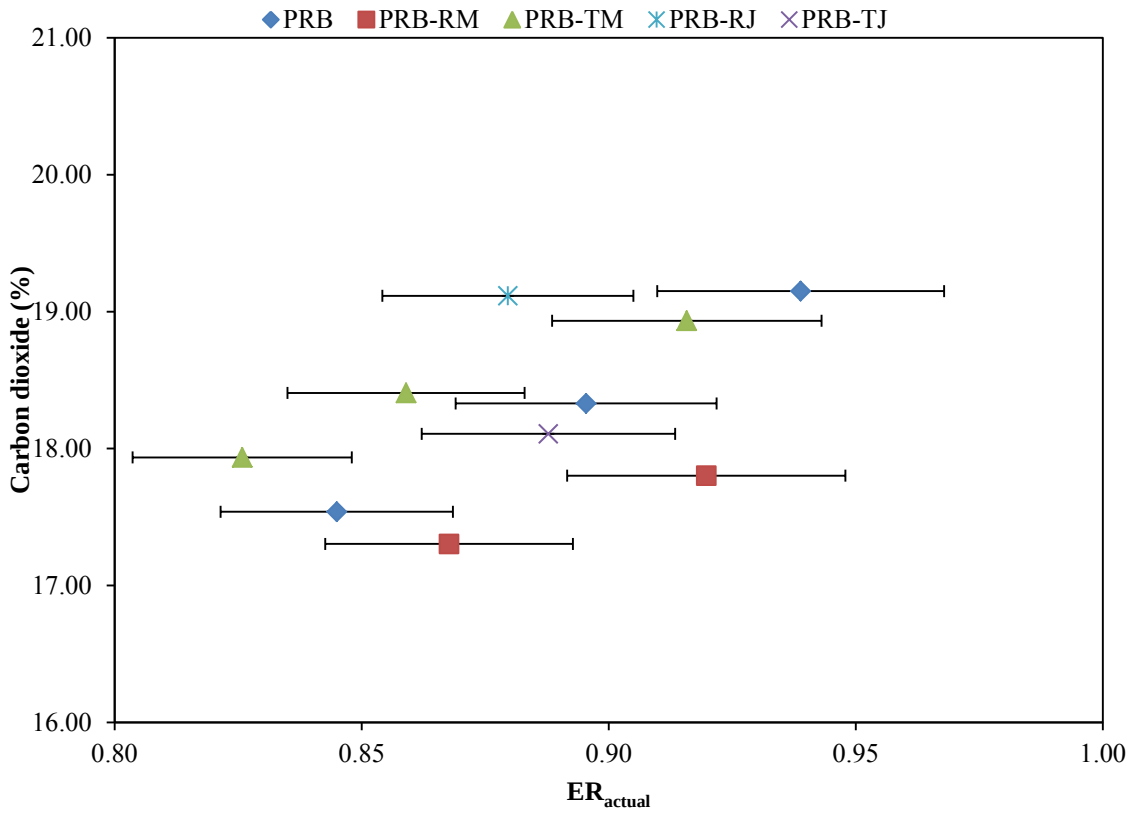

Fig. 49. Carbon dioxide percentage in the exhaust for coal and coal biomass blends (Uncertainty of the carbon dioxide percentage is 0.9%).

Carbon monoxide concentrations increased with increase in ER (Fig. 50) caused due to lower percentage of excess air available for complete oxidation of fuel. Blending of biomass fuels with coal resulted in increased production of carbon monoxide for all ER due to higher volatile matter and higher oxygen content of biomass. Similar observations on carbon monoxide emissions were observed when wood chips were co-fired with high ash lignite in a circulating fluidized bed boiler [136]. Increase in carbon monoxide levels with ER and biomass blending can be explained using the same

rationale used in describing the lower burnt fraction obtained using the zero dimensional model.

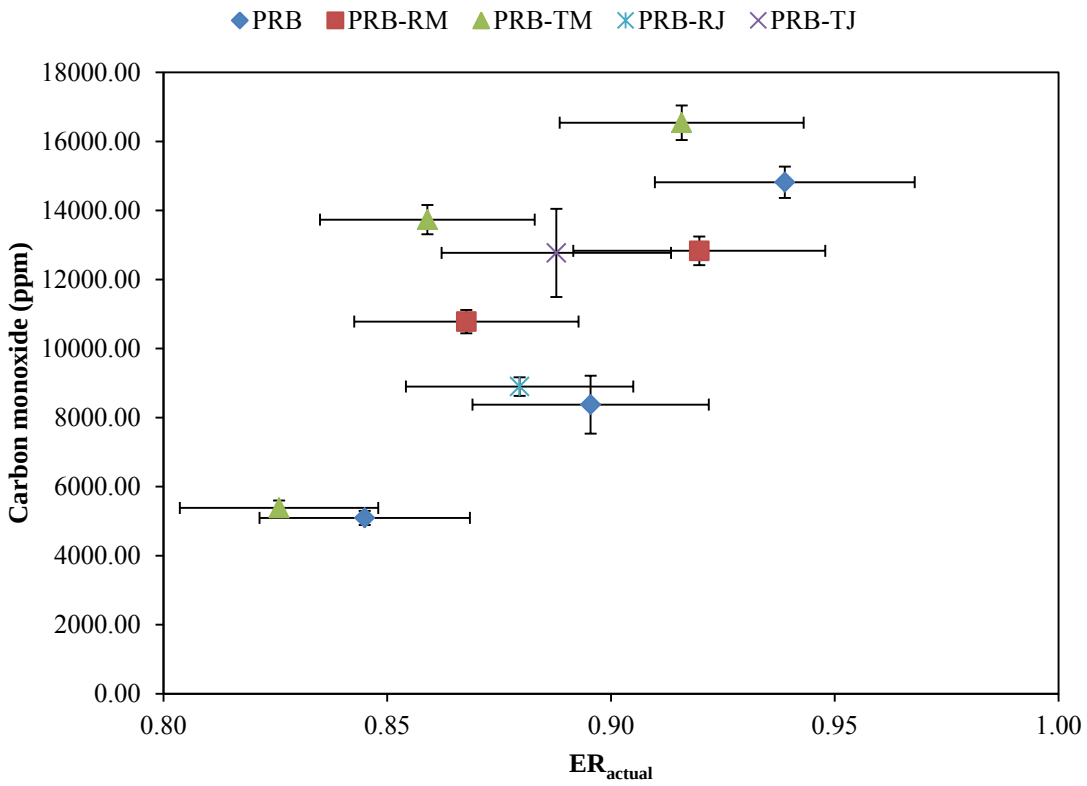

Fig. 50. Effect of ER on the CO emission from combustion of pure coal and blend of raw and torrefied biomass.

Higher amount of volatile matter in biomass causes higher rates of devolatilization near the burner nozzle and hence higher rate of oxidation of VM to CO with rapid reduction of oxygen concentration thereby resulting in incomplete combustion of CO to CO_2. The amount of oxygen available for complete combustion of fuel at higher ER is also low leading to higher levels of CO.

5.9.3. NOx emissions from the burner

The main advantages of co-firing biomass with coal are its carbon neutrality, lower sulfur content and synergistic NOx reduction effects. Similar synergistic effects were observed from the experimental results on NOx emission from the combustion of torrefied woody biomass with coal (Fig. 51). Higher amounts of volatile matter in biomass affects the NOx formation mechanism near the burner nozzle. Rapid release of volatile matter from the biomass prevents the reaction of oxygen with the fuel nitrogen and also reduces the NOx formed to molecular nitrogen. Studies on understanding the partitioning of fuel nitrogen during pyrolysis showed increased production of NH_3 from biomass and higher amounts of HCN generation from coals [133]. It was observed that the kinetics of NH_3 reducing NOx was much faster than the oxidation of NH_3 to NOx [135] which contributes to lower generation of this harmful pollutant during co-combustion of biomass with coal. Further the oxidation temperature (1480 K) of ammonia is greater than the reduction temperature (i.e NH_3 + NO) of ammonia (1145 to 1480 K) [135].

The energy density of biomass is lower than coal because of higher oxygen content in the biomass as can be observed from the dry ash free HHV of the different fuels (Table 12 and Table 22) used in the current study. Hence the NOx emission should be represented on an energy basis to take into account the energy content of the fuels.

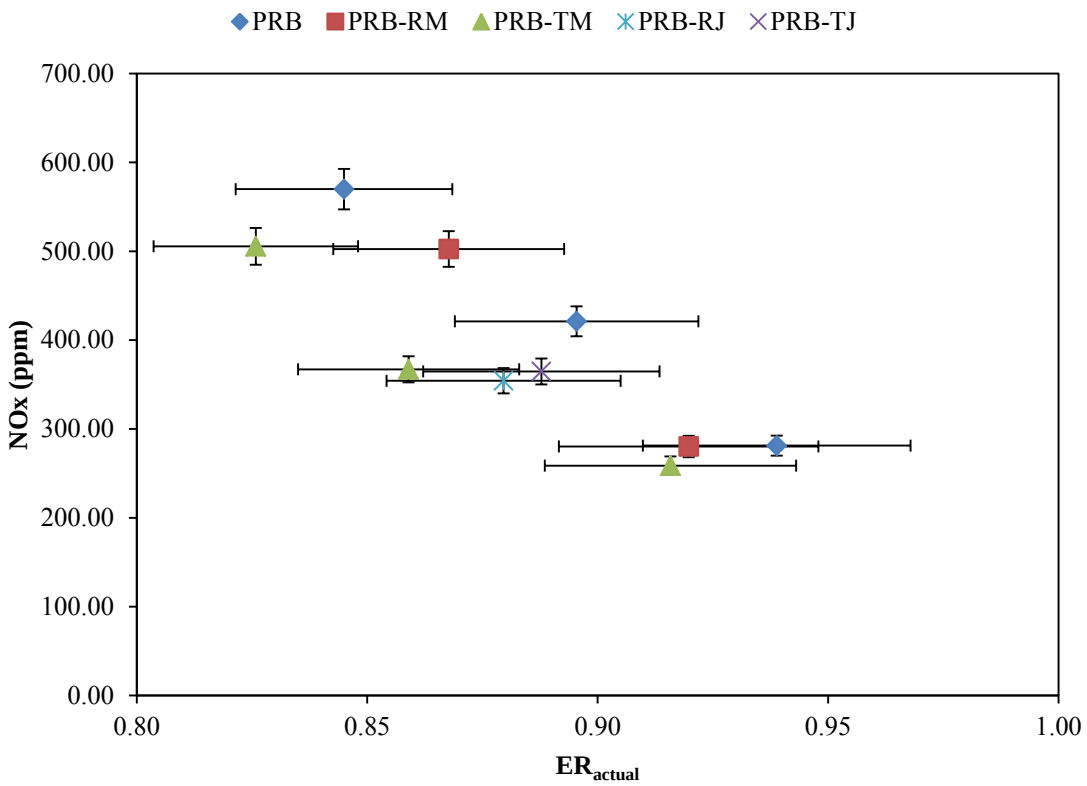

Fig. 51. Variation in NOx emission with increase in ER.

Fig. 52 shows the NOx emission levels represented in g/GJ. NOx emission in g/GJ is estimated using Eq. (45) [102].

$$NO_x in \frac{g}{GJ} = \frac{c * X_{NO_x}}{\left(x_{CO_2} + x_{CO}\right)} * \frac{M_{NO_2} * 1000}{M_F HHV_F (GJ / kg)} \quad (45)$$

where c is the number of carbon atoms in the fuel, x_i represent the mole fraction of gas species 'i' in the flue gas stream, M_i is the molecular weight and HHV represent the higher heating value of the fuel. Lower NOx levels were observed for co-combustion of

biomass with coal on an energy basis due to comparable HHV of coal and biomass. Higher amount of carbon monoxide also contributes to lower levels of NOx in the exhaust caused due to the reducing effect of CO on NOx in the presence of char. Fig. 53 shows the plot of CO vs NOx obtained for all ER and fuel blends. It can be observed that the NOx decreases when CO levels are high. The burnt fraction predicted by the zero-dimensional model (Fig. 45) also shows availability of carbon within the burner for the reduction reactions to occur.

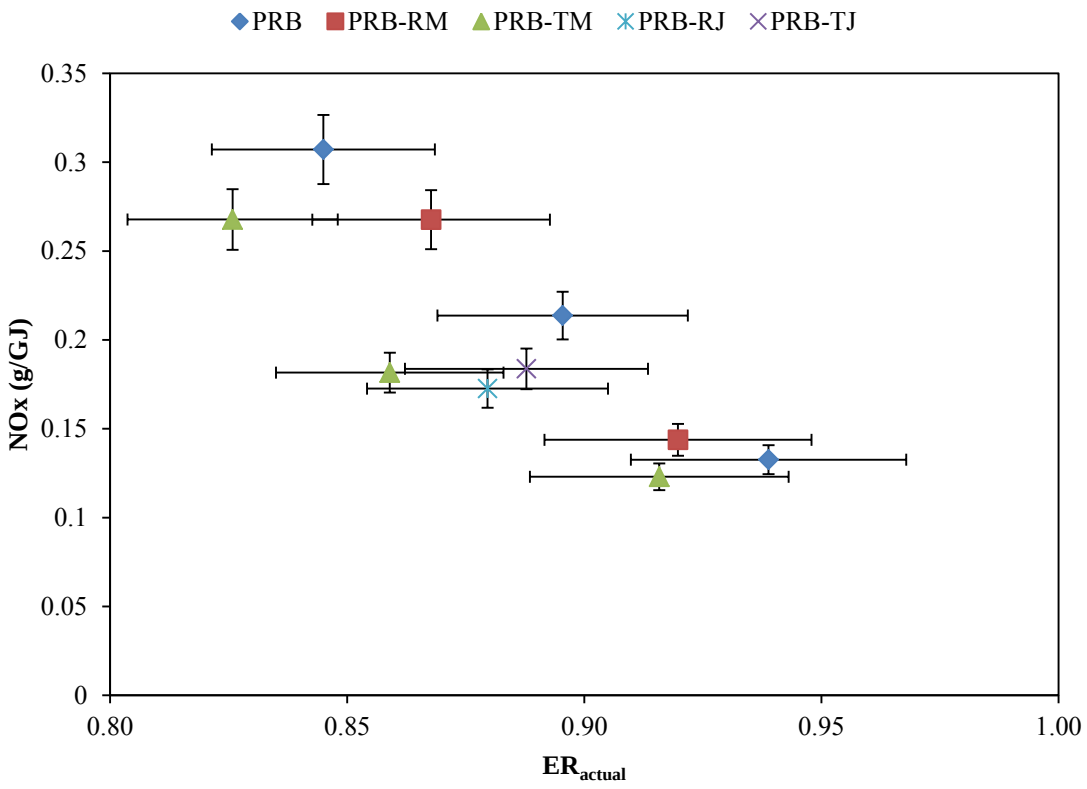

Fig. 52. NOx emission given on g/GJ basis.

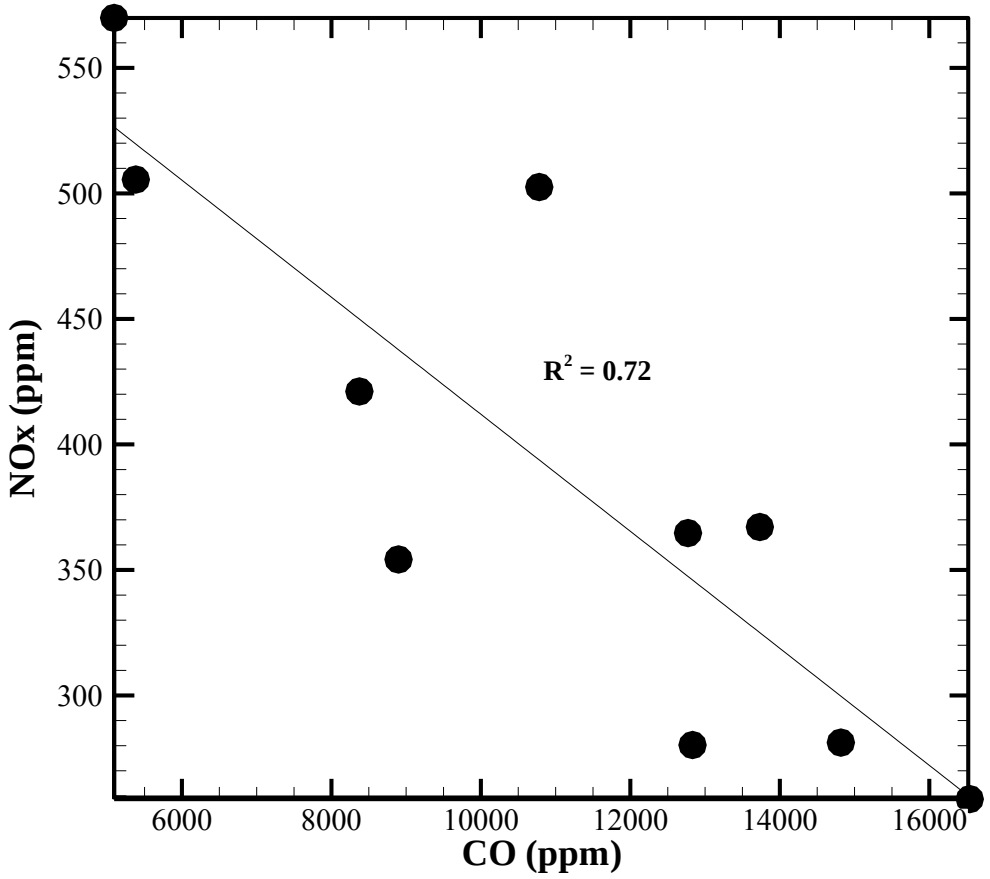

Fig. 53. NOx in ppm vs CO in ppm for all ER and fuel blend types.

It should also be observed that the raw biomass resulted in higher reduction in NOx emission when compared to torrefied biomass co-firing. Slight reduction in volatile matter in torrefied biomass when compared to raw biomass would have contributed to such a difference. 10% decrease in NOx emissions were observed for all ER studied when torrefied biomass was cofired with coal. Fig. 54 plots the NOx emission with

respect to fuel nitrogen loading for the combustion experiments carried out for all fuel types used in the current study for an ER of 0.90.

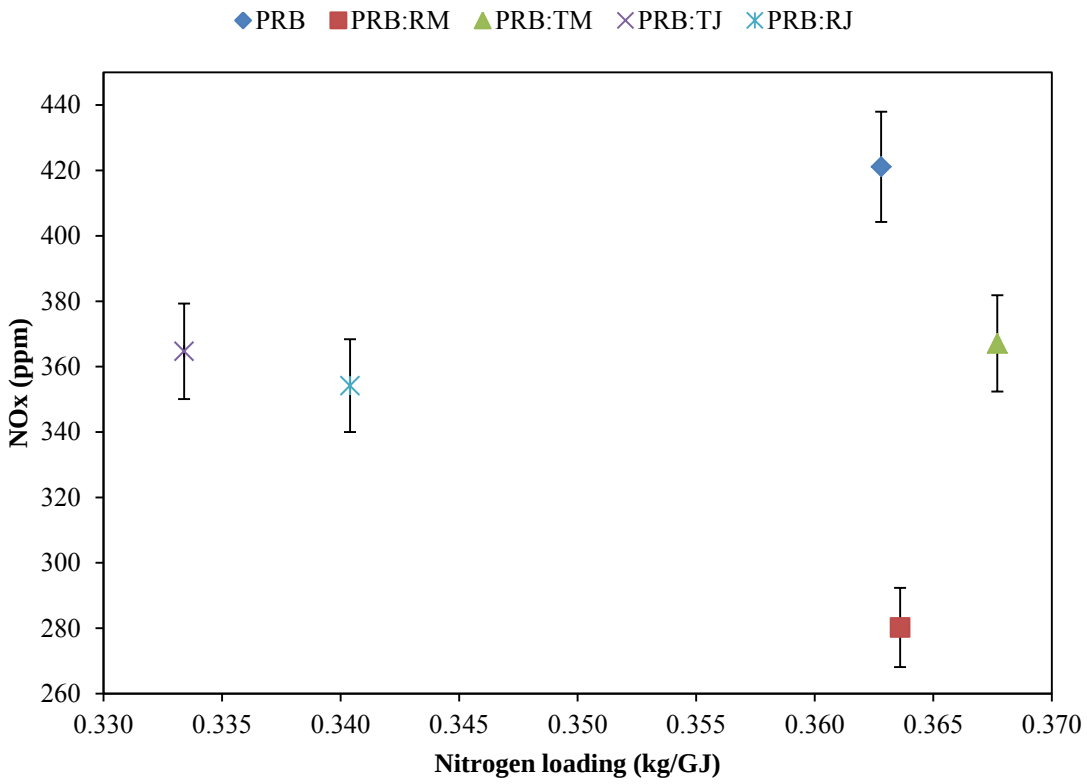

Fig. 54. NOx emission plotted against respective fuel nitrogen loading numbers for ER = 0.9.

Reduced emission of NOx would help the power plants to offset the costs associated with NOx trading. Currently the rates for NOx trading is low ($15.89 per short ton, [137]). If the trading rates are high, plants utilizing torrefied biomass can gain from trading the NOx with other plants emitting higher amounts of NOx. The major homogenous reactions which can be used to explain the NOx reductions are reactions (1)

and (2) in Table 8. The heterogeneous reduction of NO in the presence of carbon can be explained using reaction (13) in Table 9.

5.9.4. ANOVA of repeated experiments

ANOVA was performed on the repeated experimental results using a two factor analysis with replication. The two factors which were used for the current analysis was ER and the type of fuel. Pure coal and coal blended with torrefied mesquite was chosen for the analysis. The results obtained for the emissions measurement is shown below in Table 24.

Table 24. ANOVA of the emission measurement from the repeated experiments

	between ER P-value	**between biomass P-value**
O_2	4.84E-05	3.82E-01
CO_2	1.76E-03	8.59E-01
NOx	1.75E-05	2.49E-02
CO	6.70E-05	1.78E-02

The emission measurements done for different ER studied using ANOVA showed that the P-values are well below 0.05 indicating significant results and the obtained numbers are not due to experimental noise. Oxygen and carbon dioxide measurements made for different fuel types (coal and coal biomass blend) resulted in higher P-value. This is because of constant value for the oxygen concentration in the exhaust at a fixed ER even when the fuel is changed. Similarly the CO_2 percentage increases with increase in ER irrespective of the fuel used. However the NOx and CO

measurements showed a lower P-value. This is because of the synergistic NOx reduction effects when biomass is blended with coal resulting in lower NOx emission. Also, the CO levels in the exhaust increased with increase in ER during the combustion of biomass based fuels.

5.9.5. Effect of biomass cofiring on heat transfer

Three heat exchangers were used to study the heat transfer behavior during the cofiring studies. The temperature of the fluid at the inlet and exit of the HEX were monitored and recorded in addition to the temperature above and below the HEX tubes. Eq. (17) to Eq. (21) were used to calculate the heat transfer to the fluid, log mean temperature difference (LMTD) and overall heat transfer coefficient (OHTC) [8]. Deposition of ash will affect the LMTD and OHTC values. Combustion of natural gas was taken as the base case to establish the no ash scenario and all the OHTC values presented will be normalized with respect to the no ash deposition case.

Fig. 55 shows the ratio of OHTC for coal to the OHTC determined for natural gas combustion for an ER of 0.9. The uncertainty in the calculated OHTC was 0.02%. The peak temperature occurred at a distance of 30 inches from the nozzle exit and close to the first HEX system for the combustion of coal and biomass blends. As can be observed from the OHTC ratios, heat transfer coefficient is higher at the top HEX and decreases with increase in time due to the accumulation of ash on the surface of the HEX. Bottom HEX showed a considerable decrease in OHTC with increase in time due to lower temperature and higher accumulation of ash.

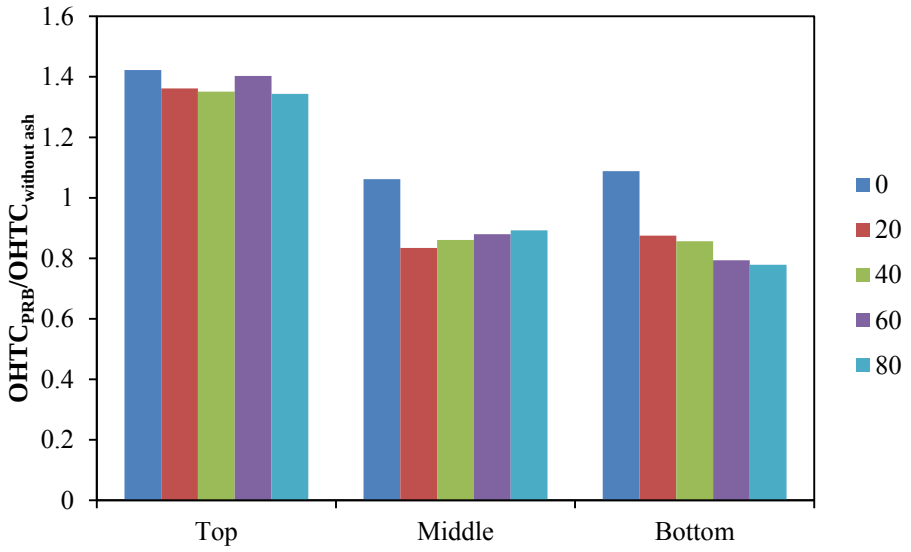

Fig. 55. Variation of OHTC ratios with time for the combustion of pure PRB coal, ER = 0.9. PRB: Powder river basin coal (Uncertainty of the OHTC ratio is 0.02%).

Axial temperature distribution within the burner after a time period of 90 minutes from the start of the experiments for the combustion of pure PRB, PRB: raw mesquite (RM) and PRB: torrefied mesquite (TM) at an ER = 0.9 is shown below in Fig. 56. The peak temperature for all the three cases occurred at a distance of 76 cm (30 in) from the fuel nozzle exit. Pure PRB coal resulted in slightly higher peak temperatures compared to coal biomass blends due to higher percentage of fixed carbon in coal. The temperatures measured along the burner axis for all the three cases were in the similar range with small differences.

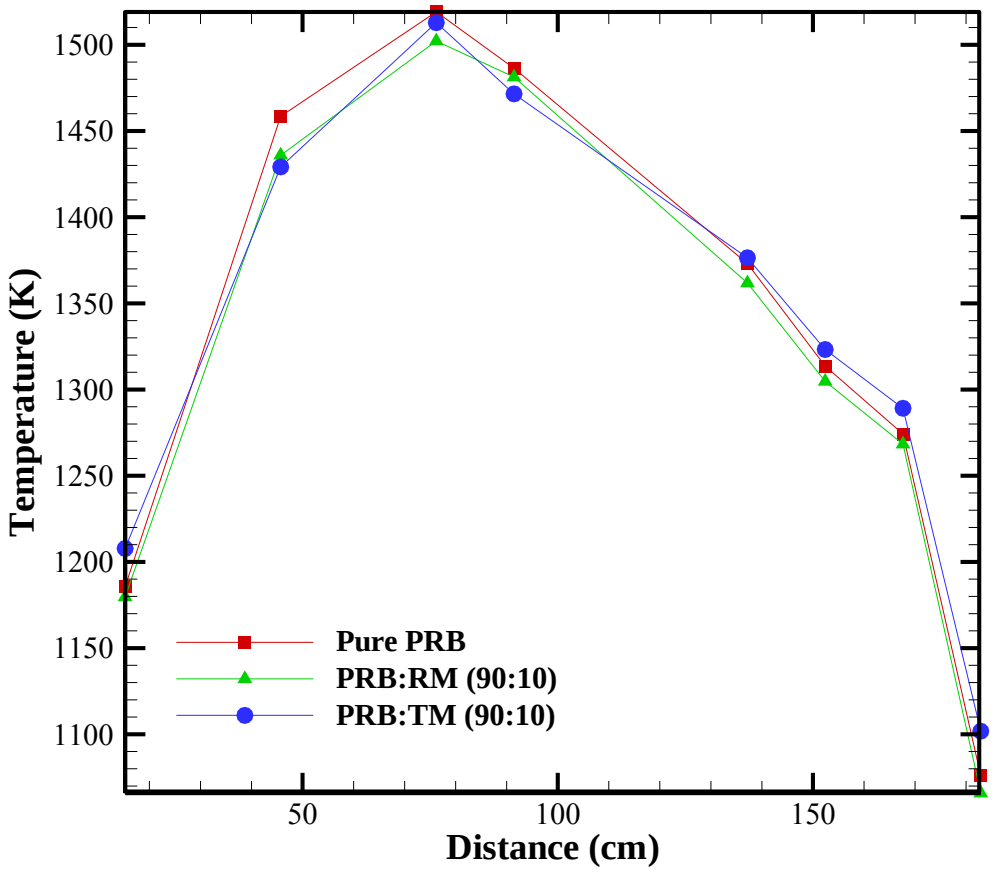

Fig. 56. Temperature profile along the axis of the burner for the combustion of pure PRB coal, PRB:raw mesquite (RM) and PRB: torrefied mesquite (TM); ER = 0.9.

Introduction of biomass along with coal resulted in lower OHTC on the top HEX and OHTC ratios comparable to that of PRB coal in the middle HEX for both torrefied mesquite (Fig. 57) and raw mesquite (Fig. 58) for an ER of 0.90. Lower OHTC for the top HEX can be attributed to the lower peak temperatures obtained for the coal biomass blends. Study on the flame characteristics of torrefied biomass revealed a movement of

the flame location further downstream [80] when compared to pure coal combustion scenario. Results obtained from the heat transfer studies also indicated a slight shift in the location of the flame resulting in higher OHTC in the middle HEX for both torrefied biomass and raw biomass. Comparatively lower OHTC ratios were obtained at the top HEX tube. The OHTC ratio decreases with increase in time. Since the experiments were carried out only for 90 minutes, formation of sticky deposits due to the alkali content in the biomass ash was not observed on the HEX tube surfaces.

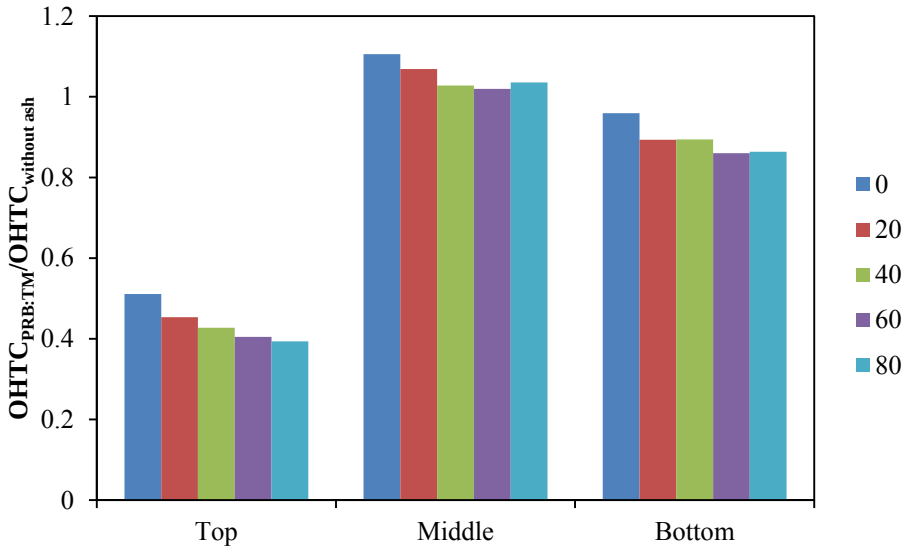

Fig. 57. OHTC ratios for cofiring torrefied mesquite with coal, ER = 0.9. TM: Torrefied mesquite (10% on mass basis) (Uncertainty of the OHTC ratio is 0.02%).

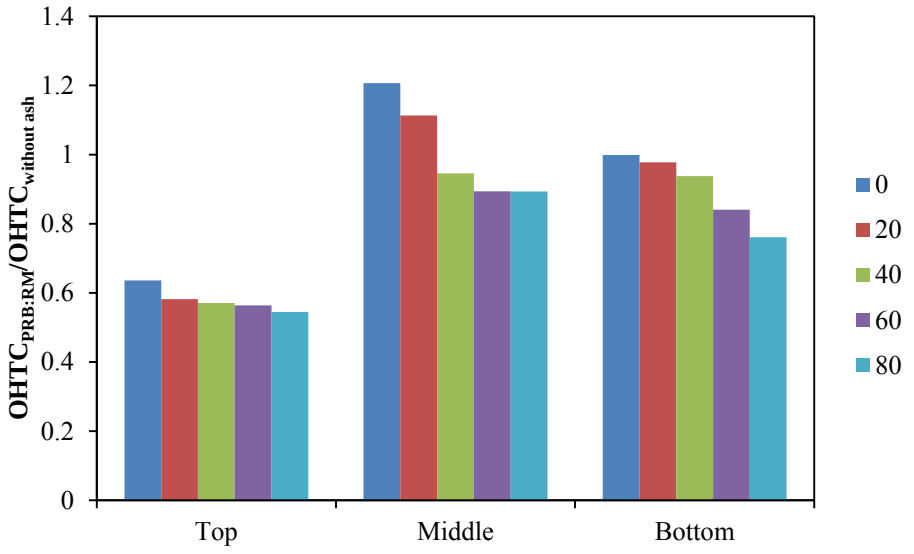

Fig. 58. OHTC ratios for cofiring raw mesquite with coal, ER = 0.9. RM: Raw mesquite (10% on mass basis) (Uncertainty of the OHTC ratio is 0.02%).

Results obtained from the current transient study indicated ash build up on the middle and bottom HEX tube surface which decreased the heat transfer to the heat transfer fluid: air with increased residence time. Evaluation of the HEX tubes after the experiments revealed brittle and non-sticky nature of the ash on the top surface of the HEX surfaces which was in the path of the exhaust gas stream. Fig. 59 shows the appearance of the deposited ash on the HEX tubes after combustion test on pure PRB for an equivalence ratio of 0.90. The ash deposited was removed easily due to brittle nature. However tests should be done for longer time periods to understand the ash behavior during cofiring torrefied biomass with coal. These tests will enable the researchers to determine the optimum time for the use of soot blowers to remove the accumulated ash from the HEX tube surfaces before the ash sticks to the surface of the HEX tubes.

Fig. 59. Ash deposited on the surface of the heat exchanger tubes from the combustion of pure PRB; ER = 0.90.

5.10. Respiratory quotient of fuels

5.10.1. Fuel properties

Properties of different gaseous, liquid and solid fuels which are commonly used for combustion applications are presented in Table 25 along with estimated RQ. The major difference which can be observed between conventional fossil fuels and renewable fuels is the amount of oxygen in these two types of fuels.

Table 25. Properties of different fuels reported on mass basis.

Fuel	C	H	S	N	O	HHV measured (kJ/kg)	Estimated HHV - Boie (kJ/kg)	Reference
Gaseous fuels								
Methane	75	25	0	0	0	55500*	55426	[102]
Ethane	80	20	0	0	0	51100*	51373	[102]
Propane	81.8	18.2	0	0	0	50300*	49914	[102]
Ethylene	80	20	0	0	0	50300*	51373	[102]
Acetylene	92.3	7.7	0	0	0	49900*	41402	[102]
Liquid fuels								
Gasoline (C_8H_{18})	84.2	15.8	0	0	0	48500	47968	[138]
Diesel ($C_{12}H_{23}$)	86.2	13.8	0	0	0	45000	46347	[138]
Biodiesel†	77.2	12.2	0	0	10.6	35900	40147	[138]
Ethanol†	52.1	13.2	0	0	34.7	29700*	29603	[102]
Methanol†	37.5	12.6	0	0	49.9	23900*	22168	[102]
Free fatty acid from peanut oil soap stock†	80.2	12.2	0.12	0.5	7	39800	41645	[138]
Bio oil (wood pyrolysis)†	56	6.25	0	0.1	37.5	17500	22801	[139]
Heavy oil	85	11	0	0.3	1	40000	42579	[139]
Canola oil†	80.2	10.9	0.004	0.14	8.62	40200	39927	[140]
Solid fuels								
WYO coal	46.5	2.73	0.27	0.66	11.3	18200	18347	[18]
TXL coal	37.2	2.12	0.61	0.68	9.61	14300	14577	[18]
Hardwood (mesquite)†	43.6	4.98	0.03	0.62	33.6	16700	17434	[111]
Softwood (Juniper)†	49.3	5.7	0.01	0.28	37	19000	19874	[111]
Fibrous (rice straw)†	41.8	4.63	0.08	0.7	36.6	16300	16068	[102]
Animal based (LAPCDB)†	35.2	3.7	0.43	1.93	18.6	12800	14780	[16]
* estimated from the enthalpy of formation data; † Renewable fuels Multiply HHV in kJ/kg by 0.43 to obtain BTU/lb								

Biomass fuels have a higher percentage of oxygen. Biomass fuels have a higher percentage of oxygen, hence lower amount of oxygen is required for combustion. This

results in higher RQ for biomass when compared to oils and gases. Boie equation can be used to study the variation of HHV with carbon, hydrogen and oxygen atoms in the fuel. Fig. 60 shows the estimated variation of HHV with fuel composition.

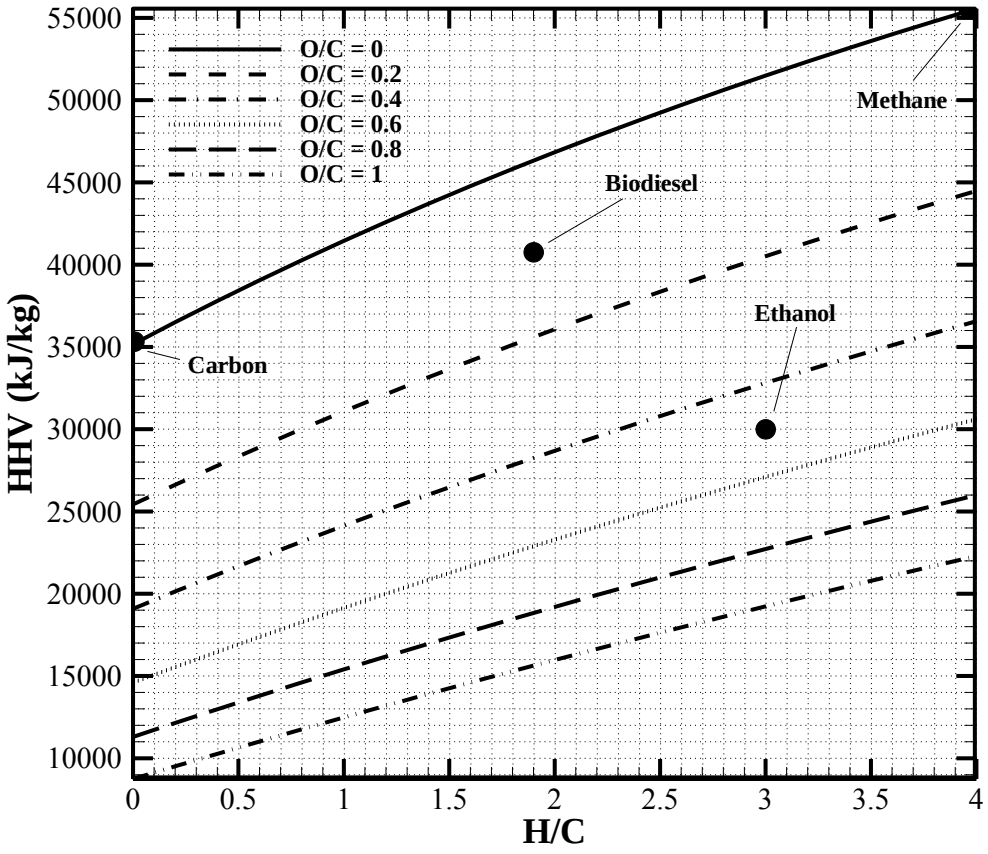

Fig. 60. Estimated variation of HHV with H/C and O/C atom ratios using Boie equation. HHV decreases with increase in oxygen content in the fuel.

It can be observed from Fig. 60 that the HHV of the fuels increases with increase in hydrogen to carbon ratio and decrease in oxygen to carbon ratio. Hydrocarbon fuels with O/C ratio of zero have the highest HHV when compared to other fuels which has some amount of oxygen intrinsically.

5.10.2. Higher heating value per unit stoichiometric oxygen

Eq. (27) was used to determine the HHV_{O2} for different fuels. Fig. 61 shows the variation of HHV_{O2} with respect to ratio of hydrogen to carbon atoms (H/C) in the fuel. It is apparent from the Fig. 61 that HHV per unit mass of oxygen burned is approximately the same of about 14250 kJ/kg of oxygen (18.6 kJ/SATP L of oxygen) or 3280 kJ/kg stoichiometric air (3.9 kJ/SATP L of air) for most fuels. It was observed that HV per unit O_2 is 13550 kJ/kg of O_2 (17.7 kJ/SATP L of O_2) for methane while Boie based equation yields 13934 kJ/kg of O_2. For n–octane, the value is 13640 kJ/kg of O_2 or 17.82 kJ/L of O_2 at standard atmospheric temperature and pressure (SATP) while Boie yields 13730 kJ/kg O_2.

Similar oxygen (O_2) % in exhaust gas after combustion implies similar excess air % (or equivalence ratio) for most solid fuels [141]. Since thermal output = HHV_{O2}* stoichiometric O_2 flow rate = HHV_{air}* stoichiometric air flow rate = HHV_{air}* actual air flow rate /(1+x/100) where x is % excess air. Thus when actual air flow rate is maintained the same, then one may switch the fuel and adjust the fuel flow rate such that same O_2 % is maintained which ensures similar thermal output. In automobiles or gas turbines, when alternate fuels are used for combustion, same thermal energy input is

assured when air flow is maintained the same and fuel flow is adjusted such that same O_2% is maintained in exhaust. For example the heating value of gasoline and ethanol blend is lower than pure gasoline and hence blend fuel flow rate must be increased until the O_2 % is maintained the same in exhaust at same air flow rate when fuel is switched from gasoline to blend.

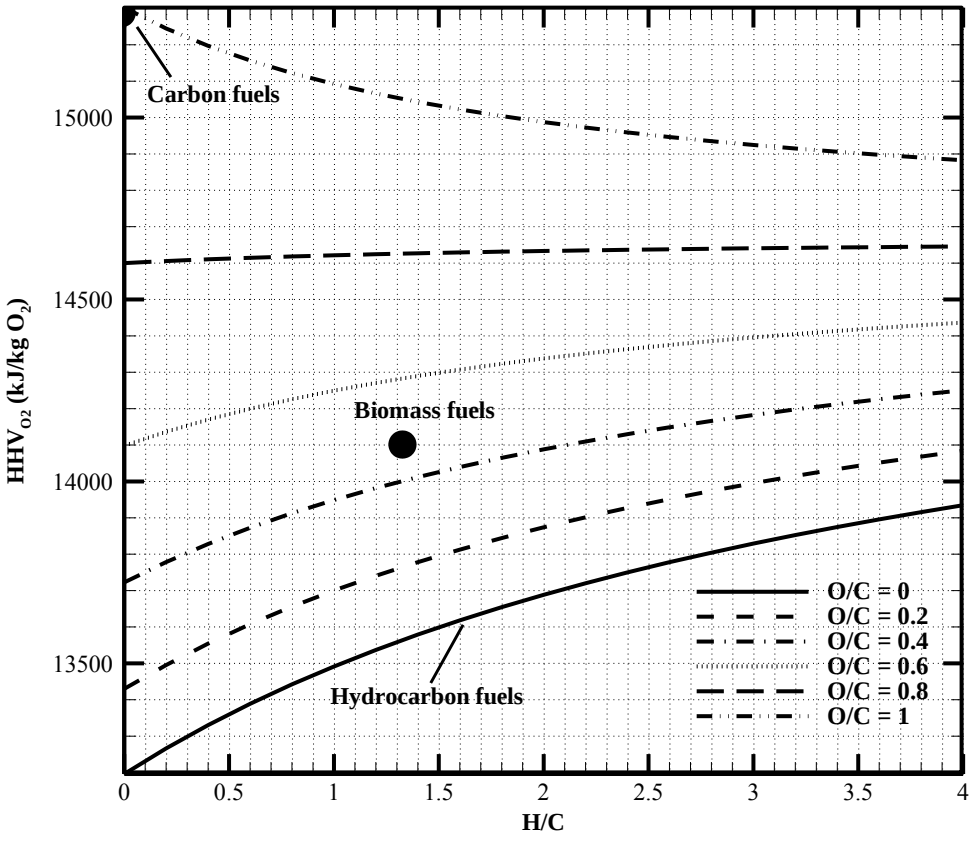

Fig. 61. Variation of Higher heating value of fuels per kg of oxygen consumed with increase in H/C ratio in fuels. It can be seen that HHV_{O2} almost remains constant for all fuels.

5.10.3. CO_2 emission in tons/GJ and RQ factor from fuel composition

Boie equation can be used to derive an expression to estimate the CO_2 emitted in tons per GJ of energy input from the fuel chemical composition as given in the Eq. (46).

$$CO_2 \text{in tons/GJ} = \frac{1*44*1000}{\left\{422270*\left(1+\left(\frac{117385}{422270}\right)*\left(\frac{H}{C}\right)-\left(\frac{177440}{422270}\right)*\left(\frac{O}{C}\right)\right)\right\}} \quad (46)$$

The CO_2 in tons per GJ of energy input is given according to Eq. (47a).

$$CO_2 \text{in tons per GJ energy input} = RQ * \frac{\text{kg } O_2}{HHV_{O_2} \text{ in GJ}} * \frac{\text{kmol } O_2}{32 \text{ kg}} * \frac{44.01 \text{ kg}}{\text{kmol } CO_2} * \frac{0.001 \text{ Tons}}{kg} \quad (47a)$$

Assuming HHV_{O2}=0.014 GJ/kg O_2,

CO_2 in tons per GJ of energy input can be reduced to ≈ RQ * 0.1. (47b)

where the approximate sign is due to assumption of constant HHV_{O2}= 0.014 GJ per kg of O_2 consumed. For RQ=1 (pure carbon), CO_2 is about 0.1 tons per GJ or 100 g per MJ.

In order to validate approximate expression for CO_2, actual measured heating values of fuels for which compositions are well known (e.g, CH_4, C_8H_{18}, $C_{12}H_{23}$, C_2H_5OH, coal, biomass, etc) are used to estimate CO_2 in tons per GJ. Results are shown

in Fig. 62. It is apparent from Fig. 62 that CO_2 in tons per GJ of energy input has a slope of 0.1 which confirms the approximation.

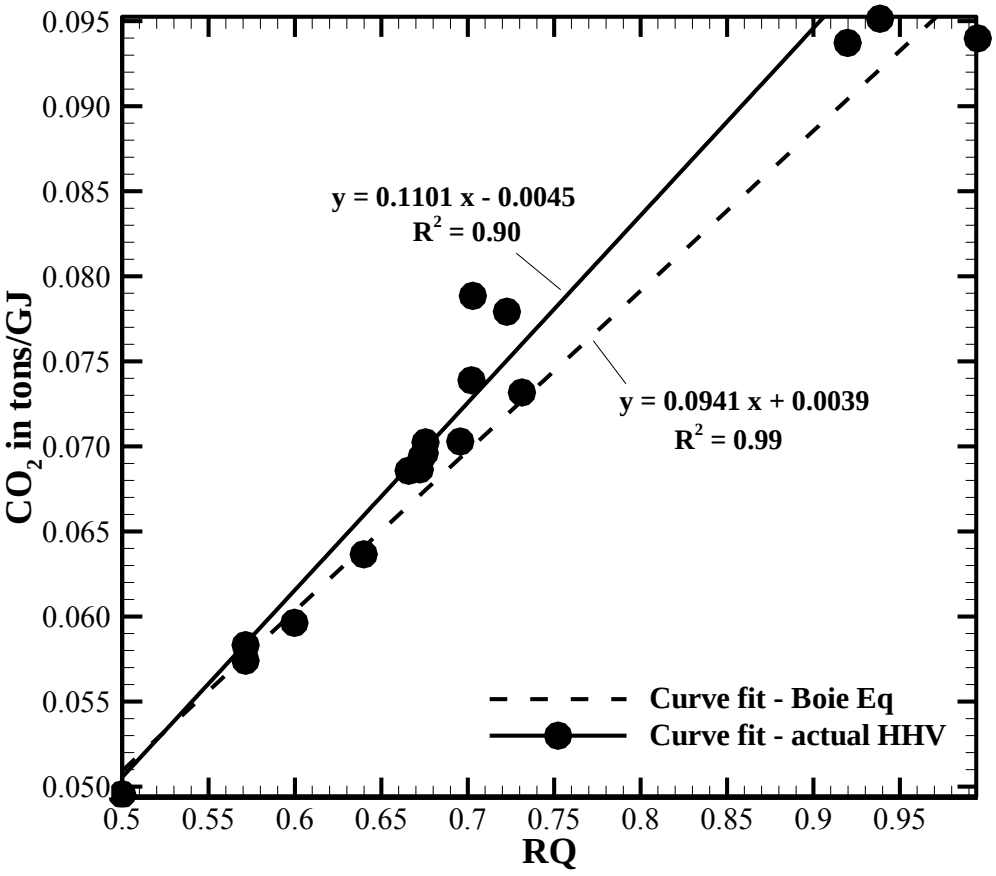

Fig. 62. CO_2 emitted in tons per GJ of energy input for fuels with different RQ factors. Fuel measured heating value and composition data was used in estimation of CO_2. Slope of both the trend lines (actual heating value and heating value estimated using Boie equation) was 0.1 which is same as the approximate value derived using Eq. (47b).

The RQ factor for fuels of known composition can be estimated using Eq. (28).

Table 26 shows the variation of RQ factor different fuels.

Table 26. RQ factor for different fuels along with their respective O/C and H/C ratios.

Fuel	**O/C**	**H/C**	***RQ***
Gaseous fuels			
Methane	0.00	4.00	0.50
Ethane	0.00	3.00	0.57
Ethylene	0.00	3.00	0.57
Propane	0.00	2.67	0.60
Acetylene	0.00	1.00	0.80
Liquid fuels			
Methanol†	1.00	4.00	0.67
Ethanol†	0.50	2.99	0.67
Gasoline (C_8H_{18})	0.00	2.25	0.64
Diesel ($C_{12}H_{23}$)	0.00	1.92	0.68
Biodiesel†	0.10	1.90	0.70
Free fatty acid from peanut oil soap stock†	0.07	1.83	0.70
Canola oil†	0.08	1.63	0.73
Heavy oil	0.01	1.55	0.72
Bio oil (wood pyrolysis)†	0.50	1.34	0.92
Solid fuels			
Softwood (Juniper)†	0.56	1.39	0.94
Hardwood (mesquite)†	0.58	1.37	0.95
Fibrous (rice straw)†	0.66	1.33	1.00
Animal based (LAPCDB)†	0.40	1.26	0.89
WYO coal	0.18	0.70	0.92
TXL coal	0.19	0.68	0.93
† Renewable fuels			

In general, the RQ factor increases with decrease in hydrogen to carbon ratio. Methane which has a H/C ratio of 4 has the lowest RQ factor for pure fuels with RQ=0.5. It can be observed from Table 26 that the solid fuels have comparatively higher oxygen content. Higher oxygen content results in higher RQ factor for solid fuels.

Gasoline and diesel fuels which are used in the automobiles have a comparatively lower RQ when compared to that of solid fuels. Lower O/C ratio of the liquid fuels is one of the factors behind the lower RQ values.

It is seen that most solid fuels (pure carbon RQ=1, biomass fuels (mesquite and juniper) RQ=0.94-0.97, most sweet sorghum sources=0.98 to 1.0 [13], coals RQ=0.92-0.93 and animal wastes RQ= 0.92-0.95) have a RQ factor of around 0.95. Gaseous and liquid fuels have RQ between 0.50 and 0.80. It is noted that renewable biomass fuels have slightly higher RQ (e.g. coal with RQ of 0.92 and biomass with RQ of 0.97).

Fig. 63 shows the plot for variation of "RQ" with H/C and O/C ratio of the fuels. Since HHV_{O2} is constant for most fuels, then for given thermal input, the O_2 moles consumed will remain the same. Hence a fuel with higher RQ produces more CO_2 for same thermal heat input i.e more tons of CO_2 per GJ. RQ scaling is applied only to oxidation processes; for example RQ tends to ∞ for anaerobic digestion which produces CH_4 and releases CO_2 since no O_2 is consumed. It does not imply that it has highest global warming potential. Here the production of CH_4 becomes important. Even in human body, senior people seem to have a higher RQ compared to young adults [142] due to anaerobic digestion in O_2 starved cells.

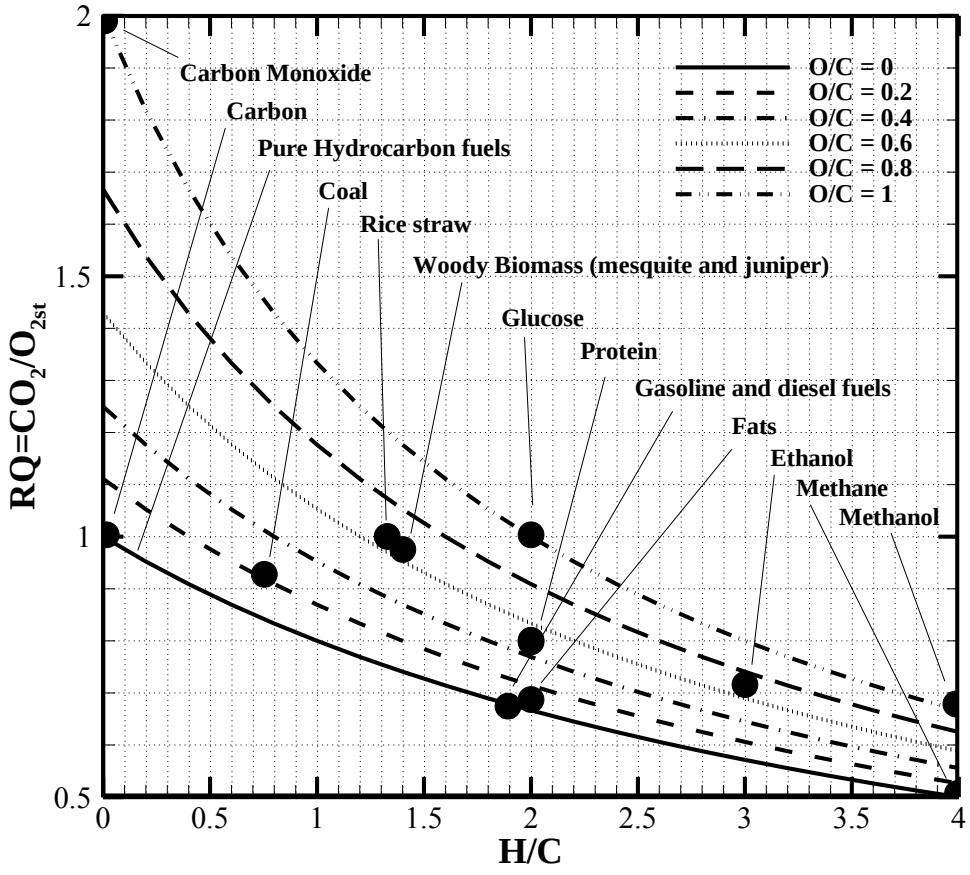

Fig. 63. Variation of RQ with H/C ratio and O/C ratio of the fuel. Gaseous and liquid fuels have lower RQ factor when compared to that of solid fossil and renewable fuels.

Using the Boie equation, one can estimate the amount of carbon emissions from a fuel. Carbon dioxide emitted on a mass basis (g/MJ or kg/GJ) determined for different fuel compositions is shown in Fig. 64. Just as Environmental Protection Agency (EPA) sets limit on NO_X in lb per mmBTU or kg /GJ, the CO_2 amount must be estimated in kg per unit GJ or lb per mmBTU rather than kg of CO_2 per kg fuel since heat input must be

maintained the same when fuel is switched. Both Fig. 63 and Fig. 64 follow the same trend in terms of increased emissions with increase in oxygen content and C/H ratio in the fuel. From results on RQ factor and carbon dioxide emissions from fuels, it can be seen that the liquid fuels currently used in automobiles have the least RQ factor next only to natural gas. Biofuels produced from renewable energy sources are limited by the energy density and oxygen content.

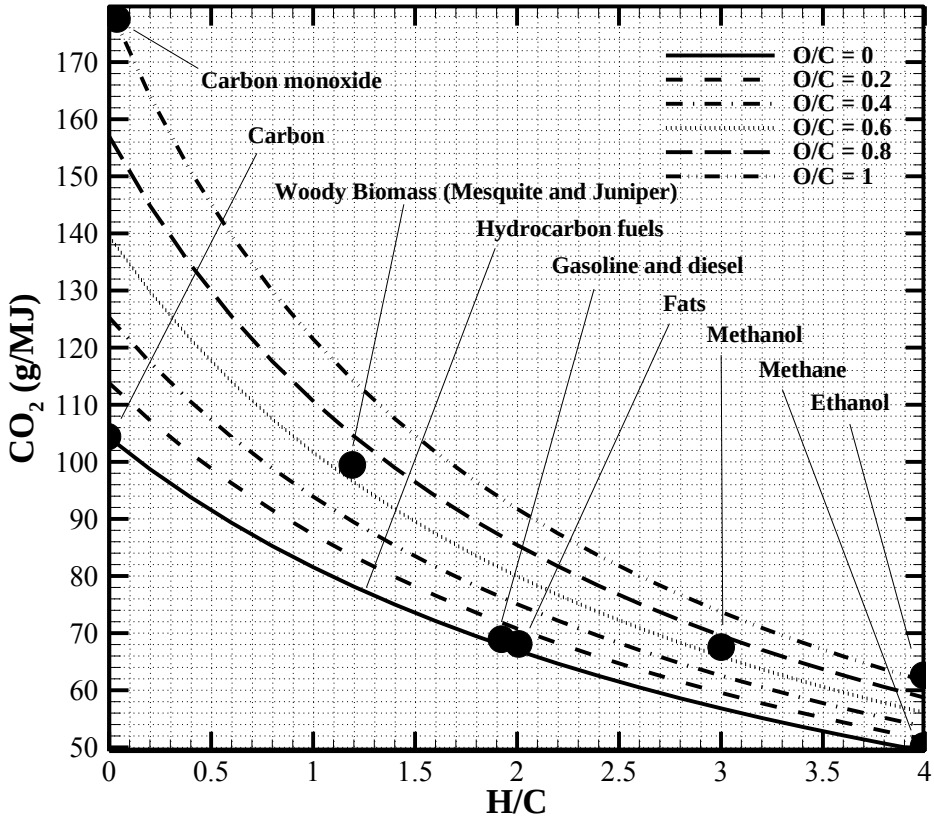

Fig. 64. Effect of H/C and O/C on the CO_2 emission from fuels. Fuels with higher RQ factor emit higher amounts of carbon dioxide.

If the oxygen content can be reduced by using torrefaction of biomass , catalytic cracking and hydrotreating [143] of bio-oils, the energy density of the biomass and bio-oils can be improved and in turn will also reduce the RQ factor of the fuels. But such a process also reduces the yield of bio oil. Though renewable fuels are argued to be carbon neutral, their potential to emit carbon is much higher (higher RQ when compared to coal). Coupled with its lower energy density, variability in production and process efficiencies and land usage pattern, studies should be done to effectively use fossil fuels with reduced RQ factor.

5.10.4. RQ factor from exhaust gas composition

Eq. (29) to Eq. (33) which gives the relation between O_2 %, CO_2 % and RQ factor of the fuel can be used to present the variation of RQ for different exhaust oxygen concentrations (X_{CO2e}). Resulting plot is shown in Fig. 65. This plot will serve as an important tool to determine the RQ factor for fuels of unknown composition (e.g. blended fuels like gasoline:alcohol, solid fuels in power plants) from the exhaust gas composition measurements. Particularly Eq. (29) can be used to determine RQ.

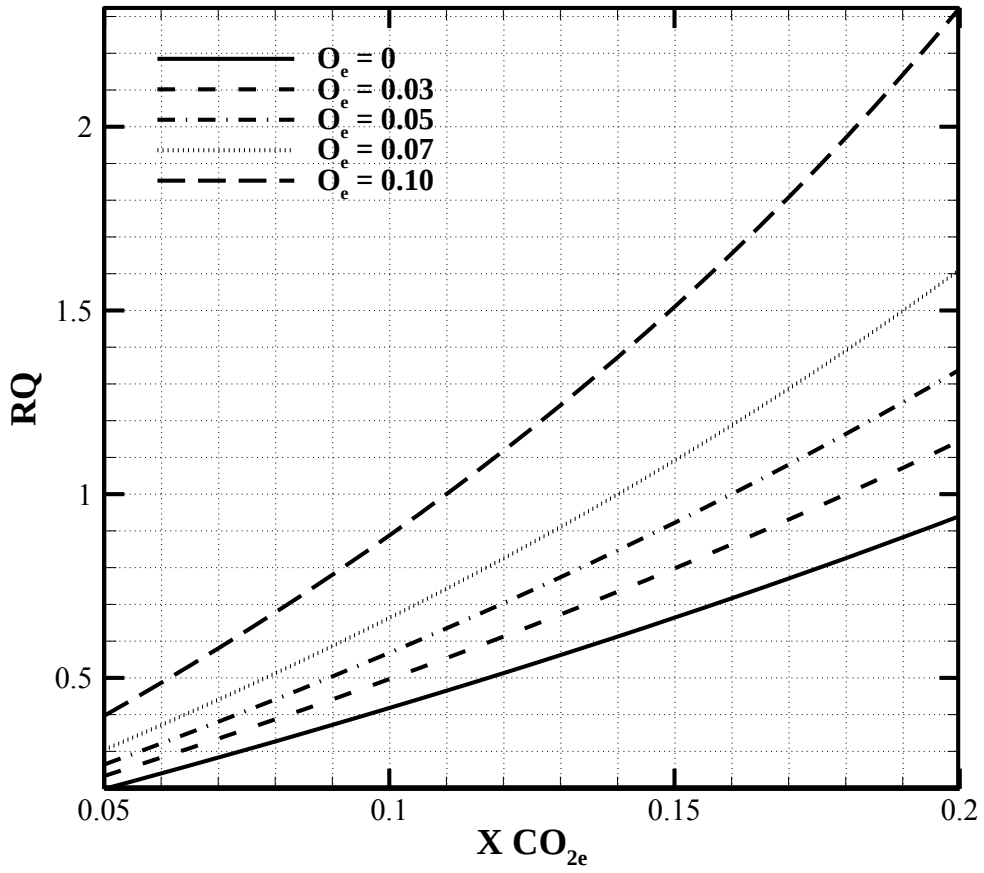

Fig. 65. Variation of RQ with respect to dry carbon dioxide and oxygen concentration in the flue gas.

An empirical relation for the total dry flue gas volume from combustion of a fuel can be estimated from the flue oxygen concentration and fuel ultimate analysis [102].

$$\text{Dry Flue gas STP volume } (m^3/GJ) = \left\{3.55 + 0.131 * O_2\% + 0.018 * (O_2\%)^2\right\}\left(\frac{H}{C}\right)^2 - \left\{27.664 + 1.019 * O_2\% + 0.14 * (O_2\%)^2\right\}\left(\frac{H}{C}\right) + \left\{279.12 + 10.285 * O_2\% + 1.416 * (O_2\%)^2\right\} \quad (48)$$

This relation is valid for oxygen concentration between 0% and 9% on a volume basis. In addition, the RQ factor of a fuel along with exhaust CO_2 concentration can also be used to determine the flue gas volume using the following relation.

$$\text{Dry Flue gas volume } (m^3/GJ) = \left(\frac{RQ*100}{CO_2\%}\right) * \frac{24.5SATP\,\frac{m^3}{kmol}}{HHV_{O_2}\,\frac{GJ}{kmol}} \tag{49}$$

Gas analysis from the experiments conducted on firing pure coal and coal biomass blends were used to determine the dry flue gas volume using Eq. (48) and Eq. (49). The values predicted using RQ factor of the fuel were also in close agreement with the values estimated from the empirical relation. The difference between the predicted flue gas volumes using the RQ method was between 0.4% and 1.5% when compared to the volume determined using the relation. Table 27 shows the values obtained for the volume of flue gas for different experimental conditions. The total flue gas volume on a dry basis varied between 260 m^3/GJ to 290 m^3/GJ when ER decreased from 0.95 to 0.85. Lower ER indicates higher amount of air supplied and hence more volume of flue gas will result due to higher percentages of nitrogen entering along with the incoming air. Based on Eq. (50) with increase in ER, the percentage of CO_2 produced increases and since the RQ of the fuel remains the same, the volume of flue gas produced will decrease.

Table 27. Dry flue gas volume determined using empirical method and RQ method for cofiring experiments.

Fuel	ER	O_2	CO_2	RQ fuel	dry flue V based on RQ (m^3/GJ)	dry flue V based on empirical relation [102] (m^3/GJ)
PRB	0.85	3.02	17.5	0.92	287.0	291.0
PRB	0.90	2.07	18.3	0.92	275.0	278.2
PRB	0.95	1.33	19.2	0.92	263.2	267.4
PRB-RM	0.85	3.12	17.3	0.92	291.4	292.5
PRB-RM	0.90	2.05	17.8	0.92	283.2	284.2
PRB-TM	0.90	2.02	18.4	0.92	273.2	274.4
PRB-TM	0.85	2.89	17.9	0.92	280.4	281.4
PRB-TM	0.95	1.28	18.9	0.92	265.7	267.6
PRB-TJ	0.90	2.23	18.1	0.92	277.8	278.8
PRB-RJ	0.90	2.06	19.1	0.92	263.1	264.9

PRB: Powder river basin sub-bituminous coal; RM: Raw mesquite; TM: Torrefied Mesquite; RJ: Raw Juniper; TJ: Torrefied Juniper.

Eq. (29) to Eq. (33) was used to determine the RQ of the fuel from the exhaust gas analysis of combustion of pure coal and coal biomass blends. The results obtained were compared to the RQ of the fuel obtained from the fuel composition (Eq. (28)). The RQ factor determined from the exhaust gas analysis were higher than the RQ determined from the fuel composition. The reason behind such high numbers is due to the assumption that the flue gas consist mainly O_2, CO_2 and N_2. However it was observed from the experimental results that considerable amount of CO is also produced at high ER. The difference in the RQ factor numbers calculated from the fuel composition and exhaust gas analysis can be attributed to the assumptions made at arriving at the

numbers. In addition the burnt fraction of a fuel can be determined from the fuel composition, exhaust gas analysis and fuel RQ factor based on Eq. (50).

$$\text{Burnt Fraction} \cong \frac{RQ_{measured}}{RQ_{theoretical}} \cong \frac{CO_{2,measured}}{CO_{2,theoretical}} \tag{50}$$

Table 28. RQ factor and Burnt fraction determined from the experimental flue gas composition.

Fuel	ER	O_2	CO_2	RQ fuel	RQ gas	Burnt Fraction (RQ)	Burnt fraction (Flue gas)
PRB	0.85	3.02	17.5	0.92	0.97	0.89	1.01
PRB	0.90	2.07	18.3	0.92	0.96	0.93	1.01
PRB	0.95	1.33	19.2	0.92	0.97	0.97	1.00
PRB-RM	0.85	3.12	17.3	0.92	0.96	0.88	0.98
PRB-RM	0.90	2.05	17.8	0.92	0.92	0.90	0.98
PRB-TM	0.90	2.02	18.4	0.92	0.96	0.94	1.05
PRB-TM	0.85	2.89	17.9	0.92	0.99	0.91	1.04
PRB-TM	0.95	1.28	18.9	0.92	0.95	0.96	1.03
PRB-TJ	0.90	2.23	18.1	0.92	0.96	0.92	1.01
PRB-RJ	0.90	2.06	19.1	0.92	1.01	0.97	1.03

Burnt fraction determined from Eq. (50) is given as Burnt fraction (RQ) and burnt fraction estimated from Eq. (44) is given as Burnt fraction (Flue gas). The burnt fraction increases with increase in ER as combustion approaches stoichiometric condition. Burnt fraction estimated from the RQ method exhibited an increasing trend with increase in ER. Burnt fraction estimated from the flue gas oxygen concentration (Eq. (44)) gave numbers greater than one for all the conditions predicting complete combustion of the fuel under all ER employed. Such high numbers are due to uncertainty

in measurements and it also shows the limitation of application of Eq. (44) for determining the burnt fraction. Since all the combustion experiments were performed at lean conditions, complete combustion of fuels in addition to higher oxygen percentages in the exhaust contributed to higher numbers for burnt fraction.

5.10.5. RQ factor for fuel processing

Even though biomass is a renewable fuel where CO_2 produced by direct combustion is neutralized by CO_2 used in production of fuel, the processing of biomass (electrical power for pumping water, heat required for drying, fertilizer used for cultivation, fuels used for collection and transportation etc) releases CO_2 if fossil fuels are used to grow and process biomass. Then one can define equivalent RQ value ($RQ_{process,biomass}$) for biomass processing by estimating tons of CO_2 released per GJ of heat content of biomass delivered to power plants. Appendix E presents the derivation for $RQ_{process,biomass}$. $RQ_{process,biomass}$ can be defined according to Eq. (51).

$$RQ_{process,biomass} = 219 * \frac{RQ_{biomass}}{\left(\frac{C\%}{12.01}\right)} \left\{ \frac{RQ_1 * p_{elec.}\left(\frac{GJ}{\text{kg biomass}}\right)}{\eta} + \frac{RQ_2 * q_{heat}\left(\frac{GJ}{\text{kg biomass}}\right)}{\eta_{burner}} + RQ_3 + RQ_4 \right\} \quad (51)$$

where RQ_1 refers to fossil fuel used for electric power generation, RQ_2 refers to another fossil fuel used for direct heat production, η: power plant efficiency, η_{burner}: burner efficiency RQ_3 refers to CO_2 released during collection and transportation, RQ_4 for CO_2 produced while producing fertilizers and C%, carbon mass % in biomass fuels. RQ (by

direct oxidation) is relatively fixed for most biomass fuels. However C% decreases when there is more oxygen, moisture and ash in biomass fuel. Thus higher amount of biomass would be needed for the same heat input and larger the CO_2 emitted during the processing of renewable biomass fuels. Hence $RQ_{process,biomass}$ increases and if it reaches same as coal, then such a biomass is not useful as renewable fuel. i.e. criteria must be $RQ_{process\ biomass} < RQ_{coal}$ if biomass is used to replace coal in order to reduce GWP. Life cycle assessment of willow biomass production was analyzed by Heller et al. [144]. Based on the analysis it was estimated that the total energy consumed for the production of willow based biomass was 98.3 GJ/ha over seven harvest rotations. Around 13.6 oven dry tonnes per hectare per year was estimated to be the average yield of the biomass. Assuming mesquite and juniper will also consume similar amount of energy when cultivated on a large scale solely for the utilization of these woody biomass for power production, $RQ_{process,biomass}$ can be determined based on the data provided by Heller et al. [144]. The $RQ_{process,biomass}$ for both mesquite and juniper was found to be 0.03 based on the life cycle analysis data. Appendix F shows the calculation of $RQ_{process,biomass}$ for mesquite and juniper biomass. Further when the raw biomass is torrefied, moisture content in the torrefied samples will be low. In addition to lower moisture content, torrefied samples will exhibit improved grindability. Hence $RQ_{process,biomass}$ for the torrefied samples will be lower than the raw biomass samples.

5.10.6. RQ factor for fuel blends

The RQ factor for the blend of biomass with coal should be less than the RQ factor for pure coal so that using biomass will result in reduced CO_2 emissions. RQ for the fuel blend can be determined using the following formula.

$$RQ_{fuel,blend} = RQ_{coal} * HF_{coal} + \left(RQ_{biomass} + RQ_{process,biomass} \right) * HF_{biomass} \quad (52)$$

where HF is the heat fraction contributed by the fuel present in the blend. Heat fraction of a fuel is defined as the ratio of heat content of a particular fuel to the total heat content of the blend (kJ of fuel/ kJ of fuel blend). For the case of 90:10 blends of coal and woody biomass which was used in the current study, the $RQ_{fuel,blend}$ was determined to be 0.82 assuming $RQ_{biomass}$ to be zero since biomass is considered carbon neutral. RQ factor for the fuel blend is lower than the coal RQ value which is 0.92. This indicates lower amount of CO_2 will be released into the atmosphere when 10% of biomass on mass basis is blended with coal. Table 29 shows the RQ_{blend} for the different biomass blends which were used in the current study.

Further it can be seen from Table 29 that the RQ_{blend} for coal and torrefied biomass is lower (0.82) than the raw biomass blends (0.84). Higher heat values of torrefied biomass resulted in higher heat fraction for biomass which led to lower numbers for RQ_{blend}. Also it should be noted that energy consumed for processing torrefied biomass will be lower than the raw biomass if hot flue gas from boiler is used for torrefaction.

Table 29. RQ factor for the 90:10 blend of coal and biomass on a mass basis.

Fuel	RQ_{coal}	HF_{coal}	$RQ_{biomass}$	$RQ_{biomass,processing}$	$HF_{biomass}$	RQ_{blend}
PRB+RM	0.92	0.91	0	0.03	0.09	0.84
PRB+RJ	0.92	0.90	0	0.03	0.10	0.83
PRB+TM	0.92	0.89	0	0.03	0.11	0.82
PRB+TJ	0.92	0.89	0	0.03	0.11	0.82
HF: heat fraction; PRB: Powder river basin sub-bituminous coal; RM: Raw mesquite; RJ: Raw juniper; TM: Torrefied mesquite; TJ: Torrefied Juniper						

6. SUMMARY AND CONCLUSION*

The following is a summary and conclusion based on current experiments dealing with mesquite, juniper and combination of a blend of i) coal and raw biomass and ii) coal and torrefied biomass.

6.1.Torrefaction

1. Torrefaction of these woody biomass serves to improve the properties of biomass in terms of increased heating value, improved grindability and hydrophobicity.
2. Comparable mass losses were observed on using the two mediums (CO_2 and N_2) for temperatures lesser than 250˚C. Lower particle size results in higher mass losses when compared to that of larger particles.
3. Comparing the mass and energy yield, torrefaction at 240˚C seems to be the optimum temperature for torrefaction of mesquite and juniper biomass.
4. Effect of using CO_2 as the torrefaction medium serves to improve the grindability of the biomass because of the increased surface area caused due to the formation of pores on the biomass samples.
5. Though a small amount of CO_2 may react with the biomass, the effect of such reaction can be controlled by varying the particle size of biomass torrefied and temperature of torrefaction.

*Reproduced in part with permission from Thanapal SS, Chen W, Annamalai K, Carlin N, Ansley RJ, Ranjan D. Carbon Dioxide torrefaction of woody biomass. Energy Fuels 2014; 28:1147–57. Copyright 2014 American Chemical Society.

6. Carbon dioxide torrefaction enables the use of exhaust gases from the boilers.

6.2.Three component modeling and TGA results

1. A simple TCM based on independent parallel reactions has been developed to model the torrefaction of woody and fibrous biomass in order to predict mass loss, heating value of biomass at any stage of torrefaction vs temperature (or time).
2. Mass loss predicted by the TCM was compared with the experimental data obtained from TGA. It is shown that heat value of the torrefied biomass increased with increase in pretreatment temperatures while the energy retention ratio decreased at high temperatures due to loss of higher amounts of combustible volatile matter at higher temperatures.

6.3.MVR model and TGA-DTG results

1. An additional model called MVR technique can be employed to extract the global reaction kinetics for the fuel samples including the determination of activation energy and order of reaction.
2. Use of non-unity order results in better mass loss prediction.
3. Increase in activation energy can be attributed to the loss in hemicellulose and cellulose components in the biomass.

4. Increased non-unity order is considered to be caused due to increased porosity in the treated biomass samples which result in increased production of gases upon pyrolysis.
5. Increased treatment temperatures result in an order comparable to that of coal.

6.4.Cofiring torrefied and raw biomass with coal

1. Effect of cofiring torrefied woody biomass mesquite and juniper with PRB coal was studied in a 30 kWt downfired burner facility on NOx emission, CO emissions and heat transfer characteristics. Parametric studies include the effect of equivalence ratio, type of fuel and amount of biomass in the blend.
2. Generally the biomass cofiring at same thermal input results in slightly higher oxygen percentage in the exhaust and higher CO% which is essentially due to higher volatile matter. Also higher levels of CO were observed at higher ER.
3. The NOx emission decreased with increase in ER and with the blending of biomass with coal. NOx emission decreased by 10% both on a volume basis (ppm) and energy basis when torrefied mesquite was cofired with PRB coal.
4. Transient heat transfer studies were done using three HEX tubes mounted perpendicular to the flow of hot flue gases. Overall heat transfer coefficients (OHTC) decreased with increase in time for the cofiring of biomass with coal due to the deposition of ash on the heat exchanger tubes. Further a slight shift in the location of the flame was observed from the higher OHTC values obtained for the middle HEX tubes.

5. Deposited ash on the HEX tube surfaces was easily removed after 90 minutes of operation. Hence soot blowers could be operated every 90 minutes to remove the deposited ash (frequency in power plants).
6. A zero-dimensional combustion model which takes into account the recirculation zones developed in a swirl burner was used to predict the emissions from the combustion of coal and biomass fuels in a 30 kWt downfired burner. Lower NOx emissions were predicted at higher ER for pure PRB combustion and with blending biomass with coal due to formation of higher percentages of NH_3 from biomass fuel nitrogen which reduces the NOx produced in the burner.

6.5.Respiratory quotient (RQ) for fuels

1. Chemical composition of the fuels and correlations developed to estimate the heating values can be used effectively to study the variation in heating values with respect to the fuel properties. The RQ term defined as the amount of CO_2 moles produced per unit mole O_2 consumed used extensively in the biological literature has been applied to combustion applications. RQ factor has been used to estimate the amount of CO_2 which is a measure of GWP.
2. Lower the RQ, lower the amount of CO_2 produced for every mole of oxygen consumed for combustion process and lower the CO_2 in tons per GJ which is shown to be approximately equal to 0.1*RQ.
3. Two methods were presented to determine the RQ factor of fuels: known composition of fuel or exhaust gas analyses. It was observed that the carbon

emission potential and hence the global warming potential was considerably low for gaseous fuels which typically have low RQ values (RQ =0.5 for CH_4). Conventional liquid fuels such as gasoline and diesel (around 0.7) and solid fossil fuels and renewable fuels such as biomass with comparatively higher oxygen content had higher RQ factor (0.93-1.0).

4. Further a term called $RQ_{process,biomass}$ is introduced to determine the effect of using a renewable fuel along with fossil fuels. $RQ_{process,biomass}$ for both mesquite and juniper (which does not use water or electricity for cultivation) was estimated to be 0.03 based on woody biomass life cycle analysis.
5. Method for estimating the RQ_{blend} for the blend of coal and biomass was presented and the RQ_{blend} for 90:10 blend of coal and torrefied biomass was 0.82 (where RQ for biomass is zero) which is lower than the RQ factor of raw coal which is 0.92.

7. FUTURE WORK*

1. Peak mass release rate of the three components hemicellulose, cellulose and lignin should be determined from the respective TGA data along with the peak temperature to determine the kinetic parameters, activation energy and pre-exponential factor from the MVR method. The determined numbers can then be used in the TCM to predict the mass loss and energy yield during torrefaction.
2. TCM should be extended to determine the conversion of the three components for non-unity orders.
3. Further the percentage of cellulose, hemicellulose and lignin in raw and torrefied biomass samples should be determined experimentally in order to understand the effect of temperature on the three components.
4. Considering the results obtained from torrefaction studies in batch reactor, it should be noted that further studies should be done to characterize the composition of the condensed tar, gases released and the changes to the percentages of the three components (hemicellulose, cellulose and lignin) along with three component modeling studies in order to gain a better understanding about increased mass losses upon using CO_2.

*Reproduced in part with permission from Thanapal SS, Chen W, Annamalai K, Carlin N, Ansley RJ, Ranjan D. Carbon Dioxide torrefaction of woody biomass. Energy Fuels 2014; 28:1147–57. Copyright 2014 American Chemical Society.

5. Extend the zero dimensional model to three dimensions to model the complex chemical reactions at each time step within the burner. Compare the results obtained with the commercially available CFD codes.
6. Develop a continuous torrefaction facility to utilize the hot flue gases for thermal pretreatment of biomass.
7. Study the effect of cofiring higher percentages of torrefied and raw woody biomass samples with coal to identify the optimum condition for maximum reduction in harmful emissions.
8. Potential of the torrefied and raw woody biomass materials as reburn fuels should also be investigated.
9. The effect of swirl number by varying the angle of the swirl blades and the effect of primary air percentage should be studied to understand how the developed recirculation zone while cofiring raw biomass affect the reduction of NOx to molecular nitrogen.
10. Further, experiments should be carried out for longer time periods to study the fouling potential of raw and torrefied woody biomass. This will help to identify the optimum time duration for the soot blowing operation to remove the deposited ash on the heat exchanger surfaces.

REFERENCES

[1] EIA, Market Trends - Natural gas: http://www.eia.gov/forecasts/aeo/MT_naturalgas.cfm, accessed February 20, 2014.

[2] BP, BP statistical review of world energy 2013: http://www.bp.com/content/dam/bp/pdf/statistical-review/statistical_review_of_world_energy_2013.pdf, accessed October 15, 2013.

[3] EIA, EIA Total Energy data: http://www.eia.gov/totalenergy/data/annual/showtext.cfm?t=ptb0804a, accessed August 12, 2013.

[4] EIA, EIA forecast: http://www.eia.gov/forecasts/ieo/, accessed August 12, 2013.

[5] EPA, EPA Greenhouse Gas Reporting Data: http://www.epa.gov/ghgreporting/ghgdata/reported/index.html, accessed August 13, 2013.

[6] Forster P, Ramaswamy V, Artaxo P, Berntsen T, Betts R, Fahey DW, et al. Changes in Atmospheric Constituents and in Radiative Forcing, in: Solomon S, Qin D, Manning M, Chen Z, Marquis M, Averyt KB, et al. (Ed.) Climate Change 2007: The Physical Science Basis. Contribution of Working Group I to the Fourth Assessment Report of the Intergovernmental Panel on Climate Change. New York: Cambridge University Press; 2007.

[7] EPA, EPA NAAQS: http://www.epa.gov/air/criteria.html, accessed August 13, 2013.

[8] Oh HJ. Reburning renewable biomass for emissions control and ash deposition effects in power generation. PhD dissertation. Texas A&M University; 2008.

[9] IEA, IEA world energy statistics: www.iea.org/publications/freepublications/publication/kwes.pdf, accessed May 15, 2013.

[10] McKendry P. Energy production from biomass (part 1): overview of biomass, Bioresour Technol 2002;83:37-46.

[11] Tillman D, Duong D, Harding N. Solid Fuel Blending; Principles, Practices, and Problems. 1st ed. Waltham: Butterworth Heinemann; 2012.

[12] Demirbas A. Combustion characteristics of different biomass fuels. Prog Energy Comb Sci 2004;30:219-30.

[13] TAMU, TAMU fuel data bank: http://cabel.tamu.edu/TAMU%20FDB.htm, accessed August 13, 2013.

[14] Tillman DA. Biomass cofiring: the technology, the experience, the combustion consequences. Biomass Bioenerg 2000;19:365-84.

[15] Demirbas A. Fuel and combustion properties of bio-wastes. Energy sources. 2005;27:451-62.

[16] Thanapal SS, Annamalai K, Sweeten JM, Gordillo G. Fixed bed gasification of dairy biomass with enriched air mixture. Appl Energ 2012;97:525-31.

[17] Di Nola G, Spliethoff H. Fuel-bound nitrogen partitioning and NOx emissions during biomass cofiring. Clean Air 2007;8:199-220.

[18] Lawrence B, Annamalai K, Sweeten JM, Heflin K. Cofiring coal and dairy biomass in a 29kWt furnace. Appl Energ 2009;86:2359-72.

[19] Baxter LL. Ash deposition during biomass and coal combustion: a mechanistic approach. Biomass Bioenerg 1993;4:85-102.

[20] Thanapal SS. Gasification of low ash partially composted dairy biomass with enriched air mixture. Masters Thesis. Texas A&M University; 2010.

[21] Magasiner N, Van Alphen C, Inkson MB, Misplon BJ. Characterising fuels for biomass-Coal fired cogeneration, in: 75th SASTA Congress, DURBAN, 2001.

[22] Wikipedia, Mesquite scientific classification: http://en.wikipedia.org/wiki/Prosopis_glandulosa, accessed August 17, 2011.

[23] Ansley RJ, Mirik M, Castellano MJ. Structural biomass partitioning in regrowth and undisturbed mesquite (Prosopis glandulosa): implications for bioenergy uses. GCB Bioenerg 2010;2:26-36.

[24] Ansley RJ, Ben Wu X, Kramp BA. Observation: long-term increases in mesquite canopy cover in a north Texas savanna. J Range Manag 2001; 171-76.

[25] Wikipedia, Juniper scientific classification: http://en.wikipedia.org/wiki/Juniperus_pinchotii, accessed August 17, 2011.

[26] Ueckert DN, Phillips RA, Petersen JL, Ben Wu X, Waldron DF. Redberry juniper canopy cover dynamics on western Texas rangelands. J Range Manag 2001;603-10.

[27] Biagini E, Barontini F, Tognotti L. Devolatilization of biomass fuels and biomass components studied by TG/FTIR technique. Ind Eng Chem Res 2006;45:4486-93.

[28] Vamvuka D, Kakaras E, Kastanaki E, Grammelis P. Pyrolysis characteristics and kinetics of biomass residuals mixtures with lignite. Fuel 2003;82:1949-60.

[29] Bradbury AG, Sakai Y, Shafizadeh F. A kinetic model for pyrolysis of cellulose. J Appl Polym Sci 1979;23:3271-80.

[30] Ozawa T. A new method of analyzing thermogravimetric data. Bull Chem Soc Jpn 1965;38:1881-86.

[31] Chen W. Fixed bed counter current low temperature gasification of mesquite and juniper biomass using air-steam as oxidizer. PhD dissertation. Texas A&M University; 2012.

[32] Hu S, Jess A, Xu M. Kinetic study of Chinese biomass slow pyrolysis: Comparison of different kinetic models. Fuel 2007;86:2778-88.

[33] Wang XY, Wan XJ, Chen MQ, Wang J. Kinetic Model of Biomass Pyrolysis Based on Three-component Independent Parallel First-order Reactions. Chin J Process Eng 2012;12:1020-4.

[34] Mészáros E, Várhegyi G, Jakab E, Marosvölgyi B. Thermogravimetric and reaction kinetic analysis of biomass samples from an energy plantation. Energy fuels 2004;18:497-507.

[35] Manya JJ, Velo E, Puigjaner L. Kinetics of biomass pyrolysis: a reformulated three-parallel-reactions model. Ind Eng Chem Res 2003;42:434-41.

[36] Varhegyi G, Antal Jr MJ, Szekely T, Szabo P. Kinetics of the thermal decomposition of cellulose, hemicellulose, and sugarcane bagasse. Energy Fuels 1989;3:329-35.

[37] Anthony DB, Howard JB, Hottel HC, Meissner HP. Rapid devolatilization and hydrogasification of bituminous coal. Fuel 1976;55:121-8.

[38] Sonobe T, Worasuwannarak N. Kinetic analyses of biomass pyrolysis using the distributed activation energy model. Fuel 2008;87:414-21.

[39] Peng Y, Wu S. The structural and thermal characteristics of wheat straw hemicellulose. J Anal Appl Pyrolysis 2010;88:134-9.

[40] Antal MJJ, Varhegyi G. Cellulose pyrolysis kinetics: the current state of knowledge. Ind Eng Chem Res 1995;34:703-17.

[41] Faix O, Jakab E, Till F, Székely T. Study on low mass thermal degradation products of milled wood lignins by thermogravimetry-mass-spectrometry. Wood Sci Technol 1988; 22:323-34.

[42] Ferdous D, Dalai AK, Bej SK, Thring RW. Pyrolysis of lignins: experimental and kinetics studies. Energy Fuels 2002;16:1405-12.

[43] Di Blasi C. Modeling chemical and physical processes of wood and biomass pyrolysis. Prog Energy Comb Sci 2008;34:47-90.

[44] Bridgeman TG, Jones JM, Shield I, Williams PT. Torrefaction of reed canary grass, wheat straw and willow to enhance solid fuel qualities and combustion properties. Fuel 2008;87:844-56.

[45] Arias B, Pevida C, Fermoso J, Plaza MG, Rubiera F, Pis JJ. Influence of torrefaction on the grindability and reactivity of woody biomass. Fuel Process Technol 2008;89:169-75.

[46] Almeida G, Brito JO, Perré P. Alterations in energy properties of eucalyptus wood and bark subjected to torrefaction: the potential of mass loss as a synthetic indicator. Bioresour Technol 2010;101:9778-84.

[47] Prins MJ, Ptasinski KJ, Janssen FJ. Torrefaction of wood: Part 2. Analysis of products. J Anal Appl Pyrolysis 2006;77:35-40.

[48] Yan W, Hastings JT, Acharjee TC, Coronella CJ, Vasquez VR. Mass and Energy Balances of Wet Torrefaction of Lignocellulosic Biomass. Energy Fuels 2010;24: 4738-42.

[49] Rousset P, Macedo L, Commandré JM, Moreira A. Biomass torrefaction under different oxygen concentrations and its effect on the composition of the solid by-product. J Anal Appl Pyrolysis 2012;96:86-91.

[50] Wang C, Peng J, Li H, Bi XT, Legros R, Lim CJ, et al. Oxidative torrefaction of biomass residues and densification of torrefied sawdust to pellets. Bioresour Technol 2012;127:318-25.

[51] Eseltine D, Thanapal SS, Annamalai K, Ranjan D. Torrefaction of woody biomass (Juniper and Mesquite) Using Inert and non-inert gases. Fuel 2013;113:379-88.

[52] Rowell RM. Handbook of wood chemistry and wood composites. 2nd ed. Florida:CRC press; 2012.

[53] Yang H, Yan R, Chen H, Lee DH, Zheng C. Characteristics of hemicellulose, cellulose and lignin pyrolysis. Fuel 2007;86:1781-88.

[54] Acharjee TC, Coronella CJ, Vasquez VR. Effect of thermal pretreatment on equilibrium moisture content of lignocellulosic biomass. Bioresour Technol 2011;102:4849-54.

[55] Medic D, Darr M, Shah A, Rahn S. Effect of Torrefaction on Water Vapor Adsorption Properties and Resistance to Microbial Degradation of Corn Stover. Energy Fuels 2012;26:2386-93.

[56] Prins MJ, Ptasinski KJ, Janssen FJ. Torrefaction of wood: Part 1. Weight loss kinetics. J Anal Appl Pyrolysis 2006;77:28-34.

[57] Repellin V, Govin A, Rolland M, Guyonnet R. Modelling anhydrous weight loss of wood chips during torrefaction in a pilot kiln. Biomass Bioenerg 2010;34:602-9.

[58] Kwon EE, Jeon EC, Castaldi MJ, Jeon YJ. Effect of Carbon Dioxide on the Thermal Degradation of Lignocellulosic Biomass. Environ Science Technol 2013;47:10541-7.

[59] Kwon EE, Yi H, Castaldi MJ. Utilizing Carbon Dioxide as a Reaction Medium to Mitigate Production of Polycyclic Aromatic Hydrocarbons from the Thermal Decomposition of Styrene Butadiene Rubber. Environ Sci Technol 2012;46:10752-7.

[60] Thanapal SS, Chen W, Annamalai K, Carlin N, Ansley RJ, Ranjan D. Carbon Dioxide torrefaction of woody biomass. Energy Fuels 2014; 28:1147–57.

[61] Hus PJ, Tillman DA. Cofiring multiple opportunity fuels with coal at Bailly Generating Station. Biomass Bioenerg 2000;19:385-94.

[62] Turn SQ, Jenkins BM, Jakeway LA, Blevins LG, Williams RB, Rubenstein G, et al. Test results from sugar cane bagasse and high fiber cane co-fired with fossil fuels. Biomass Bioenerg 2006;30:565-74.

[63] Damstedt B, Pederson JM, Hansen D, Knighton T, Jones J, Christensen C, et al. Biomass cofiring impacts on flame structure and emissions. Proc Comb Inst 2007;31:2813-20.

[64] Arumugam S, Thien B, Annamalai K, Sweeten J. Feedlot biomass co-firing: a renewable energy alternative for coal-fired utilities. Int J Green Energy 2005;2:409-19.

[65] Gogebakan Z, Selçuk N. Cofiring lignite with hazelnut shell and cotton residue in a pilot-scale fluidized bed combustor. Energy Fuels 2008;22:1620-7.

[66] Gogebakan Z, Gogebakan Y, Selcuk N. Co-firing of olive residue with lignite in bubbling FBC. Comb Sci Technol 2008;180:854-68.

[67] Sami M, Annamalai K, Wooldridge M. Co-firing of coal and biomass fuel blends. Prog Energy Comb Sci 2001;27:171-214.

[68] Narayanan KV, Natarajan E. Experimental studies on cofiring of coal and biomass blends in India. Renew Energy 2007;32:2548-58.

[69] Luschen A, Madlener R. Economic viability of biomass cofiring in new hard-coal power plants in Germany. Biomass Bioenerg 2013;57:33-47.

[70] Sampson GR, Richmond AP, Brewster GA, Gasbarro AF. Cofiring of wood chips with coal in interior Alaska. For Prod J 1991;41:53-6.

[71] Abbas T, Costen P, Kandamby NH, Lockwood FC, Ou JJ. The influence of burner injection mode on pulverized coal and biomass co-fired flames. Combust Flame 1994;99:617-25.

[72] Hansen LA, Michelsen HP, Dam-Johansen K. Alkali metals in a coal and biomass fired CFBC - measurements and thermodynamic modeling. Proc Int Conf Fluid Bed Combust, Florida, 1995;39-48.

[73] Brouwer J, Owens WD, Harding S, Heap MP, Pershing DW. Cofiring waste biofuels and coal for emissions reduction. 2nd Biomass Conf Am, Oregon, 1995;390-9.

[74] Daood SS, Javed MT, Gibbs BM, Nimmo W. NOx control in coal combustion by combining biomass co-firing, oxygen enrichment and SNCR. Fuel 2013;105:283-92.

[75] Yang H, Wu Y, Zhang H, Qiu X, Yang S, Liu Q, et al. NOx Emission from a Circulating Fluidized Bed Boiler Cofiring Coal and Corn Stalk Pellets. Energy Fuels 2012;26:5446-51.

[76] Daood SS, Nimmo W, Edge P, Gibbs BM. Deep-staged, oxygen enriched combustion of coal. Fuel 2012;101:187-96.

[77] Strege JR, Zygarlicke CJ, Folkedahl BC, McCollor DP. SCR deactivation in a full-scale cofired utility boiler. Fuel 2008;87:1341-7.

[78] Maciejewska A, Veringa H, Sanders J, Peteves SD. Co-firing of biomass with coal: constraints and role of biomass pre-treatment. Inst Energy, Petten, The Netherlands, 2006.

[79] Li J, Brzdekiewicz A, Yang W, Blasiak W. Co-firing based on biomass torrefaction in a pulverized coal boiler with aim of 100% fuel switching. Appl Energy 2012;99:344-54.

[80] Li J, Biagini E, Yang W, Tognotti L, Blasiak W. Flame characteristics of pulverized torrefied-biomass combusted with high-temperature air. Combust Flame 2013;160: 2585-94.

[81] Hall WS. A Textbook of physiology. 2nd ed. New York: Lea; 1905.

[82] Richardson HB. The respiratory quotient. Physiol Rev 1929 9:61-125.

[83] Morinaka T, Wozniewicz M, Jeszka J, Bajerska J, Limtrakul PN, Makonkawkeyoon L, et al. Comparison of seasonal variation in the fasting respiratory quotient of young Japanese, Polish and Thai women in relation to seasonal change in their percent body fat. J Physiol Anthropol 2012;31.

[84] McClave SA, Lowen CC, Kleber MJ, McConnell JW, Jung LY, Goldsmith LJ. Clinical use of the respiratory quotient obtained from indirect calorimetry. J Parenter Enter Nutr 2003;27:21-6.

[85] Annamalai K, Puri IK, Jog MA. Advanced Thermodynamics Engineering. 2nd ed. Boca Raton: CRC press; 2011.

[86] Annamalai K, Silva C. Entropy Stress and Scaling of Vital Organs over Life Span Based on Allometric Laws. Entropy 2012;14:2550-77.

[87] Sadaka S, Negi S. Improvements of biomass physical and thermochemical characteristics via torrefaction process. Environ Prog Sustain Energy 2009;28:427-34.

[88] Chen WH, Hsu HC, Lu KM, Lee WJ, Lin TC. Thermal pretreatment of wood (Lauan) block by torrefaction and its influence on the properties of the biomass. Energy 2011;36:3012-21.

[89] Chen WH, Tu YJ, Sheen HK. Disruption of sugarcane bagasse lignocellulosic structure by means of dilute sulfuric acid pretreatment with microwave-assisted heating. Appl Energy 2011;88:2726-34.

[90] Syred N, O'doherty T, Froud D. The interaction of the precessing vortex core and reverse flow zone in the exhaust of a swirl burner. Proc Inst Mech Eng: J Power Energy 1994; 208:27-36.

[91] He R, Suda T, Takafuji M, Hirata T, Sato JI. Analysis of low NO emission in high temperature air combustion for pulverized coal. Fuel 2004;83:1133-41.

[92] Colmegna G. Modeling of the reburn process with the use of feedlot biomass as a reburn fuel. Masters Thesis. Texas A&M University; 2007.

[93] Lawn CJ. Principles of Combustion Engineering for Boilers. Academic Press: 1987.

[94] Syred N, Beer JM. Combustion in swirling flows: a review. Combust Flame 1974;23:143-201.

[95] Mitchell JW, Tarbell JM. A kinetic model of nitric oxide formation during pulverized coal combustion. AIChE J 1982;28:302-11.

[96] Howard JB, Williams GC, Fine DH. Kinetics of carbon monoxide oxidation in postflame gases. Symp Comb 1973;14:975-86.

[97] Jones WP, Lindstedt RP. Global reaction schemes for hydrocarbon combustion. Combust Flame 1988;73:233-49.

[98] Van der Vaart DR. Mathematical modeling of methane combustion in a fluidized bed. Ind Eng Chem Res 1992;31:999-1007.

[99] Annamalai K, Ryan W. Interactive processes in gasification and combustion—II. Isolated carbon, coal and porous char particles. Prog Energy Comb Sci 1993;19:383-446.

[100] Hobbs ML, Radulovic PT, Smoot LD. Modeling fixed-bed coal gasifiers. AIChE J 1992;38:681-702.

[101] Yoon H, Wei J, Denn MM. A model for moving-bed coal gasification reactors. AIChE J 1978;24:885-903.

[102] Annamalai K, Puri IK. Combustion science and engineering. Boca Raton: CRC press; 2007.

[103] Incropera FP, DeWitt DP. Fundamentals of heat and mass transfer. 4th ed. New York: John Wiley & Sons Inc; 1996.

[104] E-Instruments, E 8500 Instruction and operations manual. Langhorne: 2012.

[105] Kline SJ, McClintock FA. Describing uncertainties in single-sample experiments. Mech Eng 1953;75:3-8.

[106] Johnson E. Goodbye to carbon neutral: Getting biomass footprints right. Environ Impact Assess Rev 2009;29:165-8.

[107] Mason DM, Gandhi K. Formulas for calculating the heating value of coal and coal char: development, tests and uses. Am Chem Soc Div Fuel Chem 1980;25:235-45.

[108] Channiwala SA, Parikh PP. A unified correlation for estimating HHV of solid, liquid and gaseous fuels. Fuel 2002;81:1051-63.

[109] Sheng C, Azevedo JLT. Estimating the higher heating value of biomass fuels from basic analysis data. Biomass Bioenerg 2005;28:499-507.

[110] Annamalai K, Sweeten JM, Ramalingam SC. Estimation of gross heating values of biomass fuels. Trans ASAE 1987;30:1205-8.

[111] Chen W, Annamalai K, Ansley RJ, Mirik M. Updraft fixed bed gasification of mesquite and juniper wood samples. Energy 2012;41:454-61.

[112] Yoon HC, Pozivil P, Steinfeld A. Thermogravimetric pyrolysis and gasification of lignocellulosic biomass and kinetic summative law for parallel reactions with cellulose, xylan, and lignin. Energy Fuels 2011;26:357-64.

[113] Van de Weerdhof MW. Modeling the pyrolysis process of biomass particles. Masters thesis. Eindhoven University of Technology; 2010.

[114] Raveendran K, Ganesh A, Khilar KC. Pyrolysis characteristics of biomass and biomass components. Fuel 1996;75:987-98.

[115] Liu Q, Wang S, Zheng Y, Luo Z, Cen K. Mechanism study of wood lignin pyrolysis by using TG–FTIR analysis. J Anal Appl Pyrolysis 2008;82:170-7.

[116] Cozzani V, Lucchesi A, Stoppato G, Maschio G. A new method to determine the composition of biomass by thermogravimetric analysis. Can J Chem Eng 1997;75:127-33.

[117] Orfao JJM, Antunes FJA, Figueiredo JL. Pyrolysis kinetics of lignocellulosic materials—three independent reactions model. Fuel 1999;78:349-58.

[118] Varhegyi G, Antal Jr MJ, Jakab E, Szabó P. Kinetic modeling of biomass pyrolysis. J Anal Appl Pyrolysis 1997;42:73-87.

[119] Alcock CB, Itkin VP, Horrigan MK. Vapour pressure equations for the metallic elements: 298–2500K. Can Metall Q 1984;23:309-13.

[120] Howard JB, Sarofim AF. Gasification of coal char with carbon dioxide and steam at 1200–1800 C. Report. Massachusetts Institute of Technology; 1978.

[121] Bergman PC, Boersma AR, Kiel JH, Prins MJ, Ptasinski KJ, Janssen FJJG. Torrefaction for entrained-flow gasification of biomass. Second World Conf Technol Exhib Biomass Energy Ind Clim Prot, Italy, 2004.

[122] Sweeten JM, Annamalai K, Thien B, McDonald LA. Co-firing of coal and cattle feedlot biomass (FB) fuels. Part I. Feedlot biomass (cattle manure) fuel quality and characteristics. Fuel 2003;82:1167-82.

[123] Hoffmann L. Pyrolysis and Ignition studies on Coal and Biomass blends using TGA and FTIR. Report. Texas A&M University; 2011.

[124] Lawrence BD. Investigation of Synergistic NOx reduction from Cofiring and Air Staged Combustion of Coal and Low Ash Dairy Biomass in a 30 KiloWatt low NOx furnace. PhD dissertation. Texas A&M University; 2013.

[125] Bridgeman TG, Jones JM, Williams A, Waldron DJ. An investigation of the grindability of two torrefied energy crops. Fuel 2010;89:3911-8.

[126] Phanphanich M, Mani S. Impact of torrefaction on the grindability and fuel characteristics of forest biomass. Bioresour Technol 2011;102: 1246-53.

[127] Rosin P, Rammler E. The laws governing the fineness of powdered coal. J Inst Fuel 1933; 7:29-36.

[128] Sing KSW, Everett DH, Haul RAW, Moscou L, Pierotti RA, Rouquerol J, et al. Reporting physisorption data for gas/solid systems with special reference to the determination of surface area and porosity. Pure Appl Chem 1985;57:603-19.

[129] Pilon G, Lavoie JM. Characterization of switchgrass char produced in torrefaction and pyrolysis conditions. Bioresources 2011;6:4824-39.

[130] Gray MR, Corcoran WH, Gavalas GR. Pyrolysis of a wood-derived material. Effects of moisture and ash content. Ind Eng Chem Process Des Dev 1985;24:646-51.

[131] Valenzuela-Calahorro C, Bernalte-Garcia A, Gomez-Serrano V, Bernalte-García MJ. Influence of particle size and pyrolysis conditions on yield, density and some textural parameters of chars prepared from holm-oak wood. J Anal Appl Pyrolysis 1987;12:61-70.

[132] Van Heek KH, Hodek W. Structure and pyrolysis behaviour of different coals and relevant model substances. Fuel 1994 73:886-96.

[133] Glarborg P, Jensen AD, Johnsson JE. Fuel nitrogen conversion in solid fuel fired systems. Prog Energy Comb Sci 2003;29:89-113.

[134] Smoot LD, Smith PJ. Coal combustion and gasification. New York: Plenum Press; 1985.

[135] Thien BF, Lawrence BD, Sweeten JM, Annamalai K. Co-firing Coal: Poultry Litter Biomass Blends in a Laboratory Scale Boiler-Burner. Trans ASABE 2012;55:681-8.

[136] Varol M, Atimtay AT, Olgun H, Atakül H. Emission characteristics of co-combustion of a low calorie and high sulfur–lignite coal and woodchips in a circulating fluidized bed combustor: Part 1. Effect of excess air ratio. Fuel 2014;117:792-800.

[137] EIA, Emissions allowance prices for SO2 and NOX remained low in 2011: http://www.eia.gov/todayinenergy/detail.cfm?id=4830, accessed February 8, 2014

[138] Hilten R, Speir R, Kastner J, Das KC. Production of aromatic green gasoline additives via catalytic pyrolysis of acidulated peanut oil soap stock. Bioresour Technol 2011;102:8288-94.

[139] Oasmaa A, Czernik S. Fuel oil quality of biomass pyrolysis oils state of the art for the end users. Energy Fuels 1999 13:914-21.

[140] Bhimani S, Alvarado JL, Annamalai K, Marsh C. Emission characteristics of methanol-in-canola oil emulsions in a combustion chamber. Fuel 2013;113:97-106.

[141] Lawrence B. Cofiring coal and dairy biomass in a 100,000 BTU/h Burner boiler facility. Masters thesis. Texas A&M University; 2007.

[142] Rizzo MR, Mari D, Barbieri M, Ragno E, Grella R, Provenzano R, et al. Resting metabolic rate and respiratory quotient in human longevity. J Clin Endocr Metab 2005;90:409-13.

[143] Jacobson K, Maheria KC, Kumar Dalai A. Bio-oil valorization: A review. Renew Sustain Energy Rev 2013;23:91-106.

[144] Heller MC, Keoleian GA, Volk TA. Life cycle assessment of a willow bioenergy cropping system. Biomass Bioenerg 2003;25:147-65.

[145] Powers SK, Howley E. Appendix A in: Exercise Physiology: Theory and application to fitness and performance. 8th ed. McGraw-Hill, 2012.

APPENDIX A

Derivation for reaction order 'n'

The decomposition of biomass with order n can be represented as,

$$\frac{dF_v}{dt} = -BF_v^n \exp\left(\frac{-E}{\bar{R}T}\right) \tag{A.1}$$

$$\frac{dF_v}{dT} = -\frac{B}{\beta} F_v^n \exp\left(\frac{-E}{\bar{R}T}\right) \tag{A.2}$$

At the point of maximum volatile release,

$$\frac{d^2F_v}{dT^2} = \frac{B}{\beta} F_{v,\max}^n \exp\left(\frac{-E}{\bar{R}T_{\max}}\right) * \frac{E}{\bar{R}T_{\max}{}^2} - \frac{B}{\beta} nF_{v,\max}^{n-1} \left(\frac{dF_v}{dT}\right)_{\max} \exp\left(\frac{-E}{\bar{R}T_{\max}}\right) = 0 \tag{A.3}$$

Upon simplification of Eq. (A.3), we get

$$F_{v,\max}^n \left(\frac{E}{\bar{R}T_{\max}{}^2}\right) = nF_{v,\max}^{n-1} \left(\frac{dF_v}{dT}\right)_{\max} \tag{A.4}$$

$$n = \frac{\left\{F_{v,\max}\left(\frac{E}{\bar{R}T_{\max}{}^2}\right)\right\}}{\left|\left(\frac{dF_v}{dT}\right)_{\max}\right|} \tag{A.5}$$

APPENDIX B

Derivation for RQ, ER and (A:F) from gas analysis

The current analysis was modified from the derivation presented in Powers and Howley [145]. Conisder any C-H-N-O-S fuel; assume that negligible N from air or fuel N is converted into NO and assume complete combustion. From N_2 conservation which is similar to Nitrogen tracer technique presented in Thanapal et al. [16],

$$\text{Dry or wet air mole in} * X_{N_2,i} = \text{Expired wet or dry moles} * X_{N_2,e}$$

$$\text{Thus, } \frac{\text{Expired dry or wet}}{\text{Inspired dry or wet}} = \frac{X_{N_2,i}}{X_{N_2,e}}, \text{ where } X_{N_2} \text{ can be either in wet or dry basis as appropriate} \quad \text{(B.1)}$$

$$\text{Similarly, } O_2\text{consumed} = \text{inspired} * X_{O_2,i} - \text{expired} * X_{O_2,e}$$

$$Z = \frac{O_2 \text{ consumed dry or wet}}{\text{Inspired dry or wet air}} = X_{O_2,i} - X_{O_2,e} * \left(\frac{X_{N_2,i}}{X_{N_2,e}} \right), X_{O_2} \text{ wet or dry basis as appropriate} \quad \text{(B.2)}$$

Once inspired moles are known per hour, one can compute O_2 consumed per hour and estimate metabolic rate using the known value of HHV_{O2}. When $X_{O2,e} = 0$ (stoichiometric combustion), $Z = X_{O2,i.}$

$$\text{Moles of } CO_2 \text{ expired} = \text{Expired moles} * X_{CO_2,e} - \text{inspired} * X_{CO_2,i}$$

$$\frac{CO_2 \text{ moles produced}}{\text{Inspired dry or wet air}} = X_{CO_2,e}\left(\frac{X_{N_2,i}}{X_{N_2,e}}\right) - X_{CO_2,i}, X_{CO_2} \text{ wet or dry basis as appropriate} \qquad \text{(B.3)}$$

Using Eq. (B.3) and Eq. (B.2),

$$RQ = \frac{CO_2 \text{ moles produced}}{O_2 \text{ moles consumed}} = \frac{X_{CO_2,e}\left(\frac{X_{N_2,i}}{X_{N_2,e}}\right) - X_{CO_2,i}}{X_{O_2,i} - X_{O_2,e} * \left(\frac{X_{N_2,i}}{X_{N_2,e}}\right)} \qquad \text{(B.4)}$$

$$\text{Inspired air} * X_{O_2,i} - O_2 \text{ consumed} = O_2 \text{ excess} = \text{expired moles} * X_{O_2,e}$$

$$1 - \left(\frac{O_2 \text{ consumed}}{O_2 \text{ supplied}}\right) = \left(\frac{\text{expired moles}}{O_2 \text{ supplied}}\right) * X_{O_2,e}$$

$$\varphi = 1 - \left(\frac{X_{N_2,i}}{X_{N_2,e}}\right)\left(\frac{X_{O_2,e}}{X_{O_2,i}}\right) \qquad \text{(B.5)}$$

$$\text{where, } \varphi = \left(\frac{O_2 \text{ stoich}}{O_2 \text{ supplied}}\right) = \left(\frac{O_2 \text{ consumed}}{O_2 \text{ supplied}}\right)$$

Since RQ is fixed at any equivalence ratio, then CO_2 maximum is reached when $X_{O2,e}$=0 or ϕ=1 .When CO_2 is maximum, X_{N2e}= 1- X_{CO2max}; Thus using Eq. (B.4) and solving

$$X_{CO_2,\max} = \frac{RQ * X_{O_2,i} + X_{CO_2,i}}{X_{N_2,i} + RQ * X_{O_2,i} + X_{CO_2,i}}$$

With $X_{CO2,i}$= 0 (for pure air), $X_{N2,i}$ = 1- $X_{O2,i}$

$$X_{CO_2,\max} = \frac{RQ * X_{O_2,i}}{1 - X_{O_2,i} + RQ * X_{O_2,i}} = \frac{RQ}{\left(\frac{1 - X_{O_2,i}}{X_{O_2,i}}\right) + RQ}$$

where $\left(\frac{1 - X_{O_2,i}}{X_{O_2,i}}\right) = 3.76$ for pure dry air

Air fuel ratio

If fuel has "c" Carbon atoms, then

$$\text{Air supplied} = \frac{O_2 \text{ supplied}}{X_{O_2,i}} = \frac{O_2 \text{ stoich}}{\varphi * X_{O_2,i}}$$ and using definition of RQ

$$\left(A:F\right)=\left(\frac{c}{RQ}\right)\left(\frac{1}{\varphi * X_{O_2,i}}\right) \tag{B.6}$$

If fuel fed is normalized to c atom (i e CH_xO_y, x=Hydrogen/Carbon atom, y= O atom/C atom)

$$\left(A:F\right)_{\text{emp Fuel}}=\left(\frac{1}{RQ * \varphi * X_{O_2,i}}\right), \text{ c normalized fuel } CH_xO_y. \tag{B.7}$$

APPENDIX C

Effect of heating rate and residence time in TCM

Effect of different heating rates (heating rate used to raise the temperature of the biomass from room temperature to the desired torrefaction temperature) and residence times (isothermal stage time period) on mass loss of juniper and mesquite samples were studied using three component model (TCM). Table 30, Table 31, and Table 32 shows the DAF mass remaining after torrefaction of mesquite at 10, 20 and 50 C/min respectively for different residence times.

Table 30. DAF mass remaining after mesquite torrefaction, heating rate: 10˚C/min.

T (˚C)/t (min)	**30**	**45**	**60**	**120**
200	0.9803	0.9715	0.9630	0.9324
220	0.9466	0.9255	0.9067	0.8495
240	0.8792	0.8438	0.8173	0.7611
260	0.7823	0.7463	0.7240	0.6742
280	0.6571	0.6091	0.5691	0.4469
300	0.4166	0.3406	0.2934	0.2261

Table 31. DAF mass remaining after mesquite torrefaction, heating rate: 20˚C/min.

T (˚C)/t (min)	**30**	**45**	**60**	**120**
200	0.9808	0.9720	0.9635	0.9327
220	0.9479	0.9267	0.9078	0.8501
240	0.8818	0.8457	0.8187	0.7616
260	0.7852	0.7478	0.7249	0.6746
280	0.6596	0.6108	0.5705	0.4479
300	0.4205	0.3431	0.2950	0.2264

Table 32. DAF mass remaining after mesquite torrefaction, heating rate: 50˚C/min.

T (˚C)/t (min)	30	45	60	120
200	0.9811	0.9722	0.9638	0.9330
220	0.9487	0.9274	0.9084	0.8505
240	0.8833	0.8469	0.8196	0.7619
260	0.7870	0.7488	0.7255	0.6748
280	0.6611	0.6118	0.5714	0.4484
300	0.4229	0.3446	0.2959	0.2266

The mass loss is higher for the case of 300˚C torrefaction and for higher residence times. It can also be observed from Table 30, Table 31, and Table 32 that the mass retained is slightly higher when high heating rates were used. The mass retained (F) when mesquite was torrefied at 260˚C for 30 minutes was 0.7823 for a heating rate of 10˚C/min. However the F value when the heating rate was 50˚C/min for torrefaction at 260˚C for 30 minutes was slightly higher at 0.7870 indicating that some volatiles were trapped within the biomass due to rapid heating which resulted in higher mass retention. Similar results were obtained for juniper torrefaction at different heating rates. Table shows the mass retention results obtained for juniper samples.

Table 33. DAF mass remaining after juniper torrefaction, heating rate: 10˚C/min.

T (˚C)/t (min)	30	45	60	120
200	0.9913	0.9874	0.9836	0.9700
220	0.9764	0.9670	0.9586	0.9326
240	0.9455	0.9289	0.9161	0.8861
260	0.8931	0.8711	0.8550	0.8085
280	0.7919	0.7457	0.7054	0.5802
300	0.5553	0.4783	0.4298	0.3562

Table 34. DAF mass remaining after juniper torrefaction, heating rate: 20˚C/min.

T (˚C)/t (min)	30	45	60	120
200	0.9915	0.9876	0.9838	0.9701
220	0.9770	0.9676	0.9591	0.9329
240	0.9466	0.9298	0.9167	0.8863
260	0.8946	0.8720	0.8557	0.8090
280	0.7940	0.7475	0.7070	0.5813
300	0.5595	0.4810	0.4316	0.3567

Table 35. DAF mass remaining after juniper torrefaction, heating rate: 50˚C/min.

T (˚C)/t (min)	30	45	60	120
200	0.9916	0.9877	0.9840	0.9703
220	0.9774	0.9679	0.9594	0.9331
240	0.9473	0.9303	0.9172	0.8865
260	0.8956	0.8726	0.8561	0.8092
280	0.7954	0.7485	0.7079	0.5819
300	0.5620	0.4826	0.4327	0.3570

APPENDIX D

Grindability of torrefied juniper

Juniper samples torrefied in N_2 and CO_2 were ground for 20 minutes in a Sweco Vibro Energy grinding mill. Size distribution of the ground samples were then determined using sieve shaker. Fig. 66 and Fig. 67 shows the size distribution results obtained for ground juniper samples torrefied in CO_2 and N_2 respectively.

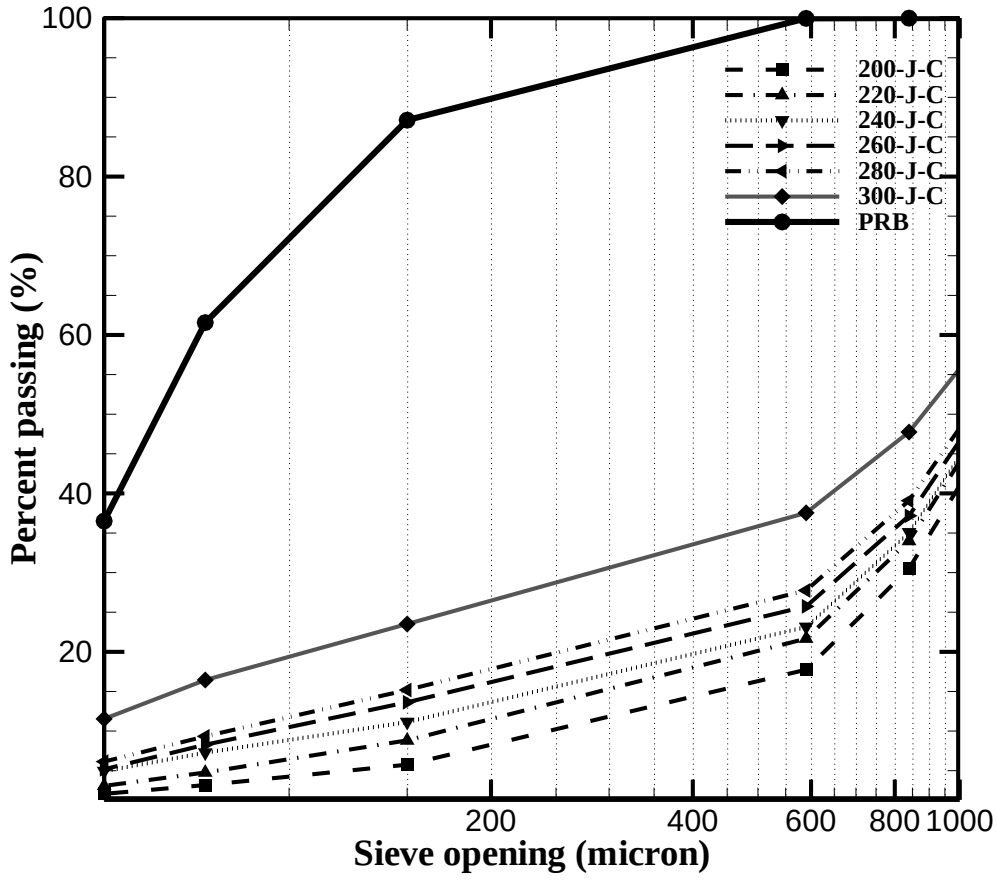

Fig. 66. Grindability of juniper samples torrefied in carbon dioxide environment.

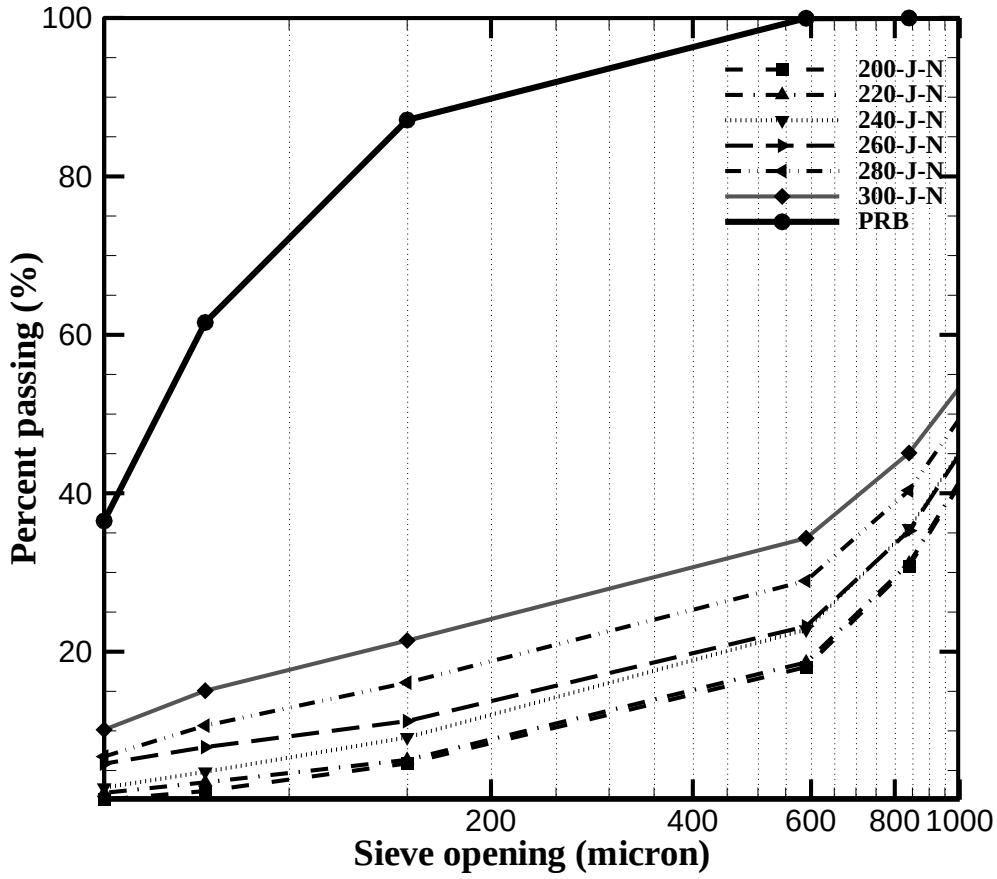

Fig. 67. Grindability of juniper samples torrefied in nitrogen environment.

It should be noted that the juniper samples which were torrefied are much smaller (2-4 mm) than the mesquite samples (4-6 mm). Also the DAF mass loss during torrefaction with CO_2 and N_2 were similar for the juniper samples. Hence the grindability results shows negligible differences for both the torrefaction mediums as similar percentage of ground samples pass through smaller sieves for lower torrefaction temperatures. At the highest torrefaction temperature of 300˚C, around 20% of the

ground samples torrefied with N_2 passes through the 150 micron sieve while around 25% of the CO_2 torrefied ground samples passed the 150 micron sieve indicating improved grindability of the CO_2 torrefied juniper samples.

APPENDIX E

Derivation for $RQ_{process,biomass}$

Respiratory quotient is defined according to the equation below.

$$RQ = \frac{CO_2 \text{moles}}{O_2 \text{ consumed moles}} \tag{E.1}$$

Consider power consumed in preparing the fuel. If the power is electric, P_{elec} (e.g grinding, transportation), then

$$\text{Heat input in GJ per kg biomass} = \left\{ \frac{p_{elec} in\left(\frac{GJ}{\text{kg biomass}} \right)}{\eta} \right\} \tag{E.2}$$

where η is the efficiency of the power plant which generates the electic power.

$$O_2 \text{ consumed in moles for electrical power moles per kg biomass} = \left\{ \frac{p_{elec} \text{in} \left(\frac{\text{GJ}}{\text{kg biomass}} \right)}{\eta * \overline{HHV}_{O_2} \text{in} \left(\frac{\text{GJ}}{\text{kmol}} \right)} \right\} \tag{E.3}$$

$$CO_2 \text{produced in moles per kg biomass} = \frac{RQ_1 * \mathrm{p}_{elec}\left(\frac{GJ}{\text{kg biomass}}\right)}{\eta * \overline{HHV}_{O_2} in\left(\frac{GJ}{kmol}\right)} \quad \text{(E.4)}$$

where RQ_1 is the RQ factor for fossil fuel used in generating the electrical power and η, power plant efficiency. If heat is used directly (example: drying, collection)

$$CO_2 \text{ produced in moles per kg biomass} = \frac{RQ_2 * q_{heat}\left(\frac{GJ}{\text{kg biomass}}\right)}{\eta_B \ \overline{HHV}_{O_2} in\left(\frac{GJ}{kmol}\right)} \quad \text{(E.5)}$$

where RQ_2 may be the RQ factor of a different fossil fuel and η_{burner}, burner efficiency. Thus total CO_2 produced in processing and transportation per kg (From Eq. (E.4) and Eq. (E.5))

$$CO_2 \text{ in moles per kg biomass} = RQ_1 * \frac{p_{elec}\left(\frac{GJ}{kg}\right)}{\eta * \overline{HHV}_{O_2}\left(\frac{MJ}{kmole}\right)} + \frac{RQ_2 * q_{heat}\left(\frac{GJ}{\text{kg biomass}}\right)}{\eta_B \ \overline{HHV}_{O_2} in\left(\frac{GJ}{kmol}\right)}, \text{moles per kg biomass} \quad \text{(E.6)}$$

The heat input is HHV_{O2} (GJ/kg of O_2)* stoich O_2 in kg consumed per kg biomass. The CO_2 in tons per GJ of energy input is given as

$$CO_2 \text{ in tons per GJ of energy from biomass} = \left(RQ_1 \frac{P_{elec}}{\eta * \overline{HHV}_{O_2}} + \frac{RQ_2 * q_{heat}\left(\frac{GJ}{\text{kg biomass}}\right)}{\eta_B \ \overline{HHV}_{O_2} in\left(\frac{GJ}{kmol}\right)} \right) \left(\frac{\left(\frac{44.01}{1000}\right)}{a_{stoich}\left(\frac{kgO_2}{\text{kg biomass}}\right) * HHV_{O_2} in\left(\frac{GJ}{\text{kg of } O_2}\right)} \right)$$

(E.7)

Assuming HHV_{O2}=0.014 GJ/kg O_2 or 0.448 GJ/kmole O_2

$$CO_2 \text{ in tons per GJ of energy from biomass} = \frac{7.017}{a_{stoich}\left(\frac{\text{kg } O_2}{\text{kg biomass}}\right)} \left\{ RQ_1 \frac{p_{elec}\left(\frac{GJ}{kg}\right)}{\eta} + \frac{RQ_2 * q_{heat}\left(\frac{GJ}{kg}\right)}{\eta_B} \right\}$$

(E.8)

For 100 kg as received biomass fuel of formula CH_mO_n (dry ash free fuel) with remainder being moisture and ash. Then

$$m = \frac{H\% * 12.01}{C\% * 1.01},\ n = \frac{O\% * 12.01}{C\% * 16}\text{; hence, } RQ = \frac{1}{\left(1 + \frac{m}{4} - \frac{n}{2}\right)}$$

$$\bar{a}_{stoich} = \left\{ \frac{C\%}{12.01} + \left(\frac{1}{4}\right)\frac{H\%}{1.01} - \left(\frac{1}{2}\right)\frac{O\%}{16} \right\} \text{ moles of } O_2 \text{ per 100 kg fuel} \qquad \text{(E.9)}$$

From Eq. (E.1).,

$$RQ_{biomass} = \frac{\left(\frac{C\%}{12.01}\right)}{\bar{a}_{stoich}} \tag{E.10}$$

$$a_{stoich} = 0.32 * \bar{a}_{stoich} = \frac{0.32 * \left(\frac{C\%}{12.01}\right)}{RQ_{biomass}} \tag{E.11}$$

Using Eq. (E.11) in Eq. (E.8)

$$CO_2 \text{ in tons per GJ of energy from biomass} = 21.9 * \frac{RQ_{biomass}}{\left(\frac{C\%}{12.01}\right)} \left\{ RQ_1 * \frac{p_{elec}\left(\frac{GJ}{\text{kg biomass}}\right)}{\eta} + RQ_2 * q_{heat}\left(\frac{GJ}{\text{kg biomass}}\right) \right\} \tag{E.12}$$

Since CO_2 in tons per GJ ≈ RQ*0.1, then

$$RQ_{\text{process,}biomass} = 219 * \frac{RQ_{biomass}}{\left(\frac{C\%}{12.01}\right)} \left\{ RQ_1 * \frac{p_{elec.}\left(\frac{GJ}{\text{kg biomass}}\right)}{\eta} + \frac{RQ_2 * q_{heat}\left(\frac{GJ}{\text{kg biomass}}\right)}{\eta_{burner}} \right\} \tag{E.13}$$

APPENDIX F

$RQ_{process,biomass}$ for mesquite and juniper

Based on the life cycle assessment of willow based biomass [144], the total energy consumed for the growth and harvesting of woody biomass was estimated to be 98.3 GJ/ha for a time period of 23 years. Assuming an average yield of 13.6 oven dry tonnes of woody biomass per hectare per year, the total energy consumed in MJ/as received kg of mesquite and juniper was found to be 0.2655 and 0.2958 respectively. 52% of the total energy consumed for the production of biomass was based on electricity generated from burning fossil fuels and 48% of the total energy consumed was from diesel fuel. Assuming the efficiency of the power plant to be 0.33 and using Eq. (E.13), the $RQ_{process,biomass}$ for mesquite and juniper was estimated to be 0.03. The energy provided by the diesel fuel was accounted for directly in the biomass processing equation.